AN ABSTRACT OF THE THESIS OF

Kanokrat Tiyapun for the degree of Master of Science in Radiation Health Physics

presented on March 12, 1997. Title: Epithermal Neutron Beam Design at the Oregon State University TRIGA Mark-II Reactor (OSTR) Based on Monte Carlo Methods.

Redacted for privacy

Abstract approved: _____

Stephen E. Binney

Filter and moderator assemblies were designed for the tangential beam port of the Oregon State University TRIGA Mark-II reactor (OSTR). The objective of this design was to achieve an adequate epithermal neutron beam (energy range from 0.5 eV to 10 keV) with low fast and thermal neutron components for boron neutron capture therapy (BNCT). A Monte Carlo neutron calculation was performed with the Monte Carlo N-Particle Transport Code (MCNP) to simulate a model of the reactor core and neutron irradiation facilities. The two-step calculations performed included criticality and epithermal neutron beam design. Results indicated that the multiplication factor (k_{eff}) was 1.032 and an optimized epithermal neutron beam can be obtained by using heavy water as a moderator in beam port 4 (radial piercing beam port), and sulfur and lithium carbonate (Li_2CO_3) as fast neutron and thermal neutron filters in beam port 3 (tangential beam port), respectively. Since the beam size is usually larger than a brain tumor, collimation of the epithermal neutron beam was required. By using different diameters of a cone-shaped collimator, a 12 cm diameter had better performance than other diameters. An epithermal flux of 1.28×10^8 n $cm^{-2}s^{-1}$, a thermal neutron flux of 1.34×10^7 n $cm^{-2}s^{-1}$ and a fast neutron flux of 1.14×10^7 n $cm^{-2}s^{-1}$ was derived for an operating power of 1 MW. In the event that a higher reactor power was available and suitable fast neutron and gamma ray shields were

designed, a modified beam port can produce a sufficient epithermal neutron intensity with negligible fast and thermal neutron and gamma ray contamination for BNCT.

Epithermal Neutron Beam Design at the Oregon State University TRIGA Mark II Reactor (OSTR) Based on Monte Carlo Methods

by

Kanokrat Tiyapun

A THESIS

submitted to

Oregon State University

in partial fulfillment of
the requirements for the
degree of

Master of Science

Presented March 12, 1997
Commencement June 1997

Master of Science thesis of Kanokrat Tiyapun presented on March 12, 1997

APPROVED:

Redacted for privacy

Major Professor, representing Radiation Health Physics

Redacted for privacy

Head of Department of Nuclear Engineering

Redacted for privacy

Dean of Graduate School

I understand that my thesis will become part of the permanent collection of Oregon State University libraries. My signature below authorizes release of my thesis to any reader upon request.

Redacted for privacy

Kanokrat Tiyapun, Author

CONTRIBUTION OF AUTHORS

I appreciate the helpful suggestions and guidance for improving my thesis from Dr. Stephen E. Binney, my major professor and advisor, who was involved in the design, analysis, interpretation and examination of various drafts. I would like to thank the member of my committees: Dr. Roy D. Haggerty, Dr. Todd S. Palmer and Dr. Fred L. Ramsey for final editing. I am grateful to Christopher E.D. Vostmyer who assisted in creating the reactor core input file and compiled MCNP executable. I also wish to thank Dr. Todd S. Palmer and Dr. Andrew C. Klein for their generous help in the interpretation of data. Special thanks are extended to Arthur D. Hall and Scott A. Crail, who provided nuclear data for the TRIGA Mark-II Reactor. I want to express my sincere appreciation to Hsing Hui Lee who has contributed to the completion of my thesis and made many wise suggestions. Finally, without the encouragement of my mother (Rachanee Tiyapun), my father (Nimit Tiyapun), my sister (Chittima Tiyapun) and my brother (Theerayut Toojinda), this work would not have been possible.

TABLE OF CONTENTS

TABLE OF CONTENTS (Continued)

TABLE OF CONTENTS (Continued)

TABLE OF CONTENTS (Continued)

LIST OF FIGURES

LIST OF FIGURES (Continued)

LIST OF FIGURES (Continued)

LIST OF TABLES

LIST OF TABLES (Continued)

EPITHERMAL NEUTRON BEAM DESIGN AT THE OREGON STATE UNIVERSITY TRIGA MARK-II REACTOR (OSTR) BASED ON MONTE CARLO METHODS.

1. INTRODUCTION

The death rate in the United States due to primary brain tumors is approximately 10,000 people per year. The glioma or glioblastoma multiforme is the most common type of brain tumor which has an incidence ranging from 31 to 49% of all intracranial tumors (Kennedy, 1972). The ideal treatment for brain tumors or several types of cancers is based on killing tumor cells without seriously damaging normal tissues.

The standard treatments which are currently successful in killing cancer today are radiation therapy, chemotherapy and surgery. In addition to the standard treatments, gadolinium neutron capture therapy (GdNCT) and photodynamic therapy (PDT) are alternative methods to treat brain tumors.

However, gliomas are difficult to treat with surgical removal, external radiation therapy or PDT, since the finger-shaped colonies of neoplastic cells that invade surrounding brain tissue are well vascularized and rapidly multiplying.

An effective therapeutic method for this type of tumor is a combination treatment which is called boron neutron capture therapy (BNCT) (Maker et al., 1972). BNCT combines two components involving boron and neutrons to produce a lethal radiation that can destroy tumor cells while the healthy tissue is relatively undamaged.

1.1 Boron Neutron Capture Therapy (BNCT) Description

BNCT is a selective treatment based on the reaction described in the following diagram: (Aizawa et al., 1980)

$$\rightarrow {}^{7}Li + \alpha + 2.79 \text{ MeV } (6.1\%)$$

$${}^{10}B + n \rightarrow {}^{7}Li^{*} + \alpha + \gamma + 2.31 \text{ MeV } (93.9\%)$$

$$\hookrightarrow {}^{7}Li + \gamma + 0.48 \text{ MeV}.$$

The two step method consists of (a) the stable isotope ^{10}B being injected into the tumor via the blood stream where the ^{10}B enriched compound can accumulate in tumor cells while the normal tissue takes up little or none and (b) the tumor area being irradiated by a beam of low energy or intermediate energy neutrons that induces the $^{10}B(n, \alpha)^{7}Li$ neutron capture reaction.

The alpha particles and recoiling ^{7}Li ions produced in the nuclear reaction have a short range and are high linear-energy-transfer particles. These ions have a range in tissue of 10 μm or less (about 1 cell diameter) so that the tumor cells will receive the highest fraction of the dose from this reaction while the normal tissues which have a lower neutron capture cross section, because of less boron present, will be relatively unaffected (Harling et al., 1990).

1.2 Advantages of BNCT

The advantage of BNCT is that a small number of alpha particles which are released from the neutron capture reaction can produce a cytotoxic reaction in the tumor cells by releasing their energy within the tumor cells. Alpha particles do not require the

present of oxygen in order to destroy tumor cells. Conventional radiation treatment and chemotherapy are the best treatment only for dividing cells (Barth et al., 1990).

Gadolinium Neutron Capture Therapy (GdNCT) is an alternative method by using Gadolinium-157 (^{157}Gd) instead of boron-10 (^{10}B) together with neutron irradiation. This method is based on the $^{157}Gd(n, \gamma)^{158}Gd$ reaction. After neutrons are captured by ^{157}Gd, energetic photons (gamma rays and x-rays) and electrons (Auger and internal conversion electrons) which were emitted result in an enhanced therapeutic effect of GdNCT (Shih and Brugger, 1992).

However, the disadvantages of this method are that (1) the gamma ray and Auger electron products of the $^{157}Gd(n, \gamma)^{158}Gd$ reaction do not appear to be as effective as the products of the $^{10}B(n, \alpha)^{7}Li$ reaction and (2) the dose from GdNCT is not well-localized so the healthy cells can be damaged (Cheng et al., 1995).

GdNCT is useful in the treatment of superficial tumors. On the other hand, it is not suitable for deep-seated tumors since the capture gamma rays and internal conversion electrons from the $^{157}Gd(n, \gamma)^{158}Gd$ reaction dose are not selective at the cellular level (Matsumoto 1995).

Photodynamic therapy (PDT) involves the selective uptake of a photosensitizer, such as a haematoporphyrin derivative, followed by irradiation of the tumor containing the sensitizer with light of a wavelength that will penetrate tissue and activate the sensitizer in the tumor cells. The results from this method are still less effective in destroying tumors compared to BNCT (Kaye, 1992).

1.3 Requirements for BNCT

The requirements for successful BNCT depend on various factors: (1) the location and the depth of the tumor involved; (2) the ratio of the ^{10}B concentration between the tumor cells and the surrounding healthy tissue; and (3) the intensity of the neutron beam used to kill the tumor cells (Barth et al., 1990).

The first factor, which is the depth of the tumor, which must be considered because a deep-seated tumor requires more penetration of the neutron beam to destroy the tumor cells than a shallow or superficial tumor. Furthermore, attenuation, absorption and scattering effects are effected by the depth of the tumor.

The second factor is the development of a tumor-selective boron compound. The boron compound used for glioblastoma multiforme treatment was first researched by Soloway and Sweet (Soloway, 1964 and Sweet et al., 1952). They used a polyhedral borane anion; however, this compound gave poor results since the concentration of boron in the tumor was lower than in normal brain tissue and blood (Soloway et al., 1990).

The first boron containing nucleoside for BNCT was synthesized by Raymond and collaborators (Schinazi et al., 1993). This compound causes a higher uptake of boron in tumors than in normal brain tissues because the tumors have a higher rate of cell division than the normal brain tissues. Therefore this compound is more suitable for capture reactions in BNCT.

Another method to deliver the ^{10}B was performed by using monoclonal antibodies. Results indicated that the boron with immunoconjugates contained a large amount of boron atoms which is enough for (n, α) reactions at the cellular level, but the antibodies

were not specific enough to deliver boron reliably to the tumor cells (Barth et al., 1990). Although highly specific antibodies (monoclonals) were developed, linking the boron with the highly specific antibodies, such as amino acid lysine, still failed to find the antigenic target (Barth et al., 1990). Until now, two types of compounds linked to antibodies that are being used clinically in BNCT are boronated porphyrins and promazines.

The third factor required for BNCT is the neutron beam intensity needed to destroy tumor cells. In BNCT, enough neutrons must be delivered to the tumor site in order for an adequate number of capture events to occur. Fast neutrons do not efficiently induce the $^{10}B(n, \alpha)^{7}Li$ neutron capture reaction. However, healthy tissue can be highly exposed and result in severe damage from fast neutrons.

On the other hand, thermal neutrons initiate the neutron capture reaction quite well, but lack the neutron energy that is adequate to penetrate to deep-lying tumors. A craniotomy must be performed to remove some tumor mass, the intact scalp and skull when thermal neutrons are utilized. An optimized neutron beam is desirable for BNCT, so epithermal neutrons are used to improve the therapy procedure.

An epithermal neutron beam is suitable for treatment since epithermal neutrons can penetrate to near the tumor before moderating to thermal neutrons, and the treatment using epithermal neutrons can be performed without surgically removing the scalp flap or removing skull bone (Harling et al., 1992a).

Although epithermal neutrons are able to treat deep-seated brain tumors with therapeutic effectiveness, producing an intense beam of epithermal neutrons without accompanying fast neutrons, thermal neutrons, and gamma rays is very difficult.

Therefore, the development of an epithermal neutron beam is considered to be important for BNCT treatment.

1.4 Neutron Sources for BNCT

The neutrons can be generated by different methods. The potential neutron sources for BNCT include a radioisotope of californium (^{252}Cf), proton accelerators, Van de Graaff accelerators, uranium (^{235}U) fission plates, inertial electrostatic confinement (IEC) systems, research reactors, and spallation.

1.4.1 Research Reactor

Among the various methods that generate neutrons, research reactors, such as the TRIGA type, are widely perceived to be the safest to install and operate in populated areas (Liu et al., 1994a). The fuel of the reactor is capable of supplying a large flux-per-watt ratio so that less steady state power is needed to supply the desired neutron flux.

The safety features of a TRIGA reactor include the large, prompt, negative coefficient of reactivity, high fuel temperature capability with a safety limit of 1150°C and large fission product retention even at high temperatures (Whittemore, 1992). The reactivity accidents that can occur from other types of reactors are unusual occurrences in research reactors.

1.4.2 Radioisotopes

Using radioisotopes such as ^{252}Cf is an alternative way to produce neutrons besides utilizing a research reactor; nevertheless, the ability to providing a therapeutic dose rate is

three to five times lower than that provided by research reactor beams. The subcritical multiplying assembly, which involves placing fissionable material (^{235}U) into the moderator to provide a secondary source of neutrons, must be considered in order to produce an acceptable neutron beam (Yanch et al., 1993a).

1.4.3 Accelerator

Proton accelerators can generate neutrons based on the $^{7}Li(p, n)$ reaction and a neutron moderator; however, 10 mA proton currents impinging on a lithium target are needed to produce a sufficient flux of epithermal neutrons for therapy. The neutron energy emerging from the accelerator target is too energetic for patient therapy. The maximum neutron energy is 800 keV for a 2.5 MeV proton beam, and the neutron yield from the lithium target itself is very low compared to a reactor source (Wang et al., 1989).

The $^{7}Li(p, n)$ and $^{3}H(p, n)$ reactions will produce high neutron fluxes in a Van de Graaff accelerator with heavy water (D_2O) with a lead reflector and in proton accelerators. On the other hand, at least 10 mA current must be used to generate a suitable number of epithermal neutrons (Yanch et al., 1992). Such currents are technically obtainable, but the problem is how to build the high current accelerator and lithium target that can resist tens of kilowatts of power.

1.4.4 Tandem Cascade Accelerator (TCA)

The Tandem Cascade Accelerator (TCA) which is under development at Science Research Laboratory can produce an intense proton beam by using a symmetrical, series-feed cascade multiplier to supply a DC accelerating potential to the high voltage terminal

(Figure 1.1). The high gradient cascade rectifier power supply is power efficient, and the ion source and target are at ground potential during operation by suitable tandem design. By operating the target at the oblique incidence, the total 10 kW of power may be spread over a large surface area, but maintaining the lithium metal target temperature below its melting point (181 °C) during the bombardment is currently being tested (Shefer et al., 1992).

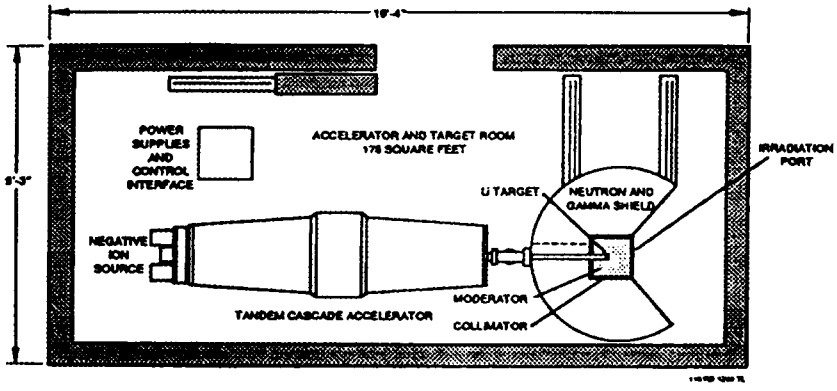

Figure 1.1 Tandem Cascade Accelerator

1.4.5 Inertial Electrostatic Confinement (IEC) System

The inertial electrostatic confinement (IEC) system generates neutron fusion reactions, where ions are accelerated toward each other by a spherical gridded structure. The IEC can produce monoenergetic 2.45 MeV deuterium-deuterium fusion neutrons without gamma radiation. A therapeutic neutron beam can be achieved by using collimators and shielding with a multiple layer composition (consisting of light water, boron, aluminum, and lead) (DeMora, 1995). Even though the IEC system is suitable as a

neutron source for BNCT, significant research and development are needed to scale the system up to the required level.

1.4.6 Spallation

Neutrons and other light particles from the nuclear reaction can be ejected when heavy elements are bombarded by protons in the spallation process (Barth et al., 1990). Neutrons can be produced by spallation in heavy elements such as copper, lead and uranium. The high energy particles must be moderated to epithermal energies. The inferior capability of this technique after measuring the spallation in copper indicates that this method will take several hours to achieve an adequate therapeutic dose (Barth et al., 1990).

1.4.7 U-235 Fission Plate

Even though the idea of using a ^{235}U fission plate located in the thermal column of a low power reactor is considered to be another method to yield an epithermal neutron beam (Rief et al., 1993), the public concern about the safety of the nuclear reactor and consequences to the environment limits the idea of using a ^{235}U fission plate. In addition, several factors limit the effectiveness of neutron production. Hence research reactors appear to be the best way to produce epithermal neutron sources for BNCT.

The objective of this study has focused on the development of an epithermal neutron beam by using modified filter materials to produce a more penetrating epithermal neutron beam for BNCT from the TRIGA Mark-II reactor.

2. LITERATURE REVIEW

Although the principle of neutron capture therapy (NCT) by using optimized thermal neutrons was proposed within four years after the discovery of the neutron (Locher et al., 1936), no clinical trials of BNCT were performed until 1951 (Godwin et al., 1955).

The first clinical trials of BNCT began in 1951 using thermal neutrons at the Brookhaven Graphite Research Reactor (BGRR). Part of the concrete shielding over the top of the BGRR was removed and an irradiation port was built to deliver thermal neutrons to irradiate brain tumors in patients. The outcome was unsatisfactory due to the high contamination of fast neutrons and gamma rays. The first clinical trials failed due to radiation injury to the normal tissue of the scalp (Sweet et al., 1952).

2.1 Clinical Trials and the Development of BNCT at the Brookhaven Medical Research Reactor (BMRR) and the Massachusetts Institute of Technology Reactor (MITR)

In 1959, the Brookhaven Medical Research Reactor (BMRR) was built and became operational to provide a higher thermal neutron flux beam for BNCT research (Liu et al., 1994b). After the BMRR was modified by a beam extraction facility to deliver a more intense beam of thermal neutrons with less contamination of the fast neutrons and gamma rays components for clinical trials of brain tumor treatment, the results showed an unsuccessful therapeutic effect.

Because of poor thermal neutron penetration and relatively high boron compound in blood or normal tissues compared to tumor cells, the neutron capture reaction occurred

in blood lining vessels more than tumor cells and damaged the blood vessels. Concurrently, BNCT clinical trials were performed at the Massachusetts Institute of Technology Reactor (MITR).

2.1.1 Clinical Trials at BMRR and MITR

The results of these clinical trials also showed discouraging results. The unsucessful research was interrupted in 1961 due to the failure to show significant efficacy. The life span or average survival of the patients was not better than conventional therapy (Perks et al., 1988).

The failure in clinical trials was attributed to the fact that the boron compound concentration was low in a tumor relative to the concentration in blood, the gamma ray background at the irradiation facility was high, and the thermal neutrons did not penetrate to an adequate depth because of their rapid attenuation in tissue. The development of better boron compounds (Soloway et al., 1990) and the construction of gamma shielding using bismuth (Kanda et al., 1975) can solve the first and second problems.

To solve the problem of rapid attenuation of the thermal neutron flux in the tissue, the following technique was used during the second therapy trial at the MITR. A craniotomy was performed to remove the main tumor mass in the brain. Subsequently a second surgery was performed in order to reflect the scalp flap and the cranium to allow an adequate penetration of incident neutrons to the tumor site. Through this technique, thermal neutrons can reach the tumor site directly and improve the depth-flux distribution. However, the results were still unsatisfactory because many patients treated with BNCT were not fresh cases (they had been treated with other treatments before BNCT treatment)

and had a high concentration of boron compound in blood and surface tissues (Deutsch et al., 1975).

2.1.2 Development for Optimal Neutron Beam at BMRR and MITR

In 1965, Fairchild performed experiments with an epithermal beam at BMRR by using a cadmium filter to eliminate the thermal neutrons from the BMRR neutron beam. The neutron beam from this experiment was intense enough for NCT. However, the fast neutron component was too high by at least one order of magnitude for therapeutic application (Fairchild, 1986).

Funding limitations was a problem for further research until 1986, when the Power Burst Facility (PBF)/BNCT program was established. The research was continued at Brookhaven National Laboratory (BNL) and Idaho National Engineering Laboratory (INEL) to modify the BMRR beam for BNCT. The first practical neutron beam applicable for biological research and clinical trials was installed at the BMRR in 1986 (Wheeler et al., 1989).

In 1988, a neutron beam at BMRR was developed involving a neutron filter design, using aluminum and aluminum oxide (Al_2O_3) as moderators to produce an intense epithermal neutron beam (Fairchild, 1992 and Wheeler et al., 1989). Thermal neutrons were minimized by a cadmium layer at the end of the filter, and the gamma component of the neutron beam was reduced by bismuth and lead (Wheeler et al., 1990). In 1991, a lithium carbonate (Li_2CO_3) in polyethylene (Li-poly) shield was added to decrease the neutron flux coming from outside the port (Liu et al., 1993).

In 1992, the configuration of the BMRR reactor core was modified in order to enhance the epithermal neutron beam and reduce the fast neutron beam. The new configuration is shown in Figure 2.1 (Liu et al., 1994a).

New fuel elements were added and shifted toward the patient port while still retaining a critical but controlled condition. The moderator assembly was redesigned by placing aluminum pallets in the moderator tank instead of an empty tank, using a combination of aluminum and aluminum oxide, replacing the outer bismuth by lead plus 0.05% atomic number density of ^{6}Li, creating an air region at the patient port and replacing the Li-poly assembly around the bismuth port with pure Li_2CO_3 sheets to reduce the background gamma dose from ^{1}H-induced gamma rays from the Li-poly shield (Liu et al., 1993). The result of the new design indicated that the fast neutron dose component was decreased, reducing the problem of severe scalp necrosis due to fast neutron dose.

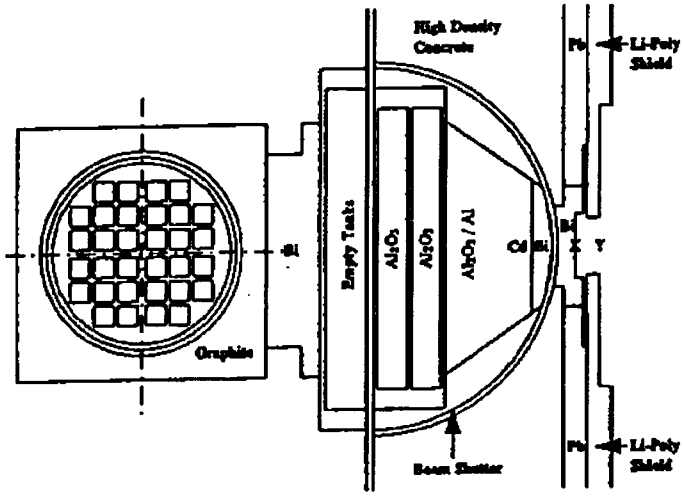

Figure 2.1 Horizontal section of the BMRR epithermal neutron beam, showing the mixing assembly of Al and Al_2O_3 in moderator tanks.

The second epithermal neutron beam which demonstrated the efficacy of NCT in animal and patient treatment was installed at the MITR (Harling et al., 1992b). The useful epithermal neutron beam for BNCT was obtained by using a heavy water (D_2O) filter and a bismuth shield. Recently, the epithermal neutron beam filter elements at MITR were modified to improve the intensity, a penetration of the neutron beam and significantly reduce fast neutron and gamma ray contaminations.

The new epithermal beam filter consisted of a cadmium, aluminum and lithium alloy, sulfur, and bismuth (Zamenhof et al., 1992). The cross section view of the MITR-II medical therapy beam with a heavy water shutter, sulfur and aluminum filters is illustrated in Figure 2.2 (Choi et al., 1990).

The results indicated that the modified epithermal beams at MITR are suitable for shallow and deep-seated tumor treatment. A single exposure irradiation using a neutron beam at MITR has shown only mild discoloration of the brain without histologically evident injury (Harling et al., 1990).

An adequate epithermal neutron intensity with a low background dose from fast neutron and gamma ray components can be produced from other high flux nuclear reactor facilities such as the Power Burst Facility (PBF), the Georgia Institute of Technology Research Reactor (GTRR) and the Missouri University Research Reactor (MURR). The PBF, GTRR and MURR can be modified to yield a high quality epithermal neutron beam for BNCT.

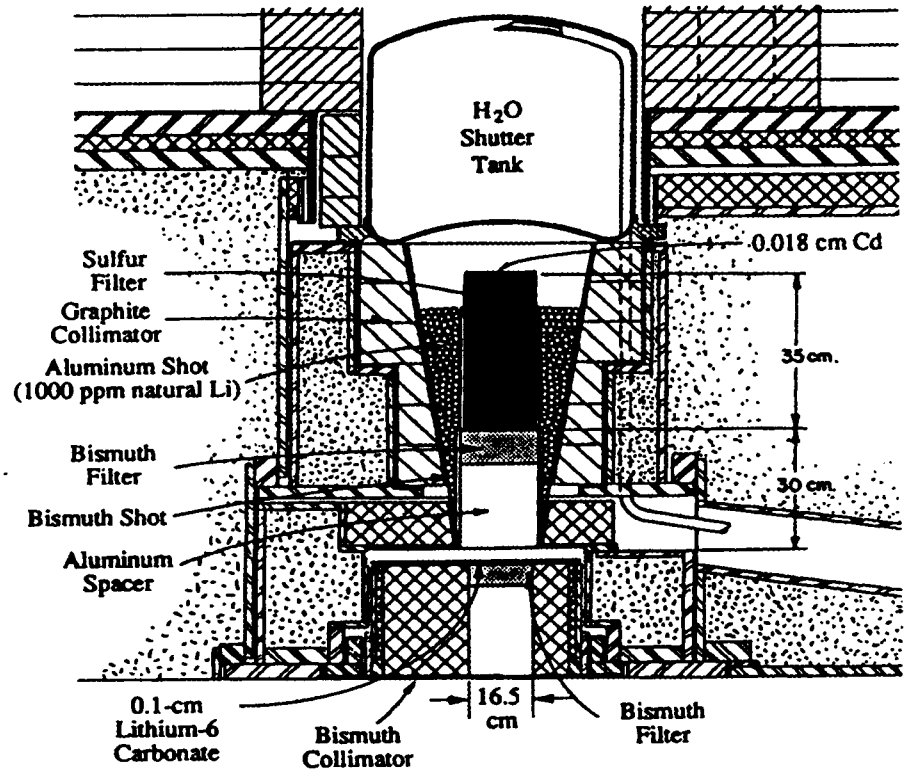

Figure 2.2 The cross section view of the MITR-II medical therapy beam with its system of shutters and sulfur and aluminum filters installed at the graphite collimator region.

2.2 Epithermal Neutron Beam Design for PBF

In the late 1960s, a high intensity epithermal neutron beam was produced from the PBF reactor located at the Idaho National Engineering Laboratory (INEL). Although the PBF is a good source of epithermal neutrons because of its high uranium loading, a low water fraction and an inefficient outer reflector, the fast neutron and gamma components are high enough that this beam was not suitable for BNCT because of high damage to healthy tissue (Wheeler et al., 1989).

In 1989, a new configuration of the PBF reactor core, which is presented in Figure 2.3, was designed for NCT (Wheeler et al., 1989). Additional fuel and filter at the patient side of the core resulted in shifting the power peak of the core, increasing reactivity and enhancing the neutron flux toward the thermal column which was used to irradiate the patient. The filter configuration consisted of aluminum plates and heavy water inside a steel cylinder to moderate and reflect neutrons, cadmium to remove the thermal neutrons and bismuth shields to attenuate the gamma rays.

The inconel-in-pile tube of PBF was changed to an aluminum tube to exclude most of the internal water so that the neutron absorption was decreased and the reactivity of the core was increased. A bismuth cone collimator can enhance the epithermal neutron flux while reducing the fast neutron component (Wheeler et al., 1989).

The results after reconfiguration indicated that the PBF beam had a higher intensity than the BMRR beam by about 10 to 100 times and has lower fast neutron components in the neutron beam.

2.3 Epithermal Neutron Beam Design for GTRR

In January 1988, a filter was designed to be added inside the beam port H-1 of the GTRR to produce an epithermal neutron beam. The filter configuration which was installed inside the H-1 beam port consisted of aluminum, sulfur to tailor neutron energies above 30 keV and pass neutron energies below 30 keV, cadmium to remove thermal neutrons below 0.6 eV, lead to decrease the gamma flux, and borated polyethylene surrounding the filter to absorb neutrons before they can scatter back into the beam (Russell et al., 1990).

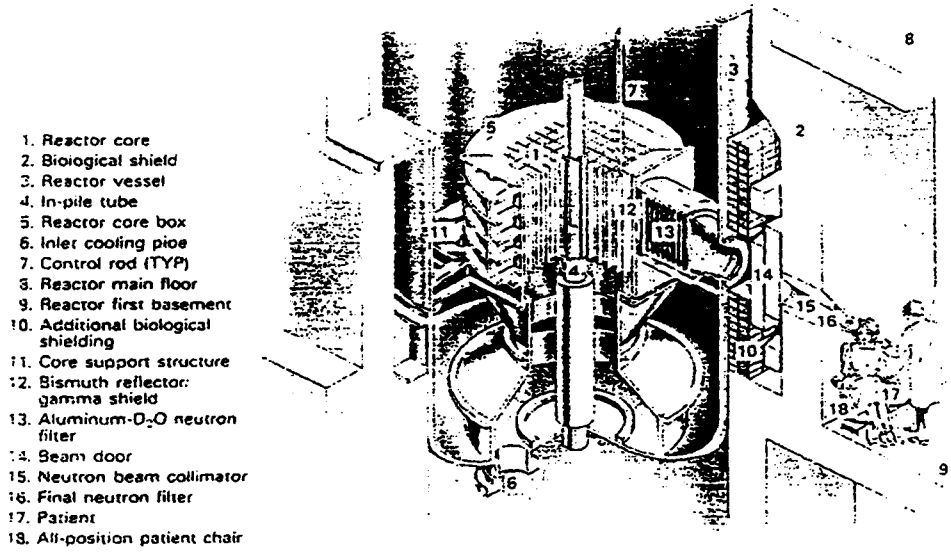

Figure 2.3 Boron NCT facility at PBF (conceptual design).

To improve the performance of the epithermal neutron beam at the GTRR, the filter was installed in the large biomedical irradiation port. The filter and moderator consisted of 90% aluminum and 10% heavy water by volume. The shielding and the reflector consisted of laminated bismuth, lead and cadmium. The horizontal cross section of GTRR with filter and moderator is illustrated in Figure 2.4 (Nigg et al., 1993).

The filter housing region was composed of dry aluminum plates, lithiated aluminum plates, and a titanium plate to shift the neutron spectrum. The bismuth, lead and lithiated-polyethylene at the exit of the port suppressed gamma rays and the thermal neutron component (Nigg et al., 1993). Results showed that the epithermal neutron beam from the GTRR is better than the BMRR in terms of intensity, fast neutron contamination, current to flux ratio, and treatment time.

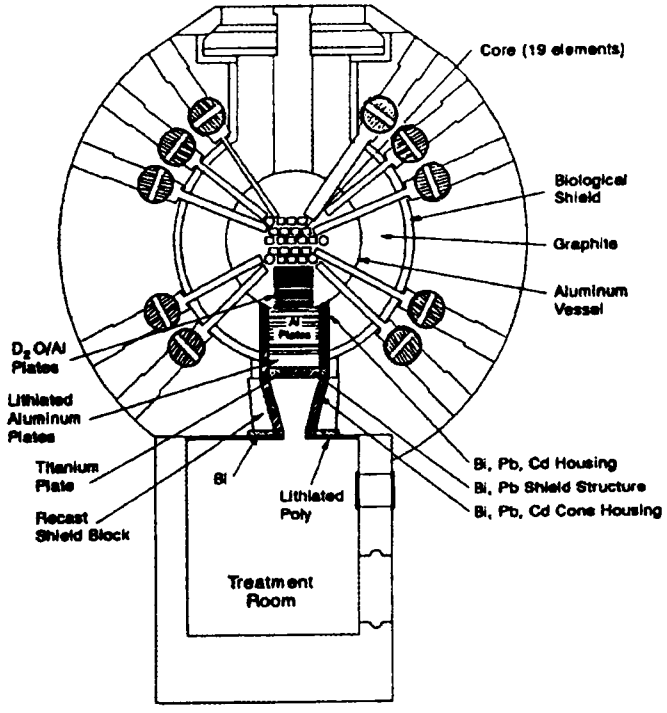

Figure 2.4 Horizontal section of GTRR including filter inside biomedical irradiation port

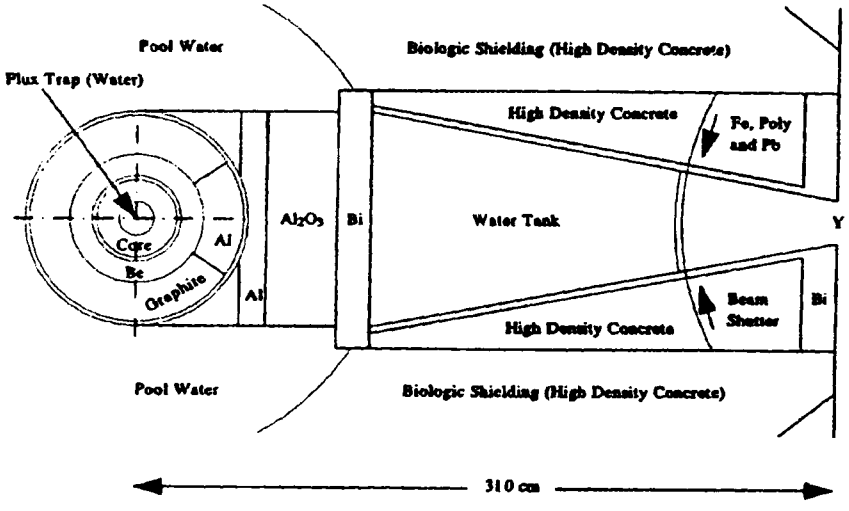

Figure 2.5 The diagram of the NCT beam in the thermal column of the MURR.

2.4 Epithermal Neutron Beam Design for MURR

Besides the PBF and GTRR, the other high flux reactor facility which can produce a therapeutic epithermal neutron beam is the MURR. The two possible positions that can produce the epithermal neutron beam are a thermal column and a beam port.

In the thermal column design, the graphite reflector which surrounded the reactor core and the thermal column were modified. Figure 2.5 shows that two graphite wedges facing the thermal column were replaced by two aluminum oxide wedges. The lead shield between the reflector ring and the reactor tank was replaced by aluminum plates. Then, a moderator was added near the reactor at the inner end of the thermal column (Brugger et al., 1992).

The moderator consisted of aluminum, aluminum oxide, lead or bismuth to reduce fast neutrons and gamma rays. 0.1% lithium (^{6}Li) was added to the moderator to eliminate thermal neutrons. The thermal neutron produced capture gamma rays in the aluminum were reduced by a bismuth or lead liner inside the beam port (Brugger et al., 1992).

In the MURR beam port F design, the epithermal neutrons were obtained with optimal moderator at the end of the beam port. Aluminum, sulfur and lead were the composition of the moderator, which was used to remove fast neutrons and gamma rays from the beam.

Although the epithermal neutrons from the beam port had a lower intensity and higher fast neutron and gamma contribution than epithermal neutrons from the thermal column, both epithermal neutron beams that were produced from thermal column and beam port F were effective for BNCT (Brugger et al., 1990).

2.5 Conceptual Design of Epithermal Neutron Beam for TRIGA Reactor

The TRIGA reactor is one of the most suitable neutron sources for epithermal neutrons because it is very safe, easy to operate, and flexible to satisfy the different needs of customers (Whittemore, 1992).

In 1990, the compact TRIGA Mark-II reactor at the University of California at Irvine was modified and redesigned for medical therapy treatment to supply the needs for BNCT in the U.S. This reactor was modified by using a thermal column with a lead plate, boron plastic, LiF and bismuth. A weak neutron poison was installed in the center of the reactor core to increase the leakage flux of the reactor and flatten the core flux distribution. Graphite surrounding the core will optimize the thermal neutron leakage for the modified thermal column. The configuration of the TRIGA Mark-II reactor is shown in Figure 2.6 (Whittemore, 1992).

Improvement of the epithermal neutron beam can be attained by using a 10 MW TRIGA U-ZrH_x fuel reactor with standard 1.37 cm fuel rods in either a 16 rod or 19 rod cluster. This design uses an extended core with a low average power density (Neuman, 1990). An efficient epithermal neutron beam can be provided from TRIGA U-ZrH_x fuel that is useful in BNCT.

2.6 Epithermal Neutron Beam Design for Low-Power Reactor

An epithermal neutron beam for BNCT can be produced in a low power reactor with two different designs (Liu et al., 1994c). The first design which is shown in Figure 2.7 utilized a ^{235}U fission plate located outside the reflector region and an Al/Al_2O_3 moderator assembly (Liu et al., 1994b). The primary source of fission neutrons comes

from the ^{235}U fission plate instead of the reactor core. Figure 2.8 presents the second design which was based on a slab reactor and Al/Al_2O_3 moderator assembly (Liu et al., 1994b).

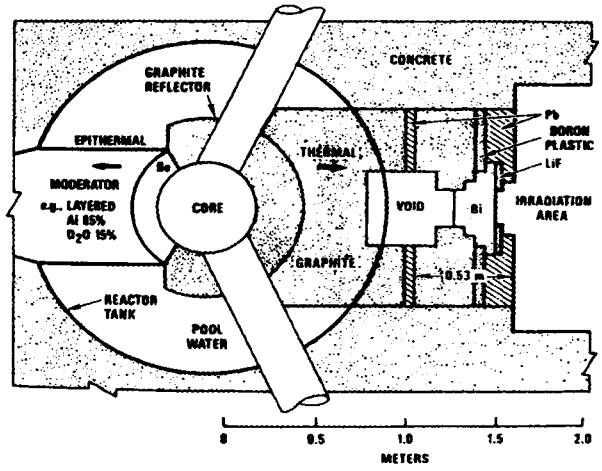

Figure 2.6 The TRIGA Mark-II reactor for BNCT using thermal and epithermal neutron

The result from both designs provided an acceptable forward directed epithermal neutron beam with a low fast neutron dose which can be used for BNCT.

2.7 Epithermal Neutron Beam Design Outside the U.S.

A high intensity epithermal neutron beam has been developed by using high flux reactors (HIFAR). Two experiments were conducted at the Harwell laboratory. In the first study, an experimental rig was fitted into a thimble of the PLUTO research reactor. In the second study, a suitable filter was installed in a different beam tube of the DIDO research reactor (Harrington and Constantine, 1995).

In addition to the DIDO and PLUTO reactors, other high flux nuclear reactor facilities which can generate an adequate epithermal neutron intensity are the high flux

reactor at Petten in Holland, and at the Australian Nuclear Science and Technology Organization (ANSTO) in Australia.

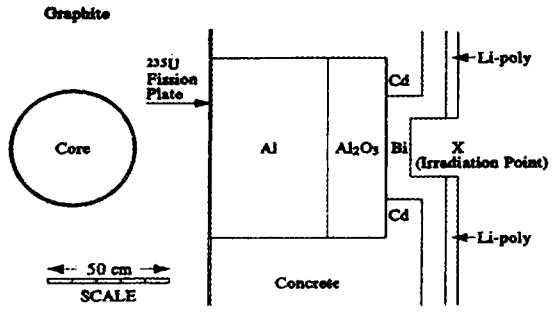

Figure 2.7 Horizontal section of a design using a ^{235}U fission plate coupled to a reactor.

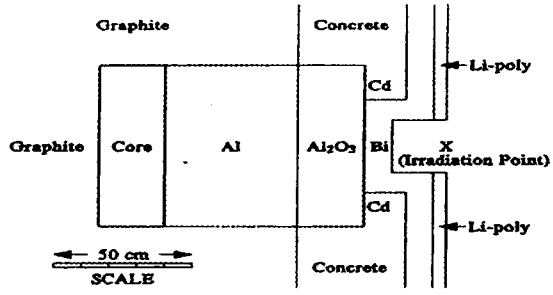

Figure 2.8 Horizontal section of a design using a slab reactor.

2.7.1 PLUTO Research Reactor

In 1988, at the Harwell laboratory, an epithermal neutron beam experiment was conducted by tailoring the neutron spectrum from the PLUTO research reactor. The high flux nuclear reactor was developed for BNCT by using the buildup in intensity of neutrons at the energy of the anti-resonance cross-section window of iron (~24 keV). The suitable materials which were used for filtering the neutron beam were a combination of aluminum, heavy water, sulfur and liquid argon. Figure 2.9 demonstrates a filter rig configuration for the PLUTO reactor (Perks et al., 1988).

A filter rig (thimble) was installed in the PLUTO reactor through a hole in the top shield, and the lower ends of the filter were located in the center of a fuel element. Iron discs were used as a neutron scatterer in the filter to scatter the maximum fluence rate of epithermal neutrons from the core of the reactor. However, the epithermal neutron beam from the iron-filter rig was not suitable for BNCT because the high fast neutron dose can damage the healthy tissue (Constantine, 1990).

2.7.2 DIDO Research Reactor

In 1987, an epithermal neutron beam model was constructed at the DIDO reactor. The DIDO reactor is a 25 MW research reactor which is cooled and moderated by heavy water. An experimental beam (B2) was produced by using a thimble tube which was formed and located at the center of a fuel element suspended by a graphite scatterer at the mid-core height within the thimble.

The combination of aluminum, sulfur, titanium, boron and liquid argon was utilized as the filter for the epithermal neutron beam in the experimental beam facility (B2 model). From the configuration which is presented in Figure 2.10 (Ross et al., 1992), the thermal neutron flux was reduced by a boron and liquid argon filter, while fast neutrons were tailored by aluminum, sulfur, liquid argon, and titanium (Ross et al., 1993).

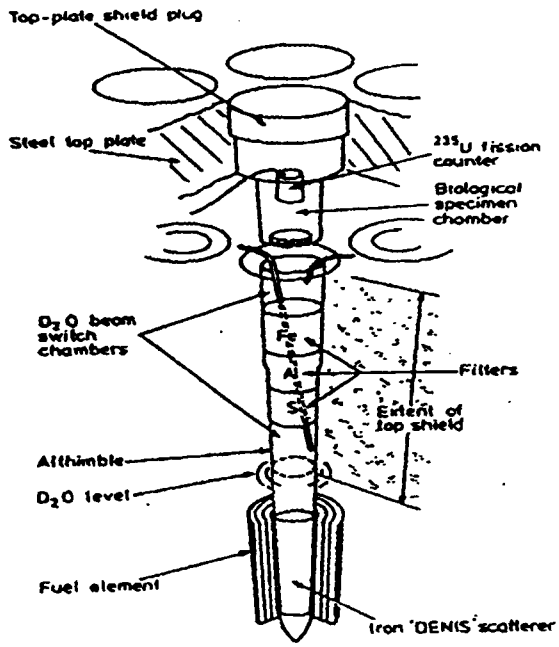

Figure 2.9 Diagram of the filter rig producing an iron-filtered 24 keV neutron beam.

The results from this experimental beam were applied to a horizontal beam port 10H which penetrated the reactor tank and extended to the reactor core (Figure 2.11) (Ross et al., 1992). While the research was carried out, the DIDO reactor was closed in 1990 for decomissioning. However, the research was still continued to select the best filter and spectrum shifter for an epithermal neutron beam.

Spectrum shifters such as Al_2O_3, AlF_3, BeO or D_2O were selected as a dry spectrum shifter. These were located at the core entrance to the beam tube. The results showed that after a dry spectrum shifter was added, the neutron kerma rate per unit neutron flux (K_n) was improved. However, photon kerma rate per unit neutron flux (K_p) was significantly increased (Ross et al., 1993). Finally, the dry spectrum shifter was removed from this design due to the high photon kerma rate per unit neutron flux.

An aluminum wet spectrum shifter which was installed between the edge of the core inside the heavy water and the entrance to the beam provided the best result in increasing the neutron flux and decreasing the photon dose. Although a positive result was obtained from a wet spectrum shifter, it had three disadvantages which involved removing an equivalent volume of heavy water, locating a wet spectrum shifter in the heavy water and decreasing the core reactivity (Ross et al., 1992). Therefore, the epithermal beam final design for the DIDO reactor consisted of the filter combination which was liquid argon, cadmium, aluminum, tin, and titanium without a wet or dry spectrum shifter.

2.7.3 High Flux Reactor (HFR) at Petten

Before the clinical trial for BNCT at Petten in 1992, the 45 MW reactor which is cooled and moderated by light water was utilized as a neutron source for epithermal neutron beam design. To achieve a high epithermal neutron beam, an experiment was conducted in the beam port HB11 which has a large diameter. Prior to modifying the beam port HB11, calculations and measurements were performed that utilized several combinations of filter components consisting of aluminum, liquid argon, titanium, cadmium, sulfur and boron in the smaller beam tube HB7 (Moss et al., 1992b). Subsequently, the epithermal neutron beam design from the beam port HB7 was applied to the beam port HB11.

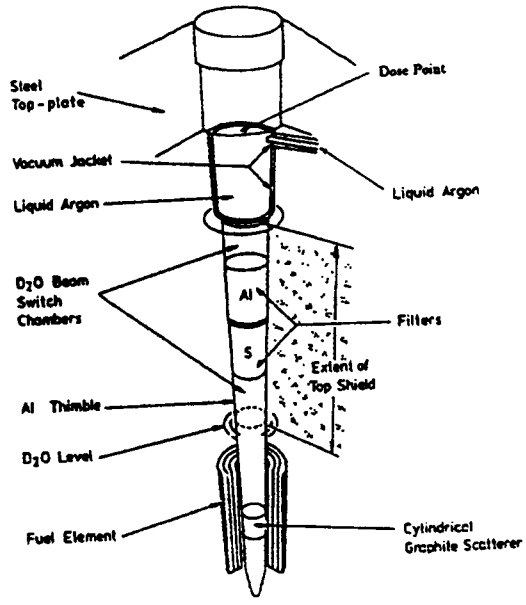

Figure 2.10 Diagram of the B2 beam located at the center of the fuel element

In addition to modifying the beam ports, the peripheral beryllium elements in the reactor core adjacent to the beam tube were replaced by an aluminum plug and a reactor fuel element to improve the beam quality (Moss et al., 1992a). The results showed that the reconfiguration of the reactor core and modified horizontal beam ports (HB7) by incorporating filters such as aluminum, sulfur, titanium, cadmium and liquid argon can deliver an intense epithermal neutron beam for BNCT (Watkins et al., 1992).

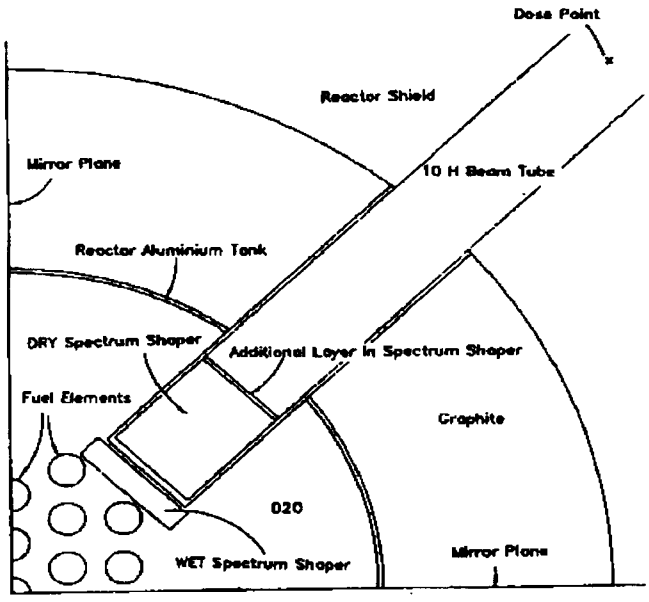

Figure 2.11 Model of the DIDO reactor

2.7.4 High Flux Australian Reactor (HIFAR) in Australia

After the High Flux Reactor at Petten was developed, the horizontal beam port facility (10H) which was located at the core mid-plane at the HIFAR in Australia was used for analysis of a filter for use with BNCT of murine melanoma xenografts. The configuration of the HIFAR reactor and 10H facility is illustrated in Figure 2.12 (Storr et al., 1992).

The filter combination at the beam port 10H included aluminum or sulfur, liquid argon, ^{6}LiF, and lead. The epithermal neutron flux was decreased due to the beam collimator, beam filters and shields. Consequently, increasing the beam diameter and power of the reactor can compensate for the low beam intensity and the appropriate epithermal neutron beam will be achieved at HIFAR in Australia (Storr et al., 1992).

Recently, a rearrangement of fuel elements was performed at HIFAR in Australia. The fuel element adjacent to the central elements was replaced by a dummy element, a dry liner tube was inserted inside the dummy element to exclude heavy water from its central region, and solid aluminum was loaded into the dry liner tube at the core middle plane. It was concluded that filter materials consisting of Al/Fe, titanium, and liquid argon were suitable for filtering the neutron beam (Harrington, 1990).

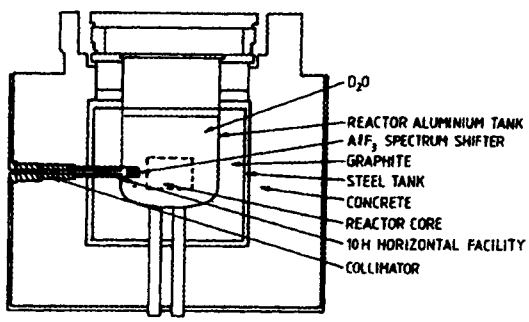

Figure 2.12 Vertical section of HIFAR and 10H facility in Australia.

2.7.5 Epithermal Neutron Beam Design for FIR-1

In addition to the TRIGA Mark-II reactors in the U.S. which can generate an intense epithermal beam for BNCT, a high epithermal flux with low fast neutron and gamma ray contamination can be produced by the FIR-1 TRIGA-II reactor in Finland without adding a neutron converter such as high or low enriched uranium plates.

Calculational results indicated that the most suitable moderator to slow fast neutrons down to epithermal energies was the mixture of 60% aluminum fluoride (AlF_3) and 40% Al. A second choice for an epithermal neutron moderator was a mixture of (1) glass and aluminum, (2) lead and beryllium fluorides, or (3) pure lead fluoride. Bismuth

and LiF were used to shield the incident gamma rays and thermal neutrons, respectively (Auterinen et al., 1993)

2.7.6 Epithermal Neutron Beam Design for LVR-15

BNCT was performed in Czechoslovakia by utilizing the VVR-S reactor at the Nuclear Research Institute at Rez to yield the appropriate neutron spectrum. The thermal column region was modified. The configuration of the thermal column consisted of moderating and shielding material, including nuclear grade graphite, heavy water, lead, and bismuth blocks. The results from the VVR-S reactor showed that an adequate epithermal neutron intensity can be obtained for BNCT. In 1988, VVR-S was shut down for reconstruction of the LVR-15 reactor.

The design for LVR-15 in Figure 2.13a and 2.13b was similar to VVR-S except for (1) a new moderator, Al_2O_3, aluminum, carbon and aluminum mixture with a cadmium sheet, (2) a bigger cavity inside the thermal column, (3) a high purity bismuth block and (4) boron carbide instead of lead (Burian et al., 1992). It was concluded that the new design of LVR-15 can generate an appropriate epithermal neutron flux with low contamination of gamma rays and fast neutrons for BNCT.

2.8 Clinical Trials and Neutron Beam Designs in Japan

Despite the failure in American BNCT clinical trials for malignant brain tumors at BMRR and MITR in 1961, Hatanaka persisted to treat glioblastoma patients with BNCT at the Musashi TRIGA reactor in Tokyo (Hatanaka, 1990). His clinical trial results have indicated that the binary system of BNCT may have great potential for superficial and

small brain tumor treatment because the 5-year survival rate was increased about 19%-58% (Hatanaka, 1990). Since the available low intensity of thermal neutron beam can not penetrate to deep-seated tumors, surgery to open the scalp was still needed in his clinical trials.

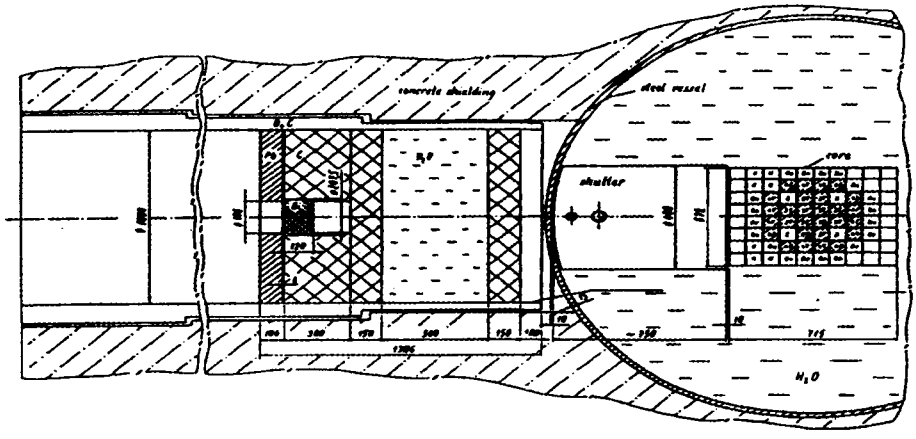

Figure 2.13a The top view configuration of the LVR-15

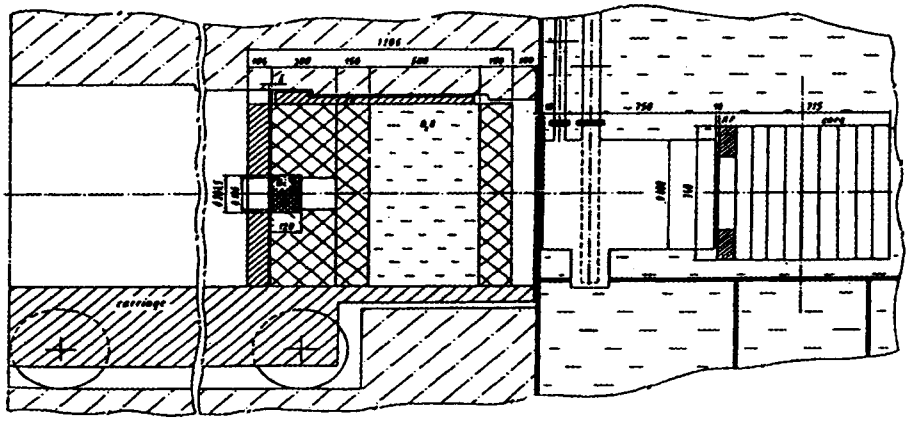

Figure 2.13b The lateral view configuration of the LVR-15

Between 1968 and 1975, the Hitachi Training Reactor (HTR) at the Tokyo Atomic Industrial Research Laboratory and Musashi Institute of Technology Reactor (MITR) used thermal neutrons for clinical trials with brain tumors (Taguchi, 1979). In 1975, the HTR was closed permanently. Therefore the MITR became the primary Japanese medical research reactor for BNCT. A remodeling of MITR was performed in 1979 to increase the thermal neutron fluence rate.

The inner structure of the thermal column was modified by increasing the internal cavity inside the thermal column to enhance the thermal neutron intensity, using bismuth to remove gamma rays from the thermal neutron beam, and using a lithium fluoride (^{6}LiF) collimator to confine the neutron beam and eliminate secondary gamma rays (Aizawa, 1990). The thermal neutron flux after remodeling was intense enough to treat the patients with superficial or small brain tumors without removing the scalp or skull.

The Musashi reactor was redesigned for an epithermal neutron beam in 1994 after it was shut down in 1990 because of a water leak in the reactor tank (Matsumoto, 1995). The spent fuel elements of TRIGA fuel (UZrH 8.4/90/1.6 wt%, 20% enrichment ^{235}U) were used as a converter assembly to produce an epithermal neutron beam placed outside the graphite reflector in a spent fuel basket (Figure 2.14). Results showed that the total fission heat from the spent fuel elements was 2.0 kW, so there was no additional cooling system in this design ((Matsumoto, 1995).

The thermal column was modified at the Musashi reactor. The new configuration consisted of Al_2O_3 to moderate fast neutrons from the reactor core and the fission converter assembly, a void region (cavity) to prevent the attenuation of useful neutron flux, a bismuth shield to attenuate the gamma dose, lead to remove fast neutrons and

incident gamma rays, a thin cadmium shield to filter out thermal neutrons and a ^{6}LiF sheet used as a collimator or thermal neutron shield (Matsumoto, 1995).

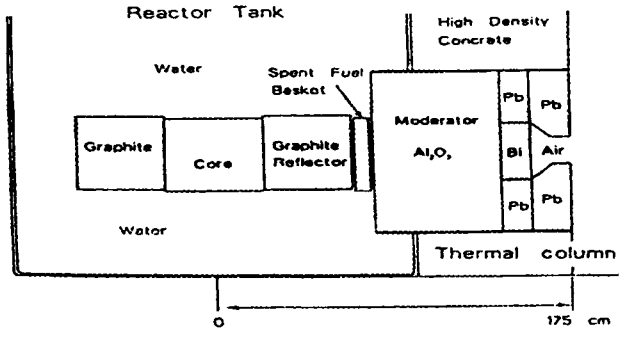

Figure 2.14 Vertical cross section of an epithermal neutron beam with the spent fuel basket at the Musashi reactor.

The resulting epithermal neutron flux was not intense enough for BNCT. However, the beam was anisotropic in the forward direction and hence had better penetration in tissue than an isotropic beam. In 1995, the thermalizing column was modified similarly to the thermal column. After modification, the results showed that the thermalizing column produced only half the intensity of the epithermal neutron beam comparing to the thermal column (Matsumoto, 1996).

Even though the higher thermal neutron flux was successful to treat superficial or small brain tumors, the attenuation effect is still a problem for deep-seated tumors. Irradiation with epithermal neutrons is desirable because they have a higher penetration depth and can thermalize within the tissue itself.

In 1980, the TRIGA reactor at the University of Tokyo was used as the neutron source to obtain an epithermal neutron beam (Yoshiaki et al., 1981). The neutrons leaking downward to the central hole of the TRIGA reactor were suitable for treating the patients (Figure 2.15).

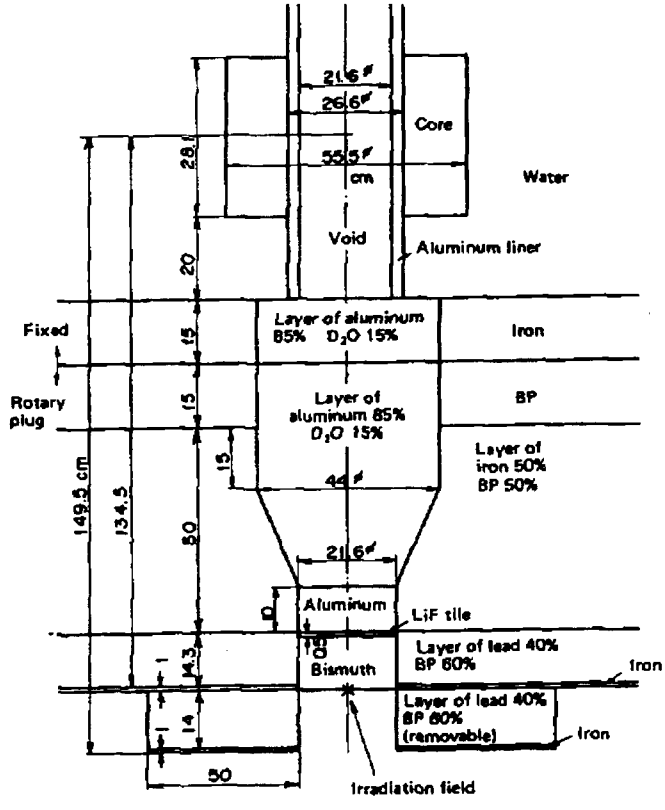

Figure 2.15 The configuration of the epithermal neutron column of TRIGA reactor in Japan

The spectrum shifter, which was a combination of aluminum and 10% - 20% heavy water, was used to fill the core region of the central hole in order to decrease the fast neutron flux with only a minor effect to the epithermal neutron flux. The incident gamma rays were shielded by bismuth and the thermal neutrons were tailored by 7.5% enriched lithium fluoride (LiF). Iron and borated polyethylene (BP) were used as the shielding

materials surrounding the moderator layer (Yoshiaki et al., 1981). Results showed that epithermal neutrons from the configuration in Figure 2.15 (Yoshiaki et al., 1981) can increase the possibility of BNCT.

Besides TRIGA reactors, a fast neutron reactor in Japan, such as the YAYOI reactor, can be used to improve the epithermal neutron beam for brain tumor treatment. In 1979, an epithermal-enriched neutron field for medical irradiation was constructed at the fast neutron source reactor YAYOI at the University of Tokyo (Shigehiro et al., 1980).

The moderator and shielding layers consisted of iron, graphite and polyethylene, lead and bismuth, borated polyethylene, natural LiF tiles and enriched ^{6}LiF flexible sheets, and heavy concrete (Shigehiro et al., 1980). Though the neutron flux from this configuration was sufficient for therapeutic treatment, the fast neutron dose was relatively high. In addition, the YAYOI reactor has a lower power than a TRIGA reactor. This in turn diminished the neutron flux with neutron moderator added, resulting in a longer treatment time. Therefore, bilateral treatment should be used with two beams each entering at the opposite of the brain laterally.

From the variety of reactors and accelerators that can generate epithermal neutron beams for BNCT, the beam parameters that can be calculated or measured should include the epithermal, thermal, and fast neutron flux densities ($n/cm^2 \cdot s$), the fast neutron dose and gamma dose per epithermal neutron fluences ($cGy \cdot cm^2/n_{epi}$) and, for more detail, it should also include the fast neutron dose per thermal neutron fluences ($cGy \cdot cm^2/n_{th}$) and the

absorbed dose from fast neutrons and gammas in free air (cGy/h). In Table 1, the beam parameters from various reactors and accelerators are compared (Moss, 1993).

Table 1. Comparison of epithermal neutron beams for BNCT

Reactor	Reactor power (MW)	epithermal neutron flux density ($x10^9$) (n/cm^2s)	D_{fast} in air $/n_{epi}$ ($x\ 10^{-11}$) $c{\cdot}Gycm^2/n_{epi}$	D_{gamma}/n_{epi} ($x\ 10^{-11}$) $c{\cdot}Gycm^2/n_{epi}$	ratio of neutron current to flux
BMRR (Al_2O_3 moderator)	3	1.8	4.2	1.1	0.67
BMRR (D_2O moderator)	3	11	27	3.2	
MITR	5	0.26	13	13	0.55
HFR, Petten	45	1.1	7.8	1.7	0.80
HIFAR, Australia	0.1	0.47		5.2	
GTRR	5	4	1.5		0.85
PBF	20	10	2	1	
MURR	10	7.9	2.8	0.3	0.78
Harwell/Pluto (Fe filter)	25.5	0.02	29	4.2	
Musashi-TRIGA	0.1	0.34	4.3	0.3	0.64
TRIGA Mark-II water reflected forced cooling	3.0	1.35			
Compact TRIGA core (16 rod) square array	10	8			
Compact TRIGA core (19 rod) hex array water reflected	10	13			
KUR-TRIGA	2	2.1			
LVR-15	1	1.4	2.38	3.57	
FIR-1 TRIGA-II	0.25	19			
TRIGA with a ^{235}U fission plate	0.1	0.8	4.4	< 1	0.78
Slab reactor with a ^{235}U fission plate	0.05	1.4	4.6	< 1	0.78
YAYOI fast neutron reactor		0.32	3.3	1.2	
Accelerator	10 mA (25 kW) in accelerator target	0.5	10		
Accelerator	10 mA (25 kW) in accelerator target	0.9	4.3	2.7	
Accelerator at MIT	10 mA (10kW) in accelerator target	1.0	12		
Accelerator	10 mA (25 kW) in accelerator target	0.78	6.6	1.4	0.94

2.9 Beam Parameters for Several Types of Epithermal Neutron Beams

Several different sources, moderator materials, filter configurations, and shielding materials have been studied to determine the suitable epithermal neutron beam design for brain tumor treatment. The design goals for epithermal neutron beams from various studies are almost the same, including a high intensity of epithermal neutrons with a short irradiation time, a low fast neutron component, a low gamma ray component, and a forward peaked epithermal neutron beam.

The requirements of an acceptable epithermal neutron beam such as an accurate model, the geometry of beam tube configuration, moderator or filter materials, angular dependence and size of the beam, the shielding and the irradiation room must be considered. The ideal epithermal neutron beam will destroy all the tumor cells while most healthy tissue will survive.

3. OSTR FACILITY DESCRIPTION

3.1 Safety Features of a TRIGA Reactor (Whittemore, 1992).

TRIGA reactors with uranium fuel and zirconium hydride moderators (U-ZrH) are widely known for their safety features. Therefore, they are suitable for producing a neutron beam for BNCT. Certain features of U-ZrH fuels inside the reactor core provide the safety factors and reduce the risk of reactor accidents. These safety features are as follows:

1. The special U-ZrH fuel matrix provides a large, prompt, negative temperature coefficient of reactivity.
2. The high temperature capability derives from the high chemical stability and the special metallurgical features of the U-ZrH matrix.
3. Fission products are trapped within the U-ZrH matrix and diffuse slowly even at a high temperature (1000°C).
4. The negative feedback coefficient of reactivity ensures that large amounts of reactivity can be added with no damage to the core.
5. In the event of loss of the cooling system, the U-ZrH fuel in a TRIGA reactor core can stay intact without an auxiliary cooling system. The temperature in the reactor core will decrease from natural convective cooling.
6. The fast startup of a TRIGA reactor is useful for BNCT purposes.
7. The normal TRIGA shielding and containment building is enough to shield radiation from the core and protect the public.

3.2 Oregon State University (OSU) TRIGA Mark II Reactor (OSTR) Description

The OSU TRIGA Mark II reactor is a pool type light-water cooled and moderated reactor built and designed for reactor safety, radioisotope production, and experimental performance. The reactor is operated at steady state power levels up to 1 MW. The reactor core consists of a solid, fuel-moderator element in which the zirconium-hydride moderator (ZrH) is homogeneously combined with 70% enriched uranium and a burnable poison which is 1.6 wt% erbium.

The configuration of the OSTR, which is presented in Figure 3.1, consists of a concrete shield containing an aluminum reactor tank, with the core, which is surrounded by a ring-shaped reflector, located near the bottom of the tank. The tank has an outside diameter of 198.1 cm and a depth of 624.8 cm. The reactor tank is filled with 487.7 cm of water above the core to provide adequate shielding in the vertical direction.

Four beam tubes and a graphite thermal column penetrate the concrete shield and reactor tank. A graphite thermalizing column also penetrates the concrete shield and terminates in a bulk-shielding experimental tank (Figure 3.2). The other irradiation facilities are shown in Figure 3.3 and include a rotating rack facility (lazy susan) which has a 40-position rotary specimen rack inside a ring-shaped well in the top of the reflector, a pneumatic transfer system (rabbit system), a cadmium-lined in core irradiation tube for irradiations with neutrons that have energies greater than the cadmium cut-off threshold, and a central thimble.

The original reactor core contained 87 fuel rods surrounded by a reflector ring which consists of graphite and lead encased in an aluminum cladding (Figure 3.4).

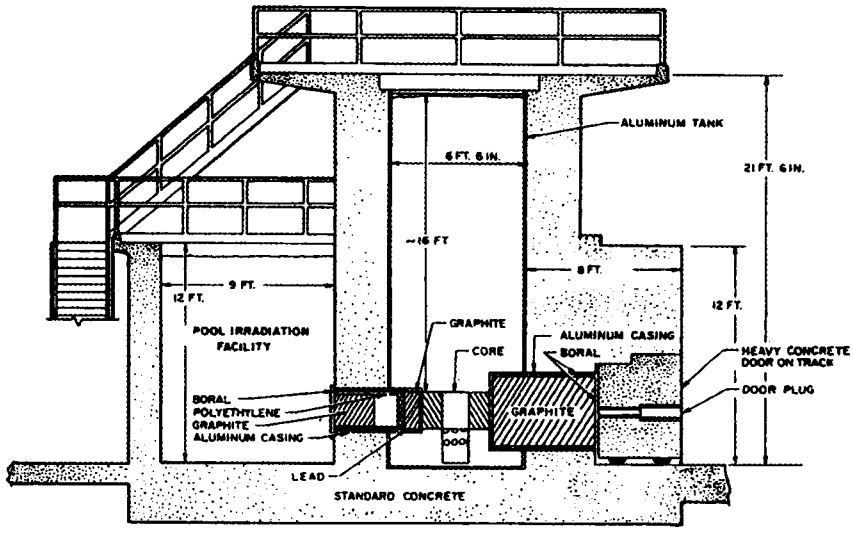

Figure 3.1 The vertical section of TRIGA Mark-II reactor

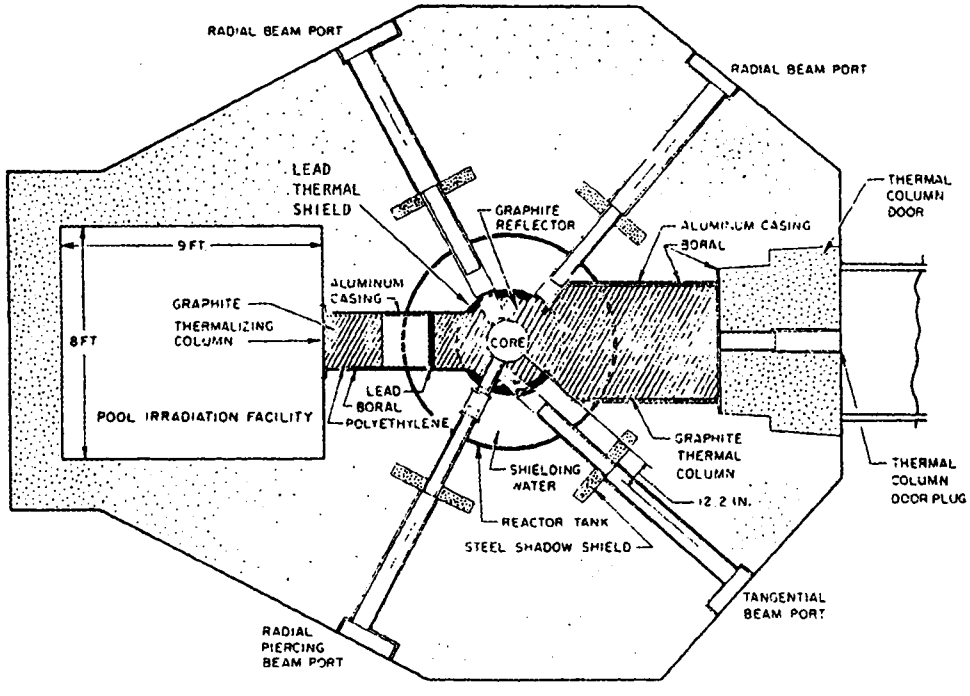

Figure 3.2 The horizontal section of TRIGA Mark-II reactor

The core is shielded radially by a 20.3 cm thick ring-shaped graphite reflector, 5.1 cm of lead inside the reflector can which is surrounded by an aluminum tank and cooled by the natural convection of water that occupies about one-third of the core volume (Figure 3.2).

NOTE: This is not the OSU TRIGA Mark III Core, but is very similar to it.

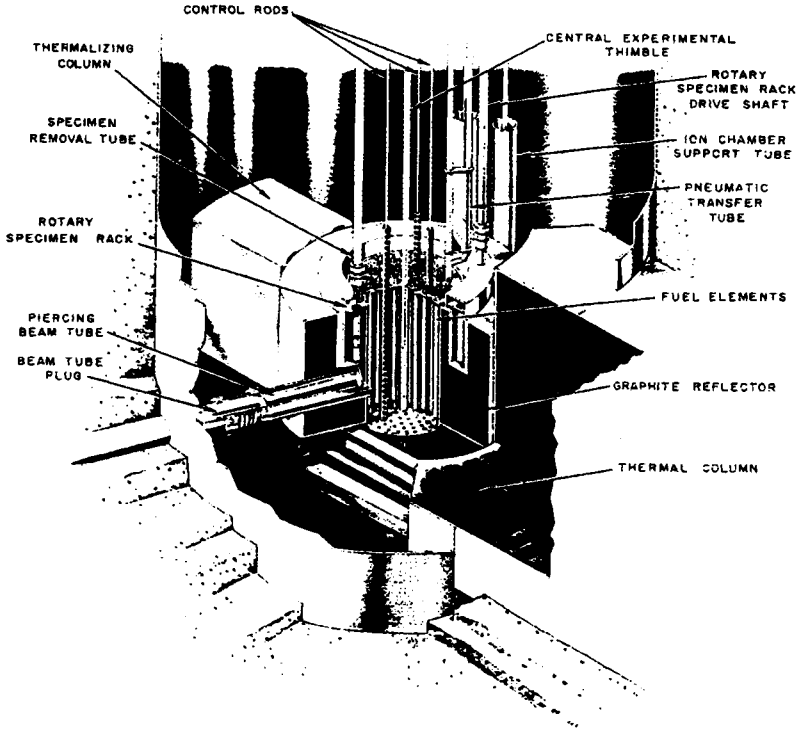

Figure 3.3 Cutaway view of a typical TRIGA Mark-II core arrangement.

3.2.1 Fuel Elements and Reflector

The fuel elements consist of an active fissile portion of the fuel element, which is 3.6 cm in diameter with a total length of 38.1 cm. Graphite reflector slugs with the length

of 16.8 cm are located at the top and the bottom of the fuel. The fuel and the graphite slugs are surrounded by a 0.05 cm-thick stainless steel cladding.

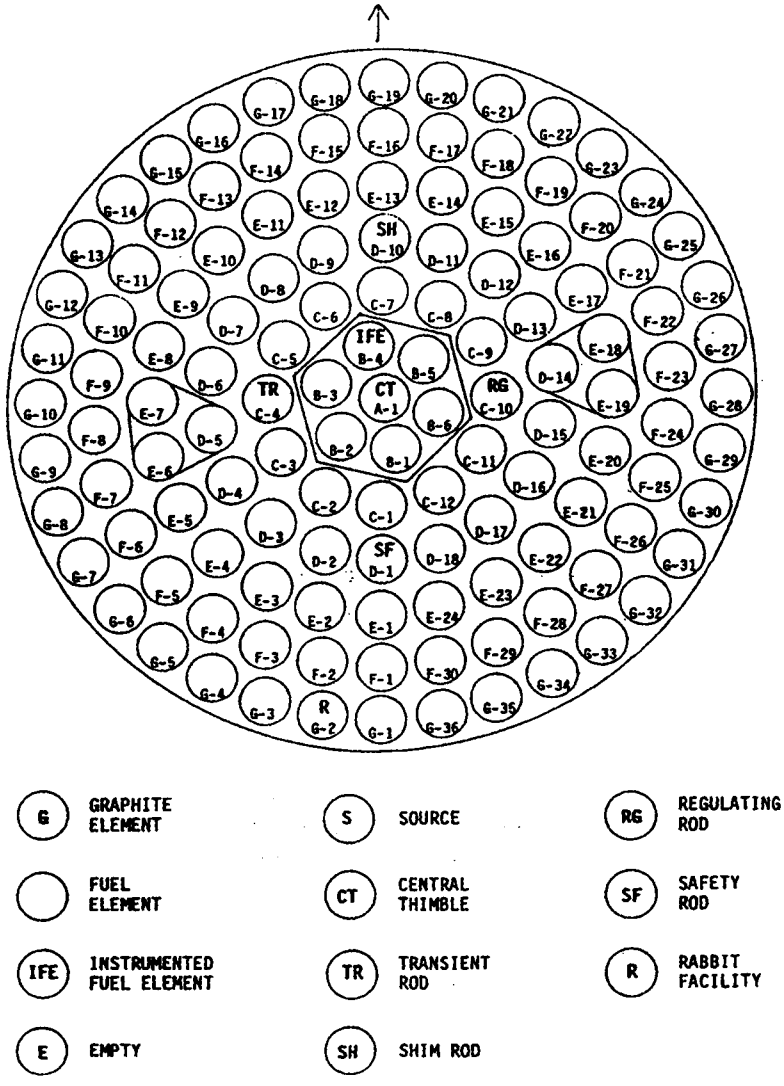

Figure 3.4 The core configuration in OSTR.

Figure 3.2 illustrates the reflector, which is a ring-shaped block of graphite radially surrounding the core with the thickness of 20.3 cm and a height of 55.9 cm. The reflector ring is clad in aluminum to prevent water from penetrating into it. Housed in the reflector

is a 5.08 cm-thick lead ring with penetrations for the beam ports, thermal column, and thermalizing column.

3.2.2 Control Rods

The OSTR uses four stainless steel clad neutron absorbing control rods to control and regulate the power, all positioned vertically between two grid plates which are fastened to the reflector assembly. Three of the control rods have the same design; the transient rod has a different design. The standard control rods are called the shim, the safety, and the regulating rod. The positions of the control rods are illustrated in Figure 3.4. The control rods are clad in 0.05 cm-thick stainless steel and are located between the top and the bottom grid plates. The top portion is borated graphite, and the bottom portion is fuel.

The transient control rod is filled with the same borated graphite poison on top and air below the graphite. The transient control rod is clad in 0.05 cm-thick stainless steel with aluminum plugs welded onto each end and is located between the top and the bottom grid plates.

3.2.3 Beam Ports

The reactor core has four beam ports extending through the concrete shield centered 6.985 cm below the centerline of the core. The tangential beam port has 15.2 cm inner diameters with 131 cm length, which increase to 20.3 cm with 164 cm length in the outer portion of the concrete shield, while the radial beam ports have 15.2 cm inner diameter with 106 cm length, which increases to 20.3 cm with 156 cm length in the outer portion of the concrete shield.

The beam tube walls are divided into two parts; the inner part closest to the reactor core is 0.80-cm thick aluminum; the outer part is 0.80-cm thick steel. The length of the radial (beam port 4) and tangential beam port (beam port 3) are 262 cm and 295 cm, respectively. The beam ports in the horizontal section view are presented in Figure 3.2.

Three of the beam ports are located radially with respect to the core center; another beam port (beam port 3) is tangential to the outer edge of the core. Two radial beam ports are aligned with cylindrical voids, located in the reflector region, and penetrate the concrete shield, pass through the reactor tank water, and terminate at the outer edge of the reflector assembly. The third radial beam port (beam port 4) penetrates through the graphite reflector and terminates at the outer edge of the core. Unlike the radial beam ports, the tangential beam port (beam port 3) terminates at the outer surface of the reflector and intersects the radial beam port (beam port 4) in the reflector graphite region.

3.2.4 Thermal Column and Thermalizing Column

The thermal column is a large boral-lined, graphite-filled aluminum vessel. The inner end of the thermal column terminates near the graphite reflector. The thermalizing column is also a boral-lined, aluminum vessel, and the outer end terminates at the bulk shield water tank while the inner end terminates near the graphite reflector ring.

4. MCNP DESCRIPTION AND MCNP MODEL OF THE OSTR

4.1 Monte Carlo N-Particle Transport Code (MCNP)

The MCNP code version 4a and version 4b, (Briesmeister, 1993) which were developed by Los Alamos National Laboratory (LANL) were used to design the beam port 3 features to produce an epithermal neutron beam relatively free of thermal and fast neutrons.

4.1.1 General Description of MCNP

The MCNP code can be applied to model the transport of neutron, photon, electron, or coupled neutron/photon/electron transport, model complex geometry and calculate eigenvalues for critical systems (Briesmeister, 1993). The advantage of MCNP for most applications is its ability to model complex geometries.

The continuous-energy nuclear and atomic data in MCNP is based on the Evaluated Nuclear Data File (ENDF), the Evaluated Nuclear Data Library (ENDL), the Activation Library (ACTL) and supplemental evaluations performed in the Applied Nuclear Science (T-2) Group. The cross sections are expressed as pointwise continuous energy cross sections (Briesmeister, 1993).

The tallies and output, such as particle current, particle flux, and energy deposition, can be obtained by simulating individual particles and recording some aspects of the average behavior of many particles. All possible reactions and interactions with materials are taken into account based on statistical processes.

4.1.2 Monte Carlo Method

Various probabilities are randomly sampled from the transport data to determine the outcome at each step of the particle's life. The individual probabilistic distributions of the particles can be specified by the source specification in the MCNP input file.

The particles start from the source specification and the number of particles crossing boundaries, number of collisions, and path lengths within volumes can be determined by the probability of reactions until the particles are lost by conversion, absorption, leakage or capture. Then another particle is sampled to start all the reactions and interactions with the material all over again.

The MCNP code is well designed and gives reasonable results. Therefore it was a good tool for the neutron beam design in this study. A combination of MCNP code version 4a, version 4b and nuclear data files based on ENDF and ENDL were utilized in this study. Only neutrons were considered in this study.

4.2 MCNP Model of the OSTR

The MCNP model using three dimensional Monte Carlo calculations was designed to simulate various areas of interest of the OSTR: the reactor core, graphite reflector, lead ring shielding, radial beam port (beam port 4), tangential beam port (beam port 3) and the other irradiation facilities, such as the pneumatic transfer system, rotating rack, thermal column and thermalizing column. After verifying the geometry model, MCNP version 4b was used to plot the two-dimensional slices of geometry that were specified in the input file.

The features of the OSTR were treated heterogenously. The origin for the MCNP calculations was chosen to be the geometric center of core. The z-axis was in the "up" (vertical) direction, the y-axis was horizontal along the thermal column axis and the x-axis was horizontal 90° clockwise from the y-axis (Figure 4.1).

A two-step MCNP calculation was performed. In the first step, the surface source write (SSW) file or KCODE fission volume source file was written to be used in subsequent MCNP calculations. In the second step, the surface source read (SSR) card was used to read the fission neutrons that were transported from the first step calculation. The subsequent MCNP calculation was used to determine the suitability of different materials as the filter configuration inside beam port 3 and beam port 4 to maximize the useful epithermal neutron flux with a minimal fast and thermal neutron flux. The detail of each step will be described in the following section.

The surface source write file or KCODE fission volume source file was written first. The geometry was divided into three main regions: the reactor core, irradiation facilities and concrete shield region, and a void region (Figure 4.1 and Figure 4.2).

1) The part of the reactor inside the water tank was modeled in two regions, inside and outside the reactor core. The region inside the reactor core contained the fuel elements, central thimble, control rods and graphite moderator. The outer region between the reactor core and reactor tank wall included the graphite reflector, lead shield, water shield and reactor tank.
2) The irradiation facilities and concrete shield region consisted of the rotating rack facility (Lazy Susan), pneumatic transfer system (rabbit system), thermal column,

thermalizing column, beam port facilities (beam port 3 and beam port 4 only) and concrete shield around the beam ports (Figure 4.2).

3) A void region outside the reactor tank and outside the irradiation facilities was used in the model since neutrons in regions far away from the beam ports would have low probabilities of entering the beam port or reactor tank. Figure 4.2 presents the void regions. Only the regions surrounding the core and some of the irradiation facilities were included in the calculation model.

4.2.1 Geometry of Reactor Core and Shielding

The reactor core was described in the input file as a large cylinder which consisted of six concentric rings of cylindrical fuel elements, cylindrical graphite dummy elements, and four cylindrical control rods around the center, which is called the central thimble.

The central thimble is located at the center of the core. The thimble in the model was defined as a 3.64 cm diameter hollow cylinder with 0.05 cm-thick cylindrical stainless steel cladding. The thimble was filled with an aluminum plug extending from the top of the grid plate to the lower grid plate to prevent flux peaking in the core center.

The fuel region inside the fuel rod cylinder was divided into three cylindrical segments: top, middle and bottom located between the upper grid plate and the lower grid plate. The middle segment of the fuel rod consisted of two concentric cylinders, a 0.64 cm diameter central zirconium rod surrounded by a 1.50 cm-thick homogeneous alloy of uranium fuel and zirconium hydride.

The fuel elements consist of a zirconium-hydride moderator, homogeneously combined with 8.5 wt.% uranium, 70% enriched in ^{235}U, and a burnable poison (~ 1.6

wt.% erbium). The ratio of hydrogen to zirconium atoms in the fuel is about 1.6 to 1. The top and bottom portions of the fuel rods contained 8.74 cm and 8.81 cm long graphite slugs, respectively. The fuel element and graphite slugs were surrounded by a 0.05 cm-thick cylindrical stainless steel cladding.

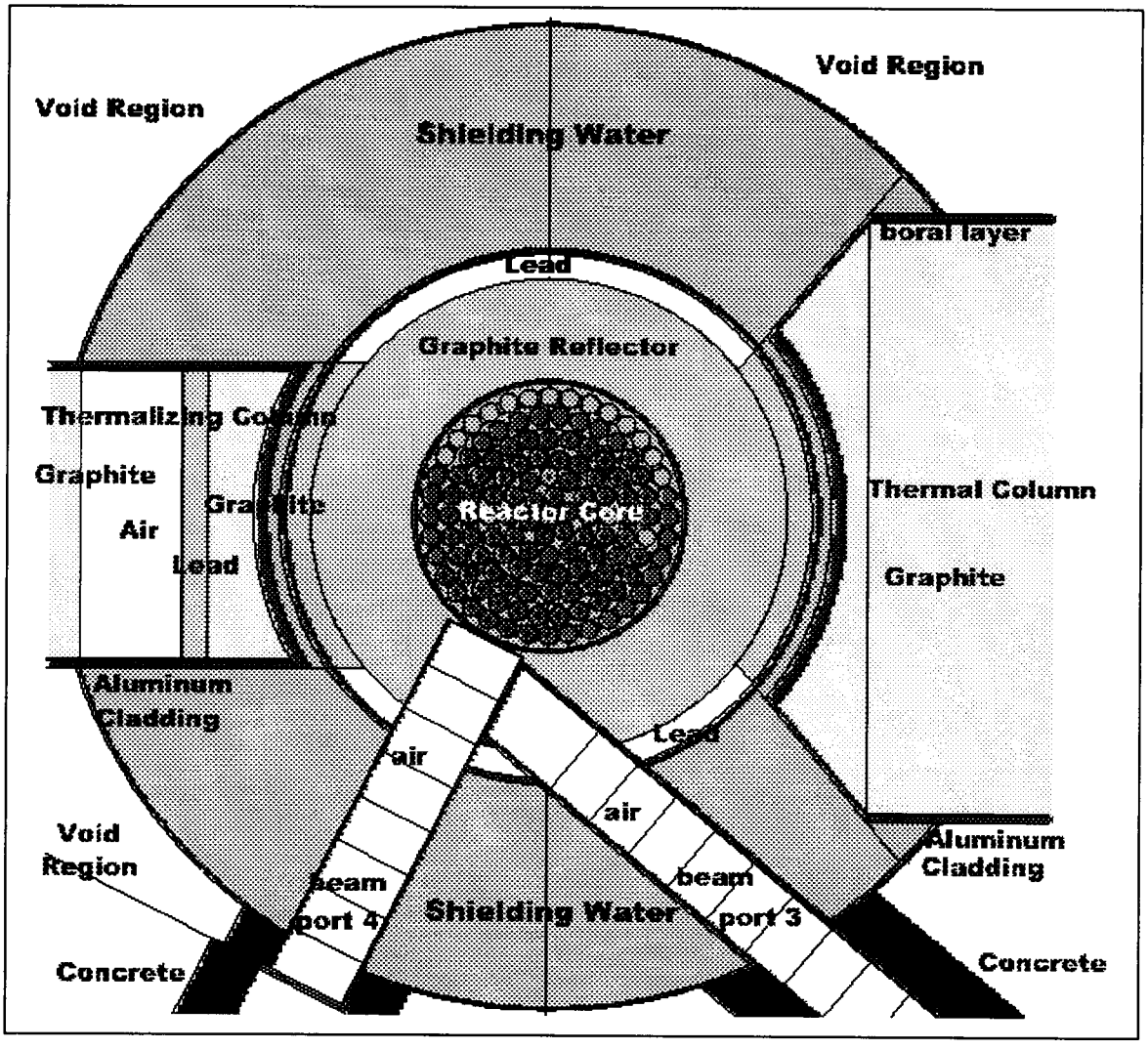

Figure 4.1. The horizontal section of the reactor core model by MCNP version 4b

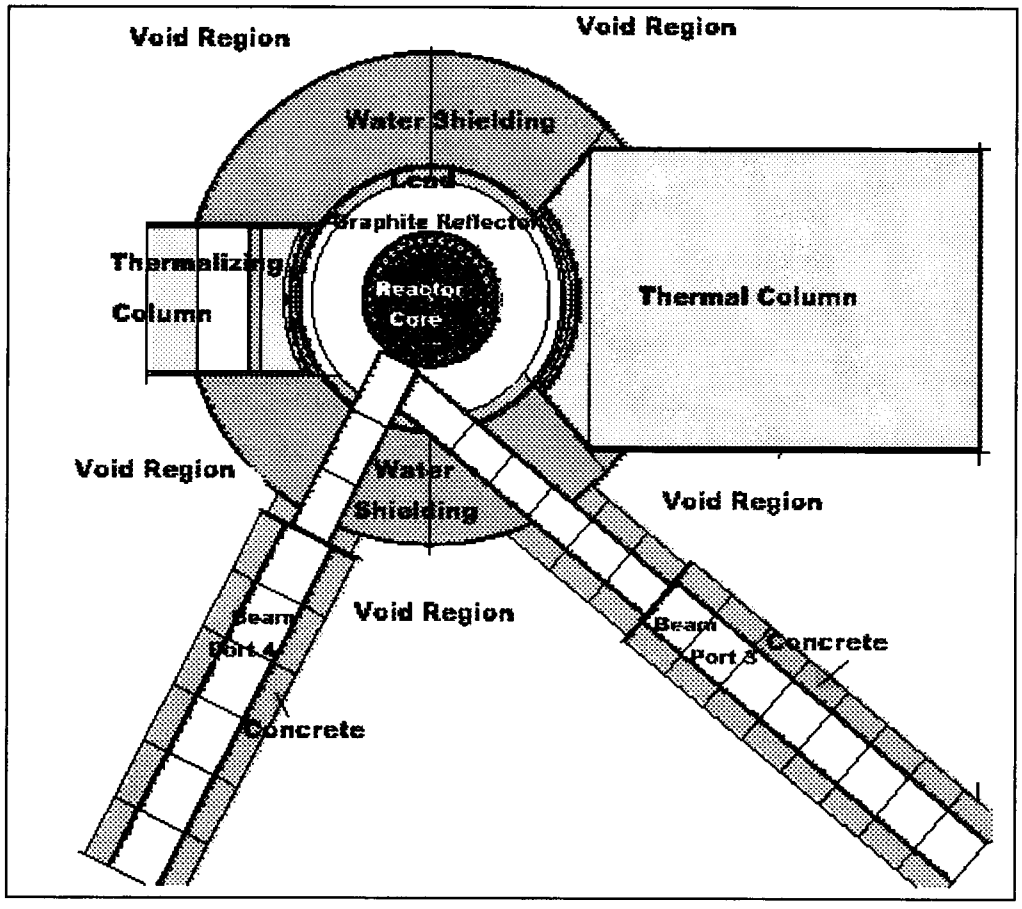

Figure 4.2. The horizontal section of the reactor core, irradiation facilities and a void region model by MCNP version 4b.

The TRIGA reactor is controlled and regulated by four control rods. Therefore, the calculation model of the reactor core also included four control rods. The control rod configuration is shown in Figure 4.3. Three control rods had the same geometry containing two cylindrical segments.

The upper section was 38.1 cm of borated graphite (graphite with 78 wt.% natural boron with a density of 2.48 g cm^{-3}). Below this was a region composed of two concentric cylinders, consisting of an inner zirconium rod surrounded by a 1.5 cm thickness of U-$ZrH_{1.6}$.

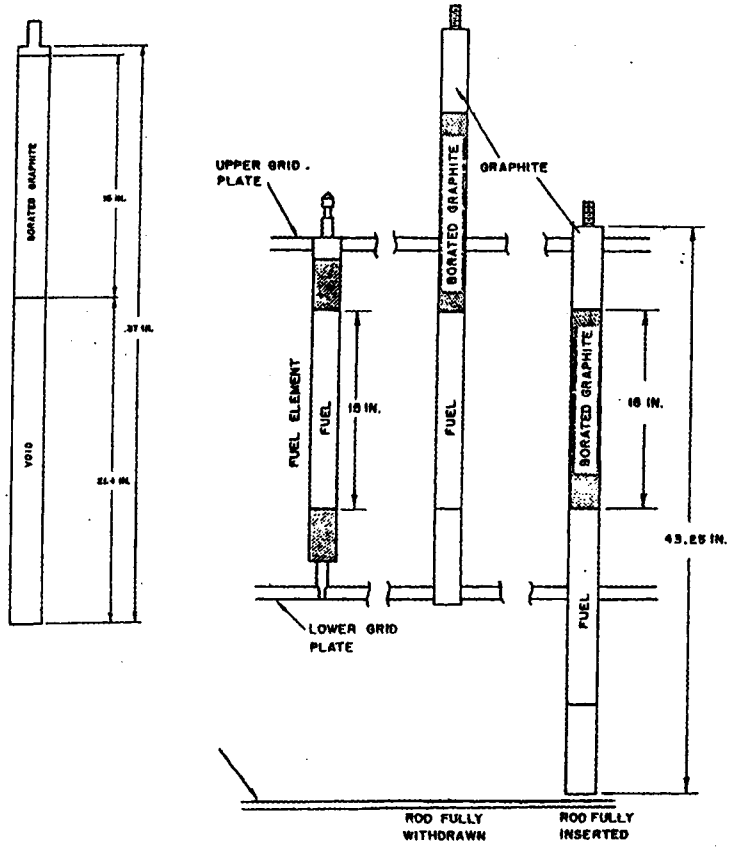

(a) (b)

Figure 4.3. The vertical section of control rods. (a) a standard control rod (b) a transient control rod

On the other hand, the transient rod had two cylindrical segments. The top part, 3.64 cm in diameter and 38.1 cm in height, was filled with borated graphite; the bottom part was filled with a 46.91 cm length of air. All the control rods were surrounded by a 0.05 cm-thick cylindrical stainless steel cladding.

Because the neutrons produced in the fission reaction are very energetic, to generate an adequate amount of neutrons for further fission, a moderator is utilized in the

reactor. The moderator can slow down or thermalize the fast neutrons to be intermediate energy or thermal neutrons. Moderation is mainly performed in the OSTR using water as the moderating material.

For cooling and moderation inside the reactor core, the design must have water occupying the space inside the reactor core around the concentric rings, about one-third of the core volume.

Also graphite dummy elements are placed at some of the positions in the outermost rings in the core. Each of the dummy elements was 55.65 cm in height and 3.64 cm in diameter, surrounded by a 0.05 cm-thick cylindrical stainless steel cladding. The vertical section of the reactor core model by MCNP version 4b is demonstrated in Figures 4.4 and 4.5.

One of the irradiation facilities which is inside the reactor core is the pneumatic transfer system or rabbit system. The rabbit system is used for producing short-lived radioisotopes. The rabbit is located in one of the positions in the outermost of the concentric rings inside the reactor core. The diameter of the rabbit in the model was 3.64 cm with the total length of 55.65 cm. The rabbit was filled with air and surrounded by 0.05 cm-thick aluminum cladding.

To reduce the number of neutrons escaping from the reactor core, a graphite reflector is used to surround the reactor core and reflect some neutrons back into the core. The ring-shaped block of graphite surrounding the reactor core was located radially in the model. The graphite reflector was clad by an aluminum tank.

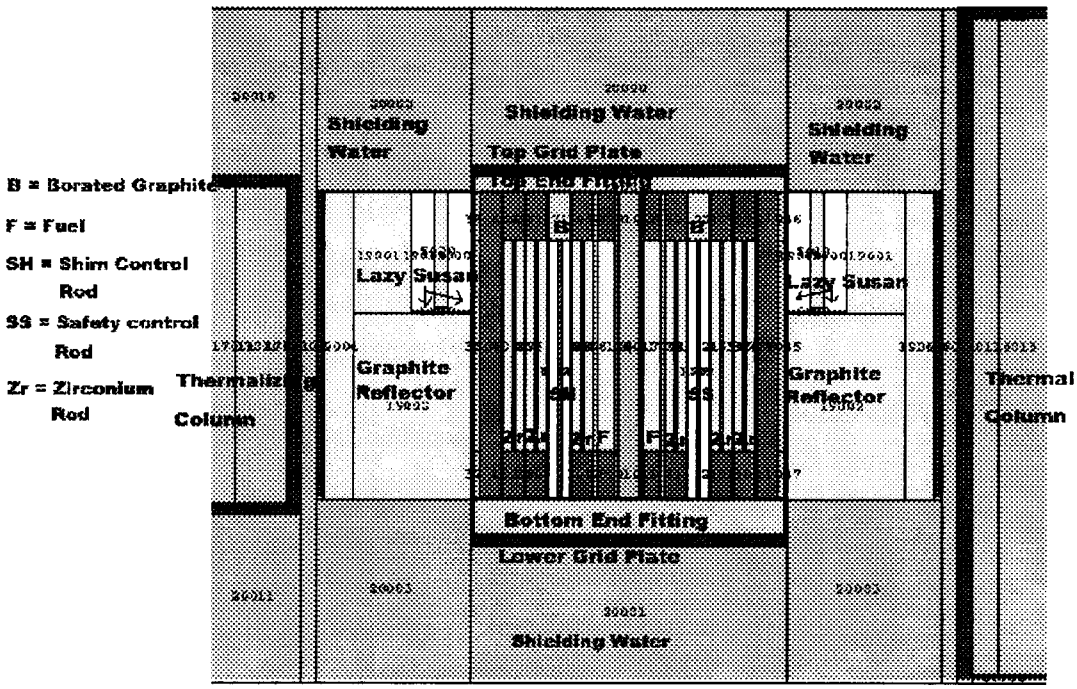

Figure 4.4 The vertical section of the reactor core model (px = 0) by MCNP version 4b

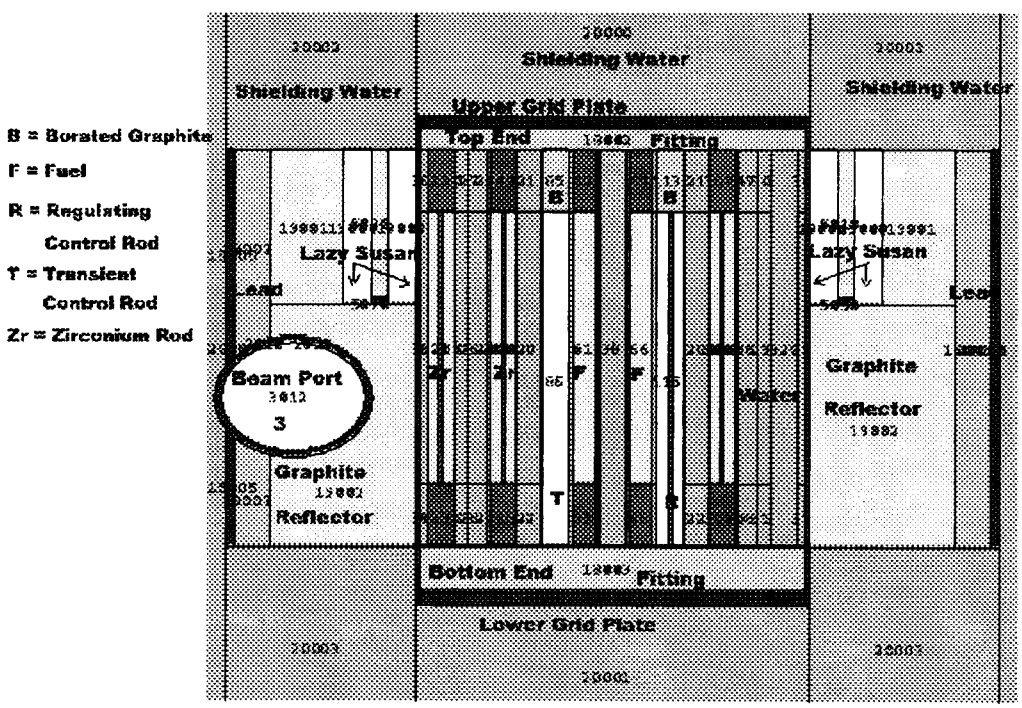

Figure 4.5 The vertical section of the reactor core model (py = 0) by MCNP version 4b

The graphite cylinder was divided into two parts, top and bottom, with a radial thickness of 20.32 cm. The top of the reflector was 21.76 cm in height, whereas the bottom part was 34.12 cm in height. Overall the reflector extends 27.79 cm above and 27.86 cm below the core midplane.

The top part of the reflector contained the Lazy Susan, which is a rotating rack facility used for producing isotopes and providing high radiation flux for research (Figures 4.6). The bottom part of the reflector has the holes for the thermal column, the thermalizing column and the beam ports.

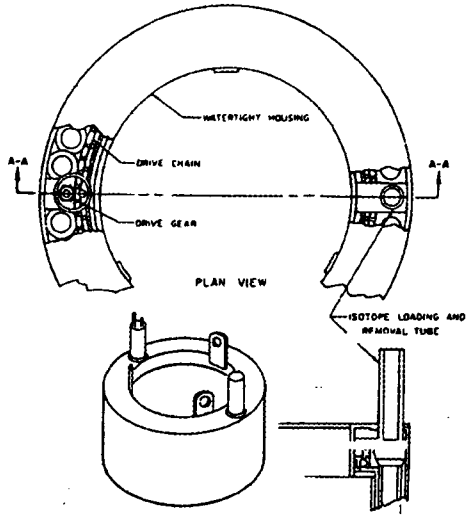

Figure 4.6 The vertical section of the reactor core and the Lazy Susan

The rotating rack facility, or Lazy Susan, is attached to the top part of the graphite reflector. Consequently, the top part of the graphite reflector includes 40 hollow cylinders with a closed lower end (Figure 4.7). Each cylinder has the same diameter, which is 2.29 cm, and the total length of the cylinder is 21.76 cm, filled with air. The rotating rack cylinder tube in this model contains two parts, 20.76 cm height at the top and 1 cm in

height at the bottom. The bottom region was used for cell flux tallies to compare with experimental measurements.

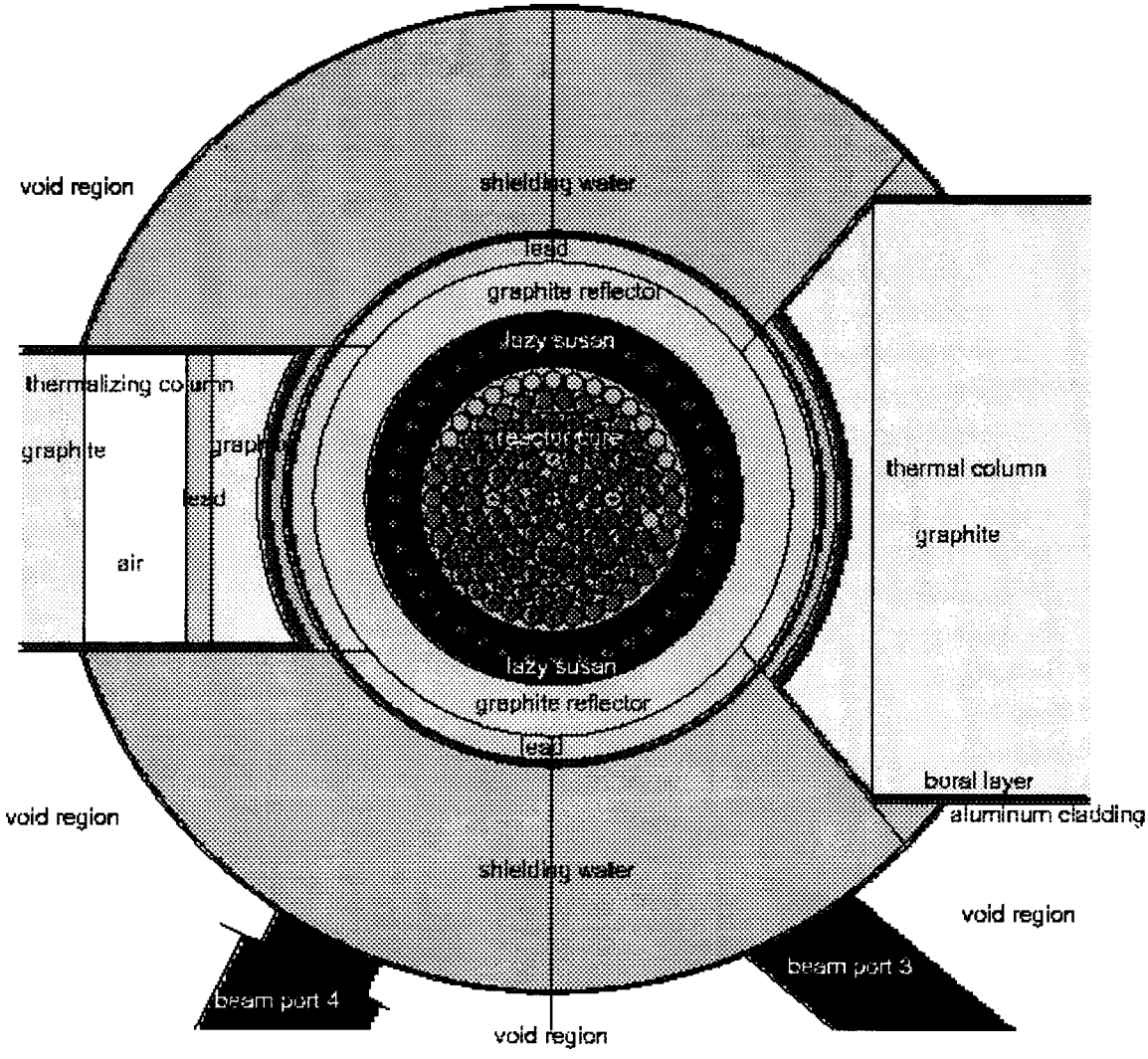

Figure 4.7 The horizontal section of the reactor core and the Lazy Susan model

Even though TRIGA reactors have good cooling systems, the concrete shield structure cannot tolerate high heat from nuclear fission. A lead shield is provided to solve this problem, serving as a thermal shield for the reactor.

A 5.08 cm-thick, 55.65 cm long lead region extending from the top to the bottom of the fuel rods was used in the model. Because the thermal column, thermalizing column,

and beam ports penetrate through the graphite reflector assembly, the lead shielding was separated into parts.

4.2.2 Geometry of Irradiation Facilities

The thermal column was simulated as a large vessel lined with a boron carbide (boral) layer, filled with graphite and encased by an aluminum container. The dimension of the thermal column is 121.92 × 121.92 cm in cross section with a length of 152.4 cm.

The thermal column was separated into an inner and outer part. The outer part was in the region outside the reactor tank. The geometry of the outer part was rectangular from the reactor tank wall out. Some of the surfaces of the inner part of the thermal column were planes that were not parallel to the coordinate axes. Consequently, the coefficients for the equation, $Ax + By + Cz - D = 0$, had to be determined in order to define these surfaces. Four planes for the inner part of the thermal column were calculated in this manner.

The boral-lined, aluminum clad thermalizing column structure was similar to the thermal column, except the dimensions are 60 cm × 60 cm × 150 cm long, and all planes are parallel to the coordinate axes. The thermalizing column is filled with a 20.32 cm-thick graphite block, a 5.08 cm-thick lead layer, a 20.32 cm-thick air space, and the rest of the thermalizing column is occupied by graphite blocks. The inner surface of the thermalizing column was matched to the contour of the graphite reflector, and the outer section was terminated at the bulk shielding tank.

Both tangential beam port (beam port 3) and radial beam port (beam port 4) geometries were described as hollow cylinders with an inner and outer section. For beam

port 3, the inner section consists of a 15.24 cm diameter region surrounded by a 0.80 cm-thick aluminum cladding, whereas the outer section consists of a 0.80 cm thick steel cladding and the diameter increases to 20.32 cm through the end of beam port 3. Beam port 4, which penetrates the graphite reflector, consists of a 16.04 cm diameter region surrounded by a 0.80 cm-thick aluminum cladding at the inner section, while the outer section consists of a 0.80 cm-thick steel cladding and the diameter steps up to 20.32 cm through the end of beam port 4.

Since both beam ports are not aligned with any of the coordinate axes, either the coefficients of the general equation for a cylinder must be determined or a surface transformation must be used. Rather than specifying the coefficients for the general equation for a cylinder which is not parallel to an x, y or z axis,

$Ax^2 + By^2 + Cz^2 + Dxy + Eyz + Fzx + Gx + Hy + Jz + K = 0$, the coordinate transformations of both the radial beam port (beam port 4) and tangential beam port (beam port 3) were included in the MCNP input file to simplify the geometry of both beam ports.

Two coordinate transformations were used in the model. Transformation 1 was used for beam port 4, and transformation 2 was used for beam port 3. The cosine of the angle was utilized to specify the relationship between the directions of the axes of the main coordinate system (x, y, z) and the auxiliary coordinate system (x′, y′, z′). In this input file, the displacement vector was the location of the origin of the auxiliary coordinate system, as defined in the main system.

Since the horizontal centerlines of beam ports 3 and 4 were 6.985 cm below the center line of the reactor core, the z value of the displacement vector was specified.

For the x and y values, a trigonometric calculation was done. Consequently, the displacement vector (cm) of beam port 4 was 0 0 -6.985, and the displacement vector of beam port 3 was -36.49 -9.37 -6.985.

The auxiliary coordinate system (beam port 3 and 4 alignment) was transformed to the main coordinate system (x, y and z axes). The angle between the x′ axis of beam port 4 (auxiliary coordinate axis) and the main x axis was 27°, whereas the angle between the x′ axis of beam port 3 (auxiliary coordinate axis) and the main x axis was 40°.

The x′y angle can be determined by the same method. The angle between the x′ axis of beam port 4 (auxiliary coordinate axis) and the main y axis was 117°, while the angle between the x′ axis of beam port 3 (auxiliary coordinate axis) and the main x axis was 130°. After using the same rotating method, the angle between the x′z angle of beam port 4 was 90°, the same as the x′z angle of beam port 3. Determination of y′x, z′x, y′y, z′y, y′z, and z′z were calculated similarly. The configuration in Figure 4.2 demonstrates the TRIGA reactor model after transformation.

The concrete shields around both beam ports (beam port 3 and beam port 4) were modeled by using the same transformation from each beam port. The concrete shield was divided into an inner and outer section. The inner sections were 10 cm-thick concrete regions surrounding the beam ports, terminating at the outside of the reactor tank. The lengths of the inner sections of the concrete were 6.83 cm for beam port 4 and 32.07 cm for beam port 3. The outer sections of beam port 3 and beam port 4 were surrounded by 10 cm-thick concrete, 163.51 cm and 155.58 cm in length, respectively.

4.2.3 Geometry of Void Region

After modeling the reactor core, reactor shielding, reactor tank, thermal column, thermalizing column, and beam port 3 and 4, the rest of the geometry was defined as a void region. Considering that the particles which were far away from the reactor core, the surrounding region, and the beam port 3 and beam port 4 regions had a small chance to enter or scatter into the beam port, a void region assumption was reasonable. Consequently, the region which is outside beam port 3 and beam port 4, outside the concrete shielding, above and below the thermal column and thermalizing column, and outside the reactor tank was modeled as a void region.

The purpose of the void region was to avoid wasting time on neutron histories which had very little probability of contributing to a tally in the beam ports, thereby improving statistical accuracy.

4.3 Material Compositions in MCNP Input File

Material cards were utilized in the input file to identify the components of the elements which were used in the reactor, surrounding material, and irradiation facilities. Furthermore, the material cards were used to specify the neutron cross section from a nuclear data file which was based on ENDF-V and ENDL.

Binding energy is involved in the formation of a nucleus from its component nucleons, and it can be stored as vibrational and rotational energy. The $S(\alpha,\beta)$ thermal scattering treatment is used to account for the binding effect of the nuclei which will affect the thermal neutron interaction with molecules or crystalline solids in a material. For this

input file, S(α,β) thermal neutron treatment was used for graphite and U-ZrH inside the reactor core when the neutron energy is lower than 4 eV.

The graphite dummy element and the axial graphite reflectors for the fuel consist of carbon with an S(α,β) treatment. The control rod contains boron carbide. The density of the graphite inside the reactor core was 1.61 g cm^{-3}.

Although the ring-shaped graphite reflector around the reactor core consists of carbon with an S(α,β) treatment, this graphite has a different density, 1.70 g cm^{-3}. The lead shield contains pure lead with a density of 11.4 g cm^{-3}. The aluminum clad for the reflector shield and lead shield is pure aluminum with a density of 2.7 g cm^{-3}.

The thermal column and thermalizing column had similar component for boral lining, graphite blocks and aluminum cladding. Both columns used graphite with the same density, 1.61 g cm^{-3}, and an S(α,β) treatment for graphite and boron carbide (B_4C). Unlike the thermal column, which was filled with graphite blocks, the thermalizing column was filled with graphite blocks, pure lead with a density of 11.4 g cm^{-3}, and air. Air used in this model was a combination of 79% nitrogen and 21% oxygen with a density of 1.029×10^{-3} g cm^{-3}.

Concrete shielding surrounded beam port 3 and beam port 4, with a density of 2.3 g cm^{-3}, and consisted of hydrogen, oxygen, sodium, magnesium, aluminum, silicon, potassium, calcium, iron and carbon. The material compositions by atomic fraction in the MCNP input file are given in Table 2. The composition of the nuclides of each component is not normalized to one. However, MCNP normalizes the unnormalized nuclide fraction entries so that the sum is one.

Table 2. Material compositions of the 1 MW OSTR (atom fractions)

Element	Fuel element	Graphite dummy	Control rod	Water	Graphite reflector	Thermal column	Thermalizing column	Concrete
Hydrogen	0.056		0.04666	0.667		0.04666	0.04666	0.01374
Carbon		0.08019	0.20		0.08521	0.08521	0.08521	
Oxygen				0.333		0.3333	0.5433	0.04606
Nitrogen							0.21	
^{10}B			0.15824			0.15824	0.15824	
^{11}B			0.64176			0.64176	0.64176	
Zirconium	0.03509		0.02916					
^{235}U	0.00089		0.00075					
^{238}U	0.00038		0.00032					
Sodium								0.00175
Aluminum						0.06031	0.06031	0.00175
Silicon								0.01662
Calcium								0.00152
Potassium								0.00069
Iron								0.00035
Lead							0.03295	
^{166}Er	0.00026		0.00027					
^{167}Er	0.00007		0.00008					

4.4 Surface Source File or KCODE Fission Volume Source File

The surface source file or KCODE fission volume source file was first used to verify the nuclear criticality or multiplication factor (k_{eff}). Besides the k_{eff} result from the surface source file, the surface source information was provided for subsequent MCNP calculations.

4.4.1 Criticality Calculation

In reactor theory, k_{eff} is defined as the ratio between the number of neutrons in successive generations, with the fission process regarded as the birth event that separates generations of neutrons (Briesmeister, 1993). The k_{eff} calculation involves the estimation of the average number of fission neutrons produced in one fission generation per fission neutron born. A fission generation is the life of fission neutrons from birth to death by

escape, parasitic capture or absorption leading to fission (Briesmeister, 1993). The k_{eff} value must be slightly above or equal to one to sustain a chain reaction.

The k_{eff} value will indicate whether the reactor core is properly simulated or not in MCNP. The initial guess of k_{eff} in this study was 1.0, which will effect the creation of fission source points for the second k_{eff} cycle. In addition to the initial guess of k_{eff}, the criticality calculation required the initial spatial distribution of fission neutrons from the reactor core, so a KSRC card was used in MCNP to locate the starting source points for the KCODE criticality calculation. To reduce the bias of the calculation, 5.0×10^4 neutrons per k_{eff} cycle with 100 active cycles were used in this KCODE fission volume source file.

4.4.2 Normalization Factor for a 1 MW Power Reactor

In the surface source write file or the KCODE fission volume source file, the tally of the fission energy deposition averaged over a cell (*F7 tally) was used to calculate a normalization factor or multiplicative constant. The unit of the *F7 tally is jerks/g, which can be changed to joule/g by using a conversion factor.

The normalization factor for a 1 MW power reactor can be calculated from the following equation:

$$Nf = \frac{Power\ of\ reactor}{amount\ of\ active\ portion\ in\ fuel\ element\ \times *F7{:}n\ \times number\ fuel\ rods \times 1.0 \times 10^9}$$

The power of the OSTR = 1.0×10^6 W.

The number of fuel elements in the reactor core in this model = 87 fuel elements.

The conversion factor to convert jerks to joules = 1.0×10^9 J/jerk.

The mass of the active portion of the fuel element = 2257.57 g /fuel element.

The amount of the active portion of the fuel element is derived from the following equation:

$$M_{fuel} = \frac{N_i \times A_i \times Vol_{fuel}}{N_a \times \%^{235}U\ enriched \times wt.\%}$$

M_{fuel} = the amount of the active portion of the fuel element (g /fuel element)

N_i = atom density of ^{235}U (atoms/cm^{-3}) = 8.928×10^{20}

% ^{235}U enriched = 70% enriched in ^{235}U

N_a = Avogadro's number = 0.6022×10^{24}

A_i = atomic weight of ^{235}U (g/mole) = 235.0439

Vol_{fuel} = volume of fuel element (cm^3) = 385.48

wt. % = the weight percent of the U in the fuel = 8.5%

After calculation, the normalization factor was determined to be 8.2056×10^{16}, which was a source strength in number of particles produced per second. Consequently, this value was used as a multiplicative constant for the input file to convert the relative results to absolute values of neutron flux and neutron dose.

The tally multiplier card (FMn) was specified for all tallies in the surface source file or KCODE fission volume source file to normalize the results to 1 MW reactor power by using the multiplicative constant.

4.5 Neutron Beam Calculation

In the second step, thermal neutron, epithermal neutron and fast neutron fluxes in the radial (beam port 4) and tangential beam port (beam port 3) were calculated using

point detectors, and cell and surface tallies. Variance reduction techniques were applied in the neutron beam calculation to reduce the relative error.

4.5.1 MCNP Tally

Three different energy bins were used to classify the boundary of neutron energies. The thermal neutron energy range was below 0.5 eV, the epithermal neutron range was from 0.5 eV to 100 keV and the fast neutron energy range was from 0.1 MeV to 10 MeV.

The point detector was located inside a spherical cell just outside beam port 3. The cells inside both beam port 3 and 4 were used to determine the average flux over the cell, and the surface tallies were calculated at the inner surface of some cells of interest. However, the result of the beam port 3 was accounted for only by the neutron fluxes inside the spherical cell at the exit of beam port 3.

4.5.2 Variance Reduction Techniques

Various techniques can be applied to improve the statistical accuracy, such as truncation methods, population control methods, modified sampling methods, and partially deterministic methods. Population control and partially deterministic methods were used in this model in beam port 3 and beam port 4 in order to reduce the fractional standard deviation of the tallies.

Geometry splitting with Russian roulette, which is one of the population control methods, was applied in the second input file (surface source read file). In order to keep the neutron track entering an adjacent cell along the beam port centerline roughly constant, cell importances were adjusted in the calculation.

When particles being tracked reach a region of higher importance (ratio of importances = I), they cross importance boundaries and are split into I particles, which are tracked separately. On the other hand, if particles cross a boundary into a lower importance region, a fraction 1 - 1/I of the particles will be killed, and a fraction 1/I of the particles will be allowed to continue.

The recommendation for geometry splitting or importance is that the thickness of the cells which will apply the importance splitting/ roulette should less than two mean free paths (Briesmeister, 1993). Therefore, 9 cm thick cells along beam port 3 were utilized in the second run of MCNP. A reliable result can be obtained when the ratio of adjacent importances is small (less than 4.0). The ratios of adjacent importance ranges in this input file varied from 0.56 to 4.0. The variance of the tallies was decreased due to sampling a larger number of particle tracks.

The potential BNCT treatment for brain tumors can be performed by using neutrons in the epithermal energy range. Therefore energy splitting with Russian roulette was used for this study. Neutrons in the intermediate energy range of 1 eV to 0.1 MeV were split into two particles whereas thermal neutrons or neutrons with energy below 0.5 eV will play Russian roulette. By this method, reasonable results can be obtained from the tallies with a low variance.

Another method to improve the variance of tallies is partially-deterministic methods. Both point detectors and DXTRAN spheres were used in this study. Since beam port 3 is very long and the neutron flux from the surface source file or KCODE fission volume source file was small so that the probability of neutron tracks to approach the exit of beam port 3 is small, the point detector was used to account for all neutrons

from every source and every collision event throughout the random walk that contributed to the point detector. Although a point detector can reduce the variance of the tallies, the time per neutron history is increased.

As long as the neutrons had a small chance of scattering toward the region of interest, which was the end of beam port 3, DXTRAN spheres can be applied to improve this situation. A contribution of the particles toward DXTRAN spheres is created from DXTRAN particles and non-DXTRAN particles or collision particles.

A combination of splitting, Russian roulette, and sampling from nonanalog probability density functions are used in DXTRAN spheres (Briesmeister, 1993). Tracking pseudoparticles inside the DXTRAN spheres and using the Russian roulette method will reduce the problem of high variance tallies.

Although DXTRAN spheres can help to decrease the variance of tallies, the time for DXTRAN sphere calculations is more than without DXTRAN spheres. The DXTRAN contribution card (DXC) card can help to solve this problem. The probability of contributing to the DXTRAN spheres was specified for each cell.

An entry of 0.001 to 0.1 (a few pseudoparticles produced) was used for cells which were far away from the point of interest, such as cells inside the steel pipe in beam port 4 and concrete shielding cells around beam port 4, because the particles had a small probability to enter, scatter or effect the point of interest. This decreases the time spent for tracking low weight pseudoparticles.

Besides the DXC card, the detector diagnostics card (DD) card was used to reduce the weight fluctuation on the DXTRAN sphere. The DD card will increase the efficiency of point detectors and DXTRAN spheres. When a positive criterion (0.5) is

utilized for Russian roulette in the DD card, the average contributing particles per history is used instead of all contributing particles to the detector. The variance reduction can be improved by using Russian roulette.

4.6 Plot Geometry Plotter and MCPLOT Tally Plotter

After a geometry was specified in the input file, geometry plots or MCPLOT were used to plot two-dimensional slices of geometry. Figures 4.1, 4.2, 4.4, 4.5 and 4.7 present the geometry plots from MCNP version 4b.

4.6.1 Plot Geometry

To run the geometry plot, the plot input and execute line option were required so that the following command must be entered: mcnp4b ip inp=file name options, where ip means initiate and plot. Drawing the plot requires the value of parameters in the plot command. For example, the orientation of the plot was defined by using basis 0 1 0 1 0 0 indicating the y-axis was pointing to the right and the x-axis was pointing up; origin 0 0 0 was the default for the middle position of the plot.

Furthermore, the cross section of geometry in a plane perpendicular to the x, y or z axis can be plotted by using PX, PY or PZ, respectively. In this input file pz -6.985 was used because this plot showed a cross section of the beam port 3 and beam port 4 geometry in a plane perpendicular to the z-axis at a distance 6.985 cm below the origin. Parameters which were entered in plot commands still effect subsequent plots unless new parameters with the same plot command or conflicting commands are written.

4.6.2 MCPLOT Tally Plotter

On the other hand, the MCPLOT tally plotter was used for viewing tally results after MCNP calculations were terminated. The MCPLOT tally was utilized in a similar method to the geometry plot, except for entering a "z" on the MCNP execute line. Therefore the following commands must be entered while running the MCPLOT tally plotters: mcnp4b z options and mcnp4b inp=file name ixrz options.

4.7 Moderator and Filter Selection for Epithermal Neutron Beam Design

The neutrons generated in the fission reaction in the reactor core have high energies and are not suitable for brain tumor treatment. The initial neutron energy from the reactor core must be slowed down or moderated before interacting with ^{10}B nuclei in the tumor cell. Fast neutrons and gamma ray components which contaminate the neutron beam should be eliminated to reduce the risk of healthy tissue damage during brain tumor treatment. Moderators, filters or attenuators were considered for the desired epithermal neutron flux intensity and the beam contaminants.

4.7.1 Characteristics of Suitable Materials for BNCT

The following conditions seem to be suitable for BNCT: (1) sufficient intensity of epithermal neutrons and (2) minimized intensities of thermal neutrons, fast neutrons and gamma rays. Therefore, types of filter materials, thicknesses, and the location in beam port 3 and beam port 4 were examined to obtain this requirement. Filter materials and thicknesses in both beam ports based on many criteria were considered for delivering enough epithermal neutrons to the tumor site and achieving an adequate number of capture events.

4.7.2 Epithermal Beam Optimization

To obtain the optimized epithermal neutron beam, the moderators, filters or attenuators should have (1) high scattering cross sections and low absorption cross sections to decrease neutron loss, (2) low (n, γ) cross sections to minimize neutron loss and gamma production, (3) a low mass number to increase the average energy loss per interaction, (4) light nuclei to maintain the angular directivity of neutrons, (5) larger interaction cross sections for fast neutrons than lower energy neutrons to limit fast neutron contamination of the therapeutic beam (Yanch et al., 1993b), and (6) a forward directed flux or high neutron current to flux ratio to increase the efficiency of producing thermal neutrons in tumor cells and decreasing the divergence of the neutron beam (Wheeler et al., 1989).

The difference between moderators and filters is defined in two ways. The first method is defined by the location (Clement et al., 1990). A moderator is very close or adjacent to the patient, whereas a filter is near the reactor core and far away from the patient.

The second method was described by the process to obtain epithermal neutrons (Brugger et al., 1990). Although filters stop fast neutrons, thermal neutrons and gamma rays, the epithermal neutrons are allowed to pass through the filters. On the other hand, moderators slow down neutrons in the fast energy range to the epithermal energy range faster than neutrons in the epithermal energy range are slowed down to the thermal energy range. Therefore, moderators produce a flux of epithermal neutrons as the source for an epithermal beam. In this study, the second method was used to describe moderators and filters.

4.8 Epithermal Neutron Beam Design at OSTR

As a first step, various materials can be used as a moderator inserted into the inner end of beam port 4 to increase the number of particles entering beam port 3. Examples of materials considered were light water (H_2O), heavy water (D_2O), aluminum (Al), sulfur (S), aluminum oxide (Al_2O_3), aluminum fluoride (AlF_3), silicon crystal (Si), and aluminum sulfate ($Al_2(SO_4)_3$). In a next step, the same materials which were used for moderator evaluation in beam port 4 were utilized as filters in beam port 3.

The MCNP run was performed by maintaining a constant beam port size while varying the filter materials and filter lengths to identify the suitable filter configuration inside beam port 3 for high epithermal neutron fluxes and low fast neutron and thermal neutron fluxes.

Collimation was required for beam port 3 since the dose rate in tumor or patient, thermal neutron penetration at the tumor site, and degree of dose uniformity throughout the tumor volume were based on the neutron collimation effect (Harling et al., 1992a and Yanch et al., 1993b). The collimator size depends on the size of tumors (Yanch et al., 1993c). Good therapeutic neutron beams should have a low fast neutron and thermal neutron component, so sulfur and lithium carbonate (Li_2CO_3) were used at the middle and the end of beam port 3 in order to remove the fast neutron and thermal neutrons from the beam, respectively.

5. RESULTS

5.1 Criticality

The ideal value of the effective multiplication factor (k_{eff}) for a critical system is one so that the number of neutrons in any two consecutive fission generations will be the same or the number of neutrons in the reactor will always remain the same (Duderstadt and Hamilton, 1976). The k_{eff} or criticality value was determined to verify that the reactor core was properly simulated. The objective of this study was to achieve $k_{eff} = 1$ which will indicate that the reactor established a stable or steady state chain reaction and the reactor core was modeled properly.

However, the result of the MCNP k_{eff} criticality calculation for the OSTR reactor core with 87 fuel elements consisting of 70 % enriched ^{235}U combining with ZrH and including reflector materials was 1.03150 with a standard deviation of 0.00172. Hence the 95% confidence interval for k_{eff} was from 1.02809 to 1.03492. The calculation accounted for the current position of three standard control rods and one transient control rod in the OSTR at full power (1 MW), and the ambient temperature ($kT = 2.53\times10^{-8}$ MeV) was assumed in this model.

The criticality calculation results showed that the number of neutrons in one generation was greater than the number of neutrons in the previous generation, or it was an unbalanced condition between the neutron production rate and neutron loss rate (absorption and leakage). Hence the chain reaction grew and increased in neutron population, which is called supercriticality.

During normal operation, the multiplication factor is maintained at one. This is achieved by partially inserting the control rods in the core. As the fuel is burned, the control rods are partially withdrawn, maintaining the reactor critical.

In order to determine the criticality condition, this study can be performed by inserting the control rods into the reactor core. It was assumed that all four control rods were driven by the same motor. MCNP calculation was showed that the k_{eff} decreased as a function of control rod insertion. The control rods were inserted in steps ranging from fully withdrawn to fully inserted. Table 3 indicates that the k_{eff} values are changed depending on the withdrawal depth of the control rods. Figure 5.1 shows the typical S-shaped control rod worth curve. Moreover, the results show that for a clean core, all the control rods must be approximately 40% withdrawn from the core to obtain k_{eff} of one.

This model was utilized to calculate the k_{eff} value for the current position of control rods in the OSTR at full power (1 MW) and low power (15 W). The results are 1.03150 ± 0.00172 at full power and 1.01085 ± 0.00362 at low power. Hence, the 95% confidence interval for k_{eff} at full power was from 1.02809 to 1.03492, and the 95% confidence interval for k_{eff} at low power was from 1.00364 to 1.01806.

Table 3. Calculated values of k_{eff} for the reactor core model with different withdrawal depths of control rods

% control rod withdrawn	k_{eff} (multiplication factor)	standard deviation	95% confidence interval
0.0	0.96686	0.00344	0.96000 to 0.97372
16.7	0.97057	0.00433	0.96195 to 0.97920
33.3	0.99516	0.00381	0.98757 to 1.00276
66.7	1.03010	0.00357	1.02300 to 1.03721
83.3	1.04922	0.00360	1.04204 to 1.05639
100.0	1.05536	0.00347	1.04845 to 1.06228

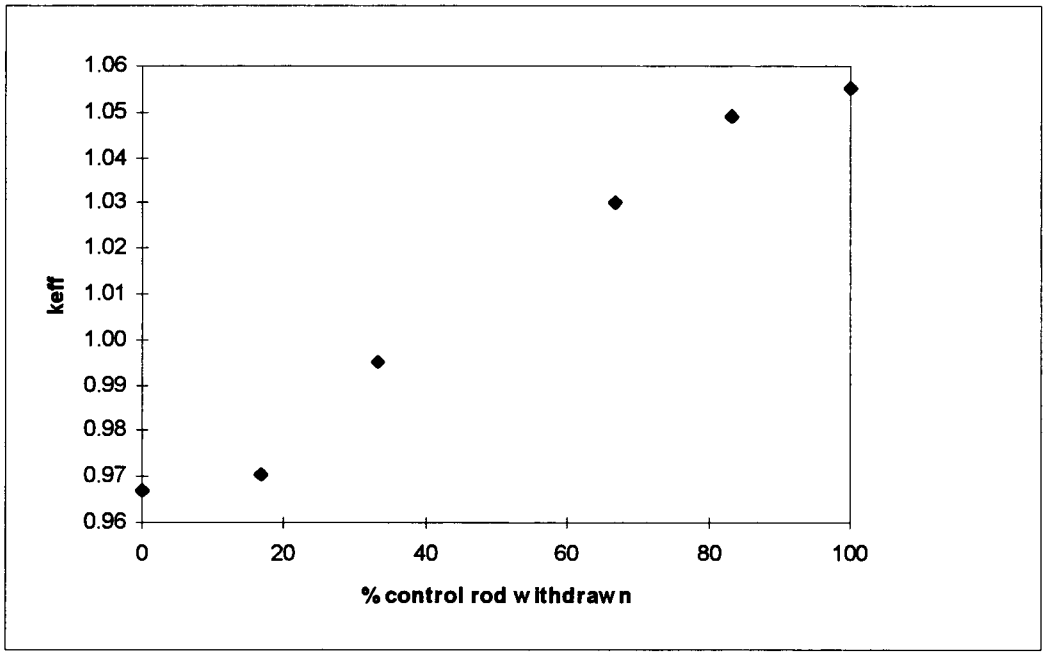

Figure 5.1 Calculated k_{eff} values with % control rod withdrawn in the reactor core model

5.2 SSW Region in Surface Source Write File

A specific region of the aluminum tank between the reactor core and the ring-shaped graphite reflector in front of beam port 4 was defined as a region of the neutron track record for subsequent MCNP calculations. A neutron track that crossed this region in the correct direction was written to the surface source write file and transported from there in a surface source read file.

From this model, 4,750,578 neutrons were used in the surface source write file and 114,598 neutrons which crossed a specified region were recorded and written to the WSSA surface source file. Subsequently, a set of 114,598 neutrons were utilized as the neutron source for the subsequent MCNP calculations.

The thermal, epithermal and fast neutron fluxes in this region in the surface source write source were 8.82×10^{12}, 3.96×10^{11} and 2.64×10^{12} n cm^{-2} s^{-1}, respectively.

The relative error for these results was in the 0.6% to 1.0% range, which is an acceptable range for MCNP.

5.3 Moderator Material Selection in Beam Port 4

The moderator parameters investigated in beam port 4 included moderator material and moderator length. Several materials were evaluated as moderators, such as aluminum, sulfur, aluminum oxide, aluminum sulfate, water, heavy water, and calcium fluoride.

The objective of this design was to produce a high intensity of epithermal neutrons with a low fast neutron and thermal neutron component at the end of beam port 3. Fast neutrons colliding with light nuclei, such as hydrogen, will lose some of their kinetic energy in elastic scattering collisions. Consequently fast neutrons can be slowed down or moderated. Hydrogen is an excellent neutron moderator since neutrons and protons have almost the same mass, so neutrons have a capability to transfer almost all the energy to protons via elastic collision. Epithermal neutrons are produced from moderated fast neutrons via scattering collisions. However, too much hydrogen may cause neutrons to scatter into and clear out of the epithermal region.

The MCNP calculations showed that the combination of 35% aluminum and 65% aluminum fluoride, and the combination of 60% aluminum and 40% aluminum oxide seemed to be outstanding optimum mixtures compared to the other combinations, so that they were also used as candidates for evaluation.

Neutron fluxes at the exit of beam port 3 with a variety of moderator materials in beam port 4 are presented in Table 4. The relative errors were less than 10% in each case, corresponding to acceptable MCNP calculation requirements.

For these calculations beam port 3 was air filled. The moderator inside the front part of beam port 4 significantly effects the neutron fluxes at the end of beam port 3. This effect is illustrated in figure 5.2.

Table 4. Calculated neutron fluxes for beam port 3 as a function of moderator material in beam port 4

material in beam port 4	thermal neutron flux with relative error E < 0.5 eV ($n\ cm^{-2}\ s^{-1}$)	epithermal neutron flux with relative error 0.5 eV < E < 0.1 MeV ($n\ cm^{-2}\ s^{-1}$)	fast neutron flux with relative error 0.1 MeV < E < 10 MeV ($n\ cm^{-2}\ s^{-1}$)
air	$1.31\times10^{8} \pm 5.4\%$	$1.69\times10^{8} \pm 3.9\%$	$1.63\times10^{8} \pm 5.3\%$
silicon	$1.21\times10^{8} \pm 5.6\%$	$1.98\times10^{8} \pm 8.3\%$	$1.83\times10^{8} \pm 9.8\%$
35% Al + 65% AlF_3	$1.10\times10^{8} \pm 7.2\%$	$1.89\times10^{8} \pm 5.8\%$	$1.29\times10^{8} \pm 9.6\%$
aluminum	$1.09\times10^{8} \pm 6.5\%$	$1.85\times10^{8} \pm 5.8\%$	$1.80\times10^{8} \pm 9.2\%$
heavy water	$1.80\times10^{8} \pm 3.9\%$	$1.83\times10^{8} \pm 3.3\%$	$8.54\times10^{7} \pm 4.5\%$
calcium fluoride	$1.18\times10^{8} \pm 4.7\%$	$1.75\times10^{8} \pm 5.4\%$	$1.32\times10^{8} \pm 9.5\%$
sulfur	$9.58\times10^{7} \pm 7.8\%$	$1.74\times10^{8} \pm 6.3\%$	$1.75\times10^{8} \pm 6.5\%$
aluminum sulfate	$1.16\times10^{8} \pm 5.3\%$	$1.69\times10^{8} \pm 5.5\%$	$1.57\times10^{8} \pm 9.5\%$
aluminum oxide	$1.17\times10^{8} \pm 5.4\%$	$1.59\times10^{8} \pm 4.5\%$	$1.27\times10^{8} \pm 5.7\%$
60% Al + 40% Al_2O_3	$1.48\times10^{8} \pm 5.9\%$	$1.16\times10^{8} \pm 4.8\%$	$1.41\times10^{8} \pm 9.5\%$
water	$1.07\times10^{8} \pm 7.5\%$	$5.50\times10^{7} \pm 8.7\%$	$6.54\times10^{7} \pm 9.8\%$

The mixture of 35% aluminum and 65% aluminum fluoride, aluminum oxide, calcium fluoride and heavy water were suitable for decreasing fast neutrons with less attenuation of epithermal neutrons than the others. The combinations of moderator material containing some aluminum gave higher epithermal neutron fluxes due to the fact that aluminum has a higher neutron capture cross section for fast neutrons than for epithermal neutrons.

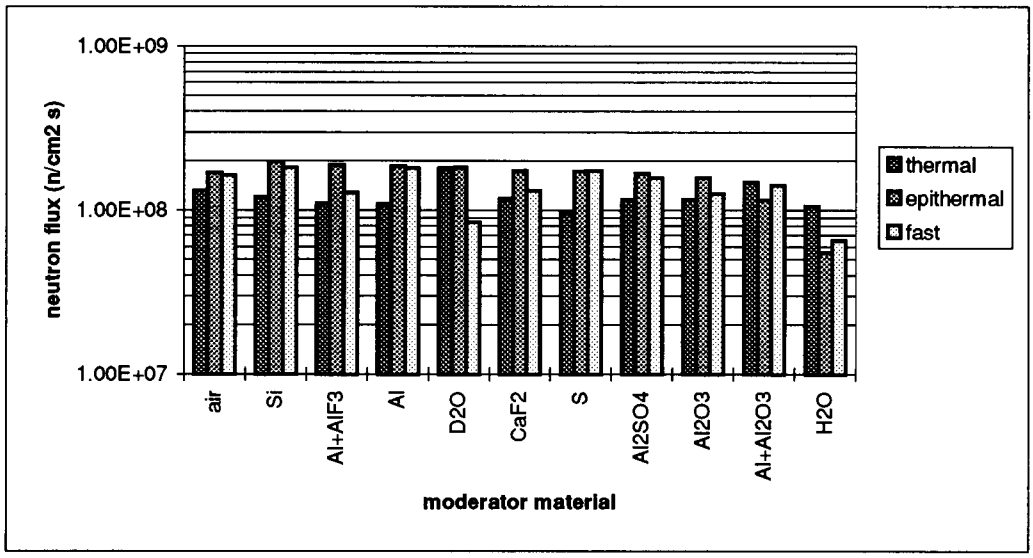

Figure 5.2 Calculated neutron flux at the end of beam port 3 (air filled) with several moderator materials in beam port 4.

Besides aluminum, adding oxygen and fluorine to the moderator improved the efficiency of the moderator. Oxygen and fluorine have low thresholds for the inelastic scattering reaction and have windows in their total cross sections which correspond to the epithermal energy range, so epithermal neutrons are preferentially transmitted through both oxygen and fluorine while fast neutrons are moderated.

In addition to water, heavy water was also utilized as a moderator. The neutron scattering and absorption cross sections of heavy water are different from light water. The macroscopic absorption cross section for heavy water is 757 times smaller than light water; correspondingly the thermal diffusion length of heavy water is 62.5 times greater than water (Wallace et al., 1995). Thus, good moderation properties and less neutron capture can be obtained by using heavy water instead of light water as a moderator.

Even though four materials (a mixture of 35% aluminum and 65% aluminum fluoride, aluminum oxide, calcium fluoride and heavy water) provided a suitable neutron

beam at the exit of beam port 3, heavy water was the best material to use as a moderator due to its superior fast neutron suppression. Hence heavy water was chosen as the moderator for the front part of beam port 4 to slow down fast neutrons from the reactor core. However it can generate fast neutrons by the $^{2}H(\gamma,n)^{1}H$ reaction.

The ratio of epithermal neutron to fast neutron flux increased as the thickness of the heavy water moderator in beam port 4 increased. However, upon reaching a certain thickness, the ratio of epithermal neutron to fast neutron flux reached an equilibrium value.

Table 5 represents the ratio of epithermal neutron to fast neutron flux at the end of beam port 3 for several thicknesses of heavy water inside beam port 4. The neutron flux ratio is plotted as a function of heavy water thickness in Figure 5.3. The optimum thickness of heavy water was 39.4 cm, so this thickness was used in the front part of beam port 4 for further calculations in the simulated model.

Table 5. The ratio between calculated epithermal neutron and fast neutron flux at the end of beam port 3 for different thicknesses of heavy water in beam port 4.

Heavy water thickness (cm)	ratio of Φ_{epi} / Φ_{fast}
9.85	2.55 ± 0.30
19.69	2.87 ± 0.33
29.54	2.88 ± 0.36
39.38	2.95 ± 0.38
49.23	2.92 ± 0.41
59.08	2.93 ± 0.43
68.92	2.93 ± 0.36
78.26	2.92 ± 0.38

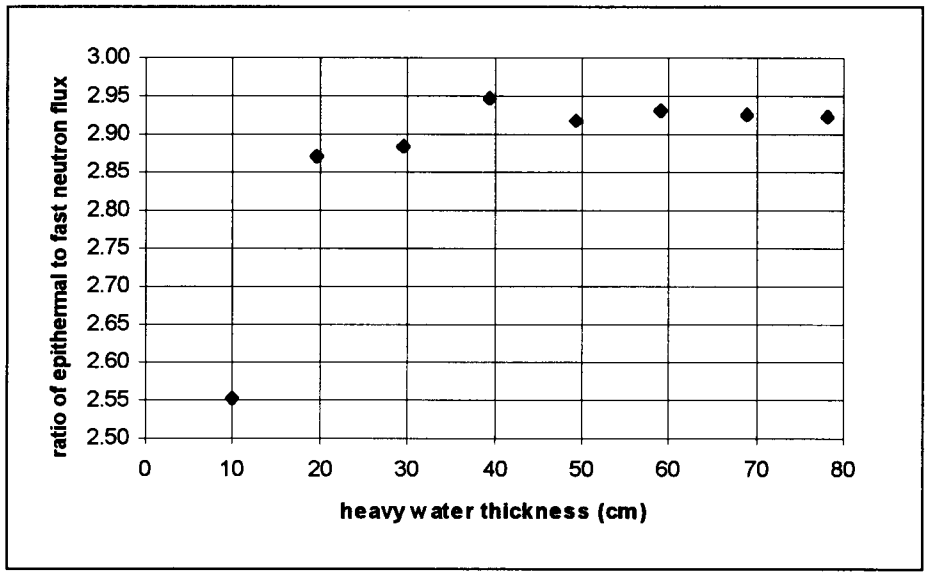

Figure 5.3 The ratio of calculated epithermal neutron to fast neutron flux at the end of beam port 3 vs. heavy water thickness in beam port 4.

5.4 Reflector in Beam Port 3

The epithermal neutron beam design in beam port 3 consisted of two parts, a reflector and a filter. Several materials were used as the candidates for the reflector and filter.

The reflector was defined as a material with a large scattering cross section and a low absorption cross section lining the inside surface of beam port 3 in order to reflect or scatter neutrons leaking out of beam port 3 back into beam port 3. The therapeutic neutron beam was maximized by using a reflector.

Three materials, graphite, silicon and beryllium oxide, were selected for consideration as neutron reflectors. Neither graphite nor beryllium oxide was suitable for this design because of low epithermal neutron fluxes produced at the end of beam port 3.

Silicon was found to have superior properties in reflectivity. Therefore an optimum thickness of silicon was determined as the neutron reflector in beam port 3.

By increasing the thickness of silicon, the ratio of epithermal neutron flux to fast neutron flux was increased until it reached a peak at an optimum thickness. Then the ratio decreased as the thickness of silicon increased further. This was due to the moderation and absorption of epithermal neutrons with increasing silicon thickness.

From Figure 5.4 the optimum thickness of silicon to use as a reflector inside beam port 3 was 0.35 cm. At this thickness, the highest epithermal neutron flux can be achieved. Results are summarized in Table 6, which shows the ratio of epithermal to fast neutron flux as a function of silicon thickness.

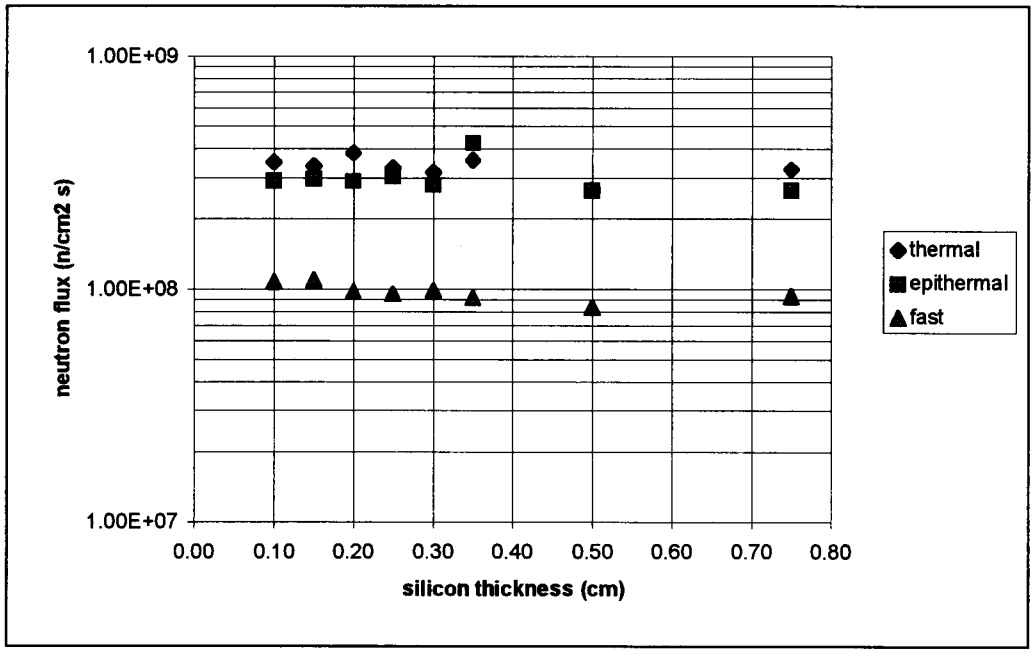

Figure 5.4 Calculated thermal, epithermal and fast neutron flux at the exit of beam port 3 vs. silicon reflector thickness in beam port 3.

Table 6. Calculated ratio of epithermal to fast neutron flux at the exit of beam port 3 for different silicon reflector thicknesses in beam port 3.

Si thickness (cm)	ratio of Φepi / Φfast
0.10	2.72 ± 0.15
0.15	2.71 ± 0.33
0.20	2.97 ± 0.33
0.25	3.17 ± 0.39
0.30	2.83 ± 0.25
0.35	4.61 ± 0.37
0.50	3.17 ± 0.30
0.75	2.83 ± 0.32

5.5 Filter in Beam Port 3

Three types of undesirable radiation components which must be considered for further reduction by filters are fast neutrons, thermal neutrons and gamma rays. The latter was not a part of this study. However, it is well known that bismuth is a very effective material for gamma ray attenuation without the accompanying production of secondary neutron or photon radiation (Choi et al., 1990).

5.5.1 Gamma Ray Filter

Bismuth is a good material for shielding against primary gamma rays due to its low neutron absorption cross section and high density. However, it can induce secondary gamma rays from the (n, γ) reaction in bismuth itself. Consequently, by increasing the bismuth thickness, the ratio of thermal neutron flux to gamma ray dose rate reached an equilibrium value (Sakurai et al., 1992). Besides gamma ray attenuation, bismuth will also attenuate useful epithermal neutrons somewhat, so the gamma ray intensity should not be reduced more than acceptable values.

5.5.2 Fast Neutron Filter

Filtering a high energy neutron component while allowing a sufficient epithermal neutron flux for treatment proved to be difficult. Partial filtering was required to remove as many fast neutrons as possible without thermalizing many epithermal neutrons. Since aluminum, sulfur, and silicon had transmission windows in the range of 4 eV to 40 keV, they were considered as filters inside beam port 3.

Although aluminum was the best filter to maximize epithermal neutrons and minimize fast neutrons, the high energy (1.78 MeV) secondary gamma rays induced from thermal neutron capture in aluminum ($^{27}Al(n,\gamma)^{28}Al$) are very difficult to shield without attenuating some useful epithermal neutrons. Therefore aluminum was not suitable for a filter material in this design.

The silicon cross section has a window at 144 keV for fast neutrons, so it would required filtering with a material such as sulfur which has a resonance cross section at approximately 144 keV (Storr et al., 1992). Moreover, the ratio of epithermal neutron flux to fast neutron flux for a silicon filter was lower than the ratio of epithermal to fast neutron flux obtained with sulfur.

Sulfur has a neutron transmission window in the epithermal energy range. MCNP simulations showed that sulfur was superior in terms of moderating efficiency when compared with silicon. On the other hand, pure sulfur does not have adequate structural strength and integrity. It is very fragile and produces toxic vapors above 100 °C, and it rapidly reacts with hydrogenous material to form toxic or corrosive compounds (Choi et al., 1990).

Due to these unsuitable properties of sulfur, a 20.12 cm diameter cylinder of sulfur was enclosed inside a thin aluminum can (0.10 cm-thick) in order to separate the sulfur from the surrounding materials. The optimum length of sulfur was calculated to yield a low fast neutron flux while maintaining an adequate epithermal neutron flux to be able to treat the tumor at an appropriate depth in the brain.

The ratio of epithermal to fast neutron flux and the ratio of epithermal to thermal neutron flux as a function of sulfur filter thickness are demonstrated in Figure 5.5 and Table 7. The results show that the epithermal neutron to fast neutron flux ratio has a linear relationship with sulfur thickness.

Table 7. The effect of sulfur filter thickness on the ratio of epithermal neutron flux to fast neutron flux.

Thickness (cm)	Φ thermal ($n\ cm^{-2}\ s^{-1}$)	Φepithermal ($n\ cm^{-2}\ s^{-1}$)	Φfast ($n\ cm^{-2}\ s^{-1}$)	ratio Φ_{epi} / Φ_{th}	ratio Φ_{epi} / Φ_{fast}
10.16	1.84×10^{8}	2.26×10^{8}	4.68×10^{7}	1.23	4.83
20.12	1.15×10^{8}	1.38×10^{8}	1.40×10^{7}	1.20	9.91
30.48	5.64×10^{7}	9.01×10^{7}	5.70×10^{6}	1.60	15.81
40.64	4.38×10^{7}	5.30×10^{7}	2.54×10^{6}	1.21	20.86
60.96	9.47×10^{6}	2.54×10^{7}	5.97×10^{5}	2.68	42.63
91.44	2.24×10^{6}	1.07×10^{7}	2.16×10^{5}	4.76	49.51

5.6 Neutron Beam Collimator

A beam collimation was considered for dose distribution in irradiated tissue. The ideal neutron beam should have a high ratio of tumor to normal tissue dose and a high current to flux ratio (J/Φ). The collimator plays an important role in the directionality of the neutron beam.

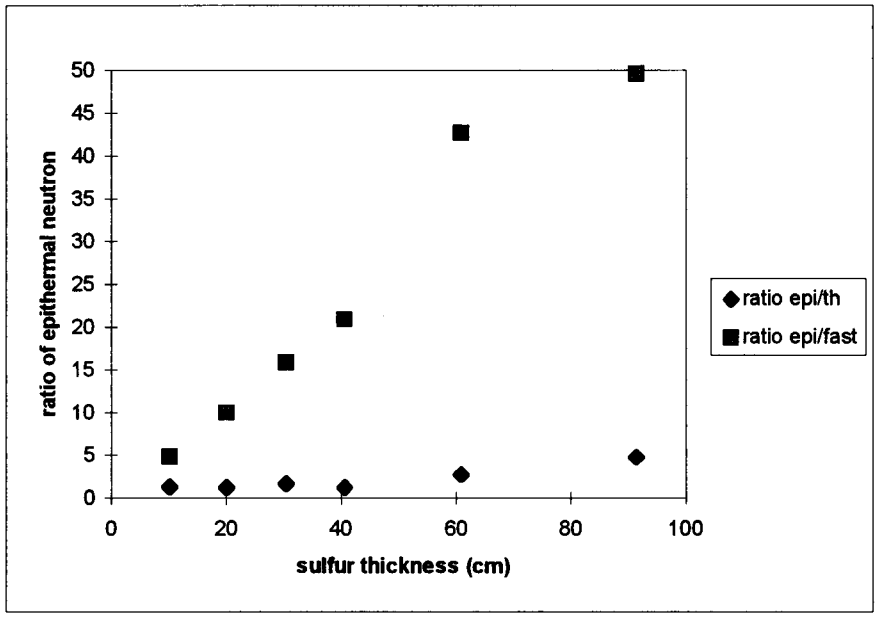

Figure 5.5 Calculated epithermal to fast neutron flux ratio and epithermal to thermal neutron flux ratio for several thicknesses of sulfur.

5.6.1 Neutron Flux and Current

To study beam size effect, the beam size was varied from 6 to 20.12 cm in inner diameter at the exit of beam port 3. Furthermore, various materials were used as a cone collimator to provide the desired flux ratios for BNCT.

The results indicated that the quality of the neutron current and neutron flux depended on the size of the collimator. The effect of the collimator diameter on neutron current and neutron flux is presented in Table 8. The neutron current, which is the number of neutrons crossing a surface oriented in a given direction, increased as a function of collimator diameter, up to a maximum value and then it changed insignificantly for larger collimator diameter. This is due to the fact that the MCNP F1 surface current tally sums over the surface.

On the other hand, the average neutron flux over a specified surface area tended to decrease as the cross sectional area increased. This is because the flux is larger near the center of the beam port and the MCNP F2 surface flux tally calculates average fluxes over the surface. Figure 5.6 shows the effect of cross sectional areas at the exit of beam port 3 on neutron currents and fluxes.

Table 8. The effect of collimator diameter on neutron currents and fluxes

collimator diameter (cm)	J thermal (n)	J epithermal (n)	J fast (n)	Φ thermal (n cm^{-2})	Φ epithermal (n cm^{-2})	Φ fast (n cm^{-2})
6	4.00×10^{8}	3.56×10^{9}	6.09×10^{8}	1.43×10^{7}	1.33×10^{8}	1.51×10^{7}
8	8.40×10^{8}	5.95×10^{9}	8.33×10^{8}	1.70×10^{7}	1.24×10^{8}	1.79×10^{7}
10	1.12×10^{9}	9.28×10^{9}	1.21×10^{9}	1.44×10^{7}	1.24×10^{8}	1.58×10^{7}
12	1.62×10^{9}	2.00×10^{10}	1.68×10^{9}	1.44×10^{7}	1.84×10^{8}	1.52×10^{7}
14	1.85×10^{9}	1.40×10^{10}	1.86×10^{9}	1.25×10^{7}	9.55×10^{7}	1.21×10^{7}
16	1.54×10^{9}	1.29×10^{10}	1.86×10^{9}	7.68×10^{6}	6.52×10^{7}	9.47×10^{6}
18	1.86×10^{9}	1.33×10^{10}	1.79×10^{9}	7.31×10^{6}	5.30×10^{7}	9.96×10^{6}
20	1.67×10^{9}	1.35×10^{10}	1.81×10^{9}	5.31×10^{6}	4.36×10^{7}	5.77×10^{6}

5.6.2 Monodirectionality

Monodirectionality (J/ Φ=1.0) is desirable in BNCT because the monodirectional beam will penetrate better to generate more thermal neutron flux at the tumor location than an isotropic beam with the same scalar flux, since the intensity of an isotropic beam falls off very rapidly as the distance from the beam port exit increases, whereas there is no diverging effect for a monodirectional beam (Wheeler et al., 1990).

In theory, increasing collimation will improve a neutron current to flux ratio and forward direction of the neutron beam (Yanch and Harling, 1993a and 1993b). However the results from this design indicate that a highly forward peaked epithermal neutron beam was achieved and it was independent of the diameter of the collimator (Table 9).

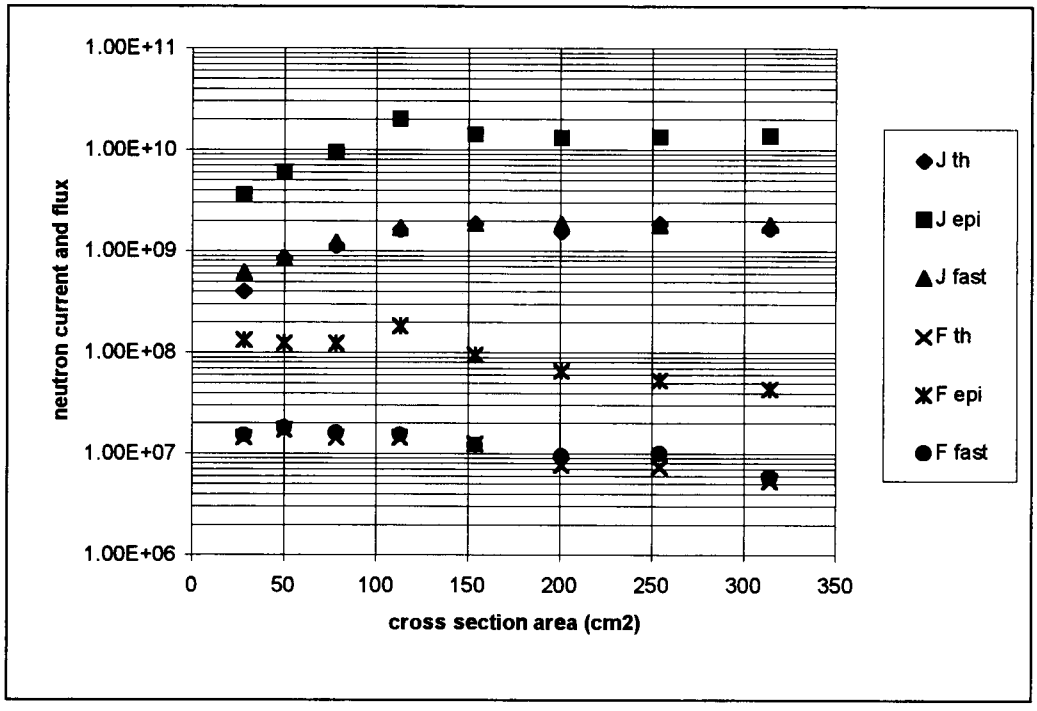

Figure 5.6 The effect of collimator cross sectional area on neutron currents and fluxes.

Table 9. The effect of collimator diameter on the directionality of the epithermal neutron beam.

Collimator diameter (cm)	ratio Φ_{epi}/Φ_{th}	ratio Φ_{epi}/Φ_{fast}	J_{epi}/Φ_{epi} ± (% relative error)
6	9.31	8.82	0.95 ± 2.63
8	7.28	6.92	0.96 ± 2.10
10	8.59	7.82	0.96 ± 1.28
12	12.77	12.05	0.96 ± 1.21
14	7.66	7.86	0.95 ± 4.85
16	8.49	6.89	0.98 ± 6.63
18	7.25	5.32	0.98 ± 6.11
20	8.20	7.54	0.98 ± 6.15

The average of the epithermal neutron current to flux ratio is 0.97 ± 0.13. Since the highest epithermal neutron flux to fast neutron flux was obtained from a 12 cm diameter collimated beam, a 12 cm was used as the collimator diameter in beam port 3 to deliver the epithermal neutron beam for BNCT applications in this study.

5.6.3 Collimator Length

Besides the collimator diameter, the collimator length was calculated to determine the optimum length that will provide a sufficient epithermal neutron intensity while minimizing the thermal and fast neutron backgrounds. The length of the collimator was varied from 70.8 cm to 111.4 cm. The results are summarized in Table 10. Figure 5.7 and Table 10 show that the neutron fluxes are nearly independent of the length of the collimator.

The average of thermal, epithermal and fast neutron fluxes were 1.64×10^8 with 5% relative error, 1.62×10^8 with 5% relative error and 7.91×10^7 with 9% relative error, respectively. After calculating and accounting for the angular divergence, 91 cm was chosen as the optimum length for the collimator in this study.

Since the ratios between the epithermal to fast neutron flux and the epithermal to thermal neutron flux changed insignificantly, there was no benefit derived from increasing the collimator length more than 91 cm to improve the angular neutron flux. Therefore, the collimator with 91 cm in length was used in the model and the horizontal cross section of beam port 3 after modification by the collimator is shown in Figure 5.8.

Table 10. The effect of collimator length on neutron flux

Thickness (cm)	Φ thermal ($n\ cm^{-2}\ s^{-1}$)	Φ epithermal ($n\ cm^{-2}\ s^{-1}$)	Φfast ($n\ cm^{-2}\ s^{-1}$)	ratio Φ_{epi} / Φ_{th}	ratio Φ_{epi} / Φ_{fast}
70.80	1.54×10^8	1.60×10^8	9.16×10^7	1.04	1.75
80.96	1.50×10^8	1.64×10^8	7.73×10^7	1.09	2.12
91.12	1.82×10^8	1.65×10^8	7.42×10^7	0.91	2.23
101.28	1.58×10^8	1.63×10^8	7.74×10^7	1.03	2.10
111.44	1.73×10^8	1.56×10^8	7.48×10^7	0.90	2.09

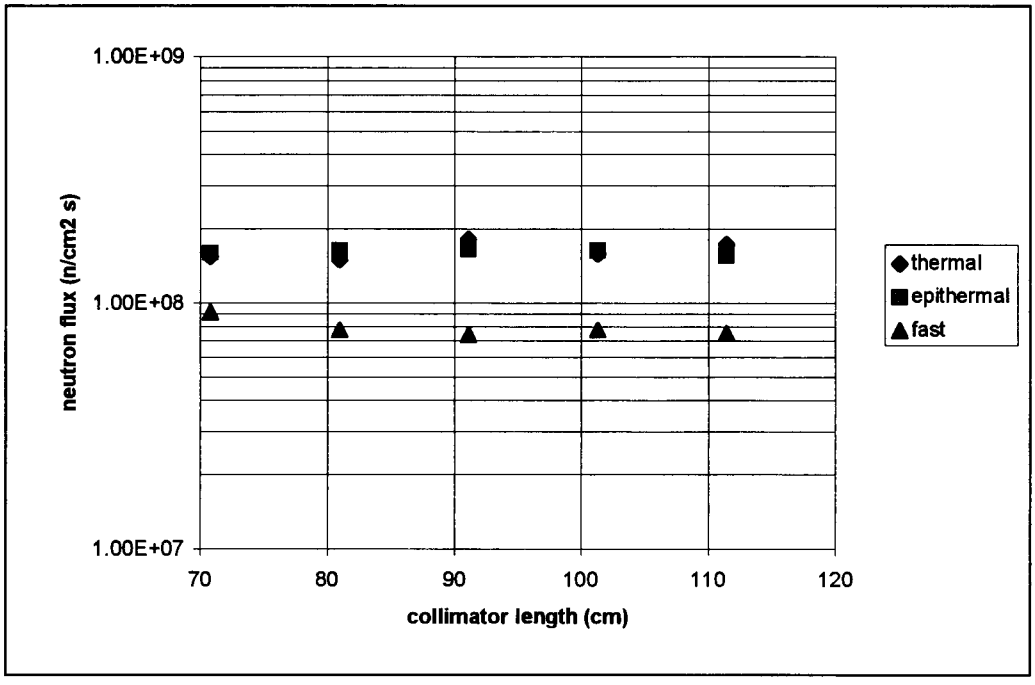

Figure 5.7 The effect of collimator length on neutron flux in beam port 3.

5.7 Thermal Neutron Filter

Due to the fact that ^6Li has a high thermal neutron capture cross section and a low gamma production cross section, it has the ability to remove thermal neutrons from the beam with an insignificant production of secondary radiation. Lithium carbonate (Li_2CO_3) with 95% enriched ^6Li was utilized at the end of beam port 3 in the design to effectively shield thermal neutrons with little secondary radiation. The desired thickness of Li_2CO_3 can be estimated from the following equation:

$$I / I_o = e^{-\Sigma_a x}$$

where $\Sigma_a = N \sigma_a$, N is the atomic number density of Li_2CO_3 (cm^{-3}), σ_a is the microscopic absorption cross section (barn or cm^2), x is the thickness of the shielding material (cm), Σ_a is the macroscopic absorption cross section (cm^{-1}), I_o is the incident neutron beam intensity (n $cm^{-2}s^{-1}$), and I is the neutron intensity after attenuation (n $cm^{-2}s^{-1}$).

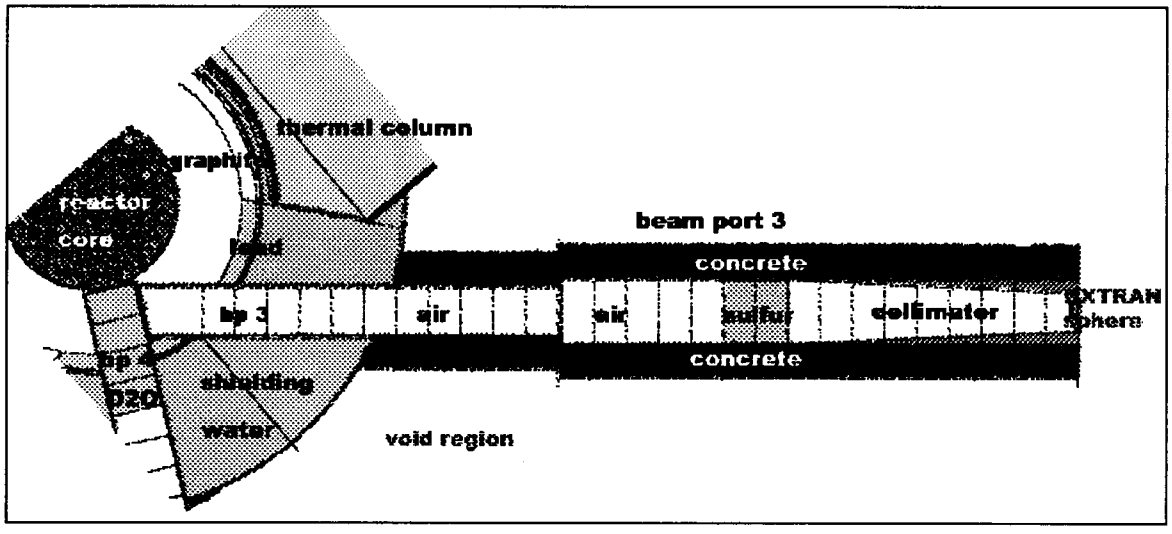

Figure 5.8 The horizontal view of beam port 3 model with collimator.

A suitable Li_2CO_3 thickness was calculated to be between 0.07 and 0.10 cm, which was then used in the MCNP model. The results in Table 11 show that a 0.10 cm thickness of Li_2CO_3 reduced the thermal neutron flux without a detrimental effect on the epithermal neutron flux better than 0.07 cm of Li_2CO_3.

Although increasing the thickness of Li_2CO_3 further can remove more thermal neutrons from the beam, no significant advantage can be gained by further increasing the Li_2CO_3 thickness more than 0.10 cm. In addition, a significant reduction in the epithermal therapeutic beam resulted as the Li_2CO_3 thickness increased.

Table 11. Comparison of thermal neutron reduction in beam port 3 for different thicknesses of Li_2CO_3

Thickness (cm)	Φ thermal ($n\ cm^{-2}\ s^{-1}$)	Φ epithermal ($n\ cm^{-2}\ s^{-1}$)	Φfast ($n\ cm^{-2}\ s^{-1}$)	ratio Φ_{epi} / Φ_{th}	ratio Φ_{epi} / Φ_{fast}
0.00	1.36×10^{8}	1.44×10^{8}	7.13×10^{7}	1.06	2.02
0.07	3.14×10^{7}	1.44×10^{8}	7.70×10^{7}	4.58	1.87
0.10	1.88×10^{7}	1.41×10^{8}	7.57×10^{7}	7.50	1.87

5.8 Final Design of Beam Port 3

The final design of beam port 3 consisted of a 0.35 cm thick silicon layer lining the inside of beam port 3, a 20 cm diameter and 20 cm long sulfur filter in an aluminum can, a 91 cm long truncated conical collimator, and a 0.10 cm thick Li_2CO_3 shield. Figure 5.9 demonstrates the beam port 3 final model by using an MCNP plot from MCNP version 4b.

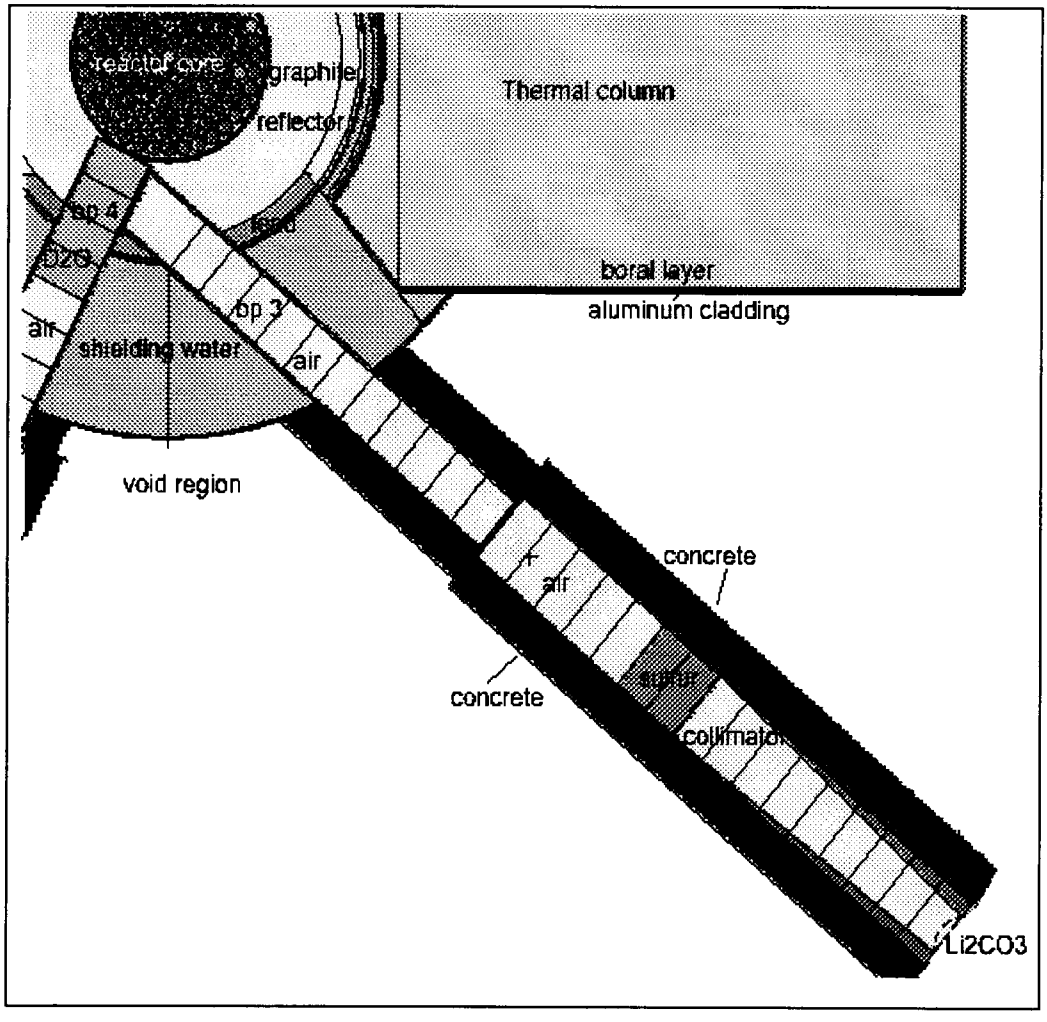

Figure 5.9 The geometry of the beam port 3 final design

5.8.1 Collimator Material

Both a DXTRAN sphere and a point detector were utilized for tracking the neutron fluxes at the exit of beam port 3. A multiplication factor was used to account for the 1 MW reactor power.

Aluminum, aluminum oxide, aluminum fluoride, aluminum sulfate, calcium fluoride and silicon were evaluated as collimator materials. Even though similar results were obtained for the different collimator materials, silicon was superior in achieving a high epithermal neutron flux with low fast and thermal neutron components.

The calculated data in Table 12 and Table 13 indicate that the silicon layer lining along beam port 3 insignificantly effected the neutron intensity, so it was removed from the design.

Table 12. Effect of collimator material on neutron flux in modified beam port 3 with the silicon layer coating along beam port 3.

Collimator material	Φ thermal ($n\ cm^{-2}\ s^{-1}$)	Φ epithermal ($n\ cm^{-2}\ s^{-1}$)	Φfast ($n\ cm^{-2}\ s^{-1}$)	ratio Φ_{epi} / Φ_{th}	ratio Φ_{epi} / Φ_{fast}
silicon	1.36×10^{7}	1.26×10^{8}	1.20×10^{7}	9.22	10.49
Al_2O_3 + Al	1.21×10^{7}	1.11×10^{8}	1.47×10^{7}	9.11	7.51
AlF_3 + Al	1.28×10^{7}	9.55×10^{7}	1.40×10^{7}	7.46	6.80
aluminum sulfate (Al_2SO_4)	1.63×10^{7}	9.66×10^{7}	1.27×10^{7}	5.93	7.62
calcium fluoride(CaF_2)	1.37×10^{7}	1.14×10^{8}	1.30×10^{7}	8.35	8.76
aluminum oxide (Al_2O_3)	1.15×10^{7}	9.43×10^{7}	1.39×10^{7}	8.17	6.80
aluminum (Al)	8.59×10^{6}	7.24×10^{7}	1.02×10^{7}	8.42	7.08

Table 13. Results of neutron flux without the silicon layer coating along beam port 3.

Collimator material	Φ thermal ($n\ cm^{-2}\ s^{-1}$)	Φ epithermal ($n\ cm^{-2}\ s^{-1}$)	Φfast ($n\ cm^{-2}\ s^{-1}$)	ratio Φ_{epi} / Φ_{th}	ratio Φ_{epi} / Φ_{fast}
silicon	1.34×10^{7}	1.28×10^{8}	1.14×10^{7}	9.53	11.29
Al_2O_3 + Al	1.21×10^{7}	1.02×10^{8}	1.23×10^{7}	8.41	8.27
AlF_3 + Al	1.25×10^{7}	9.85×10^{7}	1.24×10^{7}	7.89	7.94
aluminum sulfate (Al_2SO_4)	1.14×10^{7}	1.01×10^{8}	1.14×10^{7}	8.84	8.81
calcium fluoride(CaF_2)	1.03×10^{7}	1.02×10^{8}	1.31×10^{7}	9.91	7.75
aluminum oxide (Al_2O_3)	1.20×10^{7}	9.61×10^{7}	1.26×10^{7}	8.02	7.60
aluminum (Al)	1.35×10^{7}	7.70×10^{7}	1.04×10^{7}	5.72	7.39

Figures 5.10 and 5.11 present the calculated neutron flux at the exit of beam port 3 for the final design including the silicon layer and without the silicon layer coating along beam port 3, respectively.

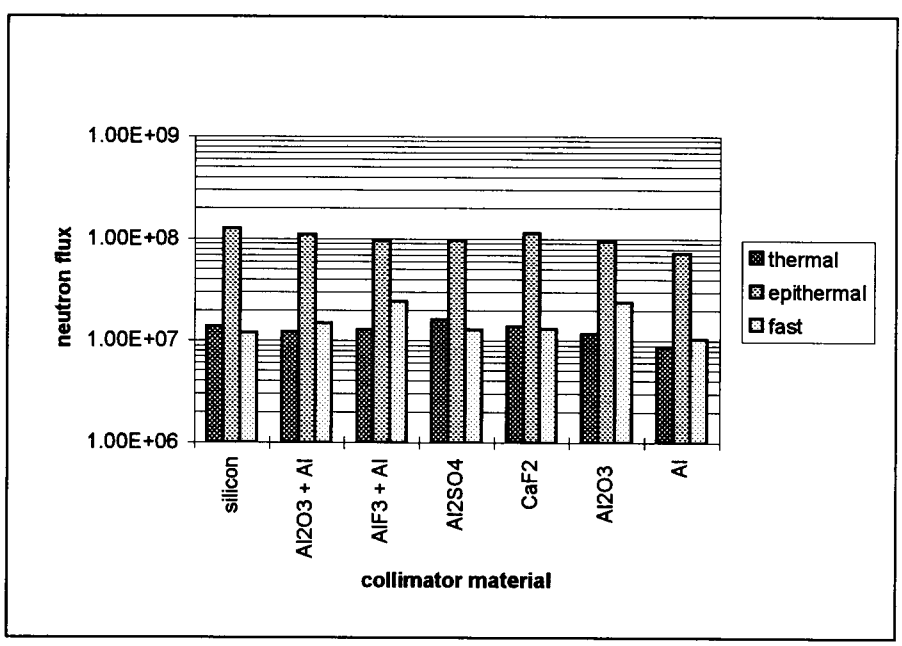

Figure 5.10 Calculated neutron flux at the end of beam port 3 (final design) with silicon layer coating along beam port 3.

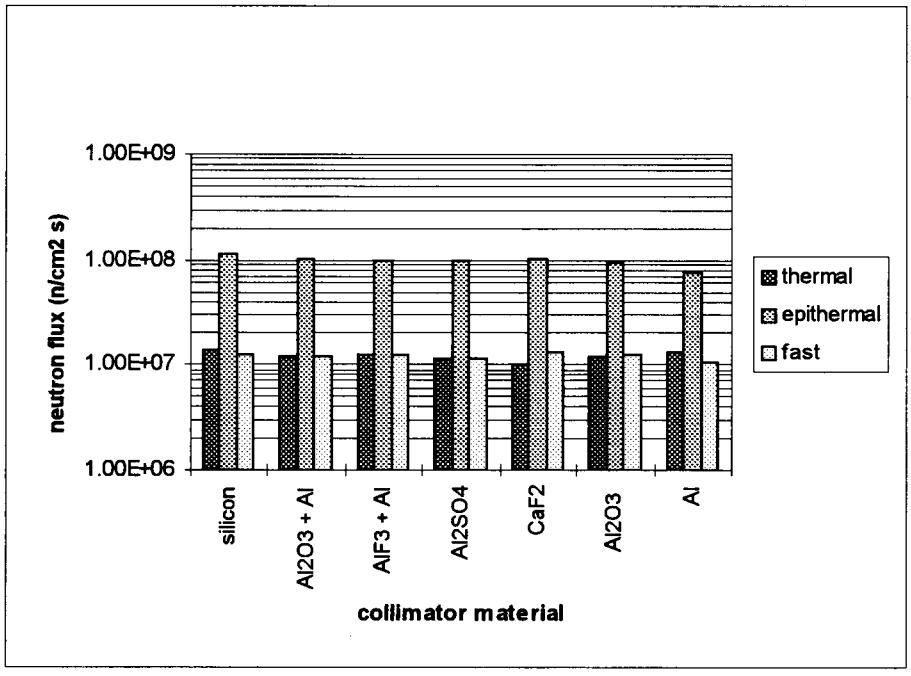

Figure 5.11 Calculated neutron flux at the end of beam port 3 (final design) without silicon layer coating along beam port 3.

The neutron beam at the exit of beam port 3 without a silicon layer coating inside beam port 3 are summarized in Table 13. The best configuration was derived from a silicon collimator inside beam port 3 providing a high intensity of epithermal neutrons, 1.28×10^{8} n $cm^{-2}s^{-1}$ with 5% relative error, with a low contribution of thermal neutrons and fast neutrons, 1.34×10^{7} n $cm^{-2}s^{-1}$ with 3% relative error and 1.14×10^{7} n $cm^{-2}s^{-1}$ with 3% relative error, respectively. This resulted in an epithermal neutron flux that was 9.53 and 11.29 times higher than the thermal and fast neutron fluxes, respectively.

5.8.2 Final Beam Direction

Directionality was determined from the neutron current to flux ratio for the final design. The area inside beam port 3 was divided into two parts: before the collimator and after the collimator. The first part was located from the beginning of beam port 3 to

the collimator and consisted of an inside beam port 3 segment and a cladding segment. The second part was the segment from the collimator to the exit of beam port 3, which was divided into 3 segments: inside collimator, collimator cladding and steel cladding.

Tally segment and segment divisor cards were used to calculate the current and flux tallies at the exit of beam port 3. Variance reduction techniques which included a population control method (geometry splitting and Russian roulette) by using importance ratio and a partially-deterministic method (DXTRAN) were utilized in this calculation.

The epithermal neutron current and flux decreased roughly exponentially with the distance down the beam port. The exponential relationship between the epithermal neutron current and flux, and the distance from the inner end of beam port 3 were plotted in Figures 5.12 and 5.13, respectively.

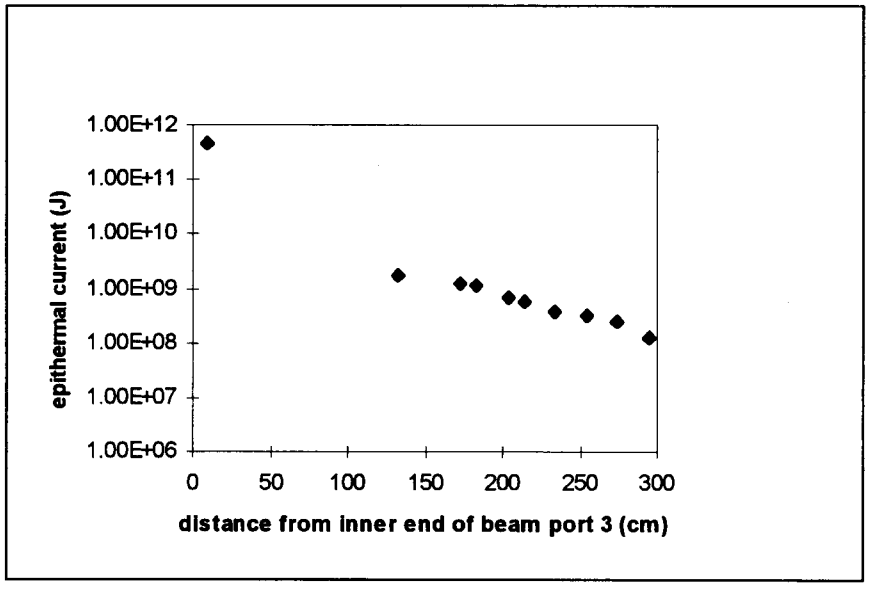

Figure 5.12 Calculated epithermal neutron current at the exit of beam port 3 (DXTRAN method) vs. distance

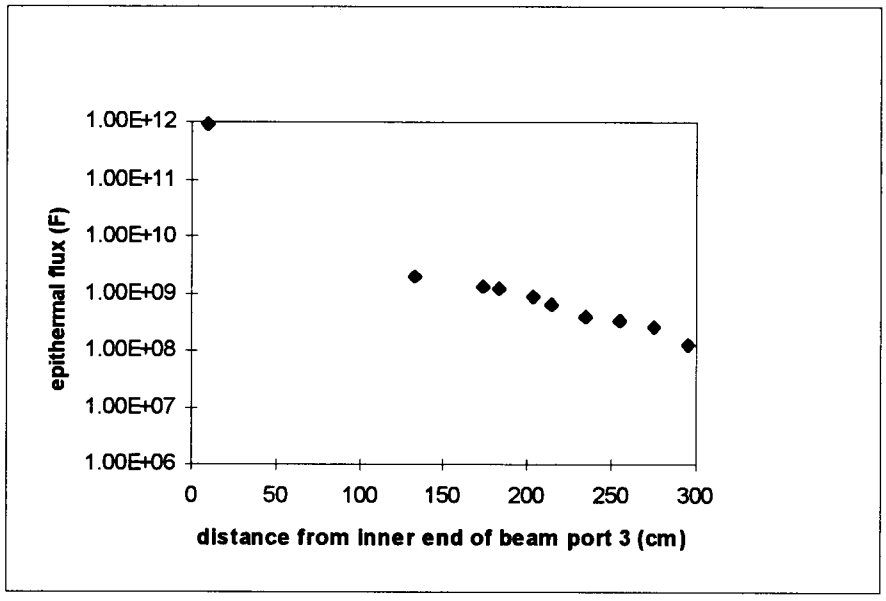

Figure 5.13 Calculated epithermal neutron flux at the exit of beam port 3 (DXTRAN method) vs. distance.

The comparison of the calculated epithermal neutron current to flux ratio (directionality) with percent relative error by using a DXTRAN sphere and an importance ratio as variance reduction techniques are presented in Figures 5.14 and 5.15. The relative error in the importance ratio method increased as the distance from the inner end of beam port 3 to the tally plane increased.

However, the relative error in the DXTRAN method seemed to be roughly constant from the inner end of beam port 3 to the exit of beam port 3 and smaller than for the importance method. Consequently, the DXTRAN method was used as a variance reduction technique in this calculation instead of the importance ratio method.

In the surface source write region, the current to flux ratio (J/Φ) for thermal, epithermal and fast neutrons were ~ 0.50 with a 1.34 % relative error, and hence was an isotropic beam.

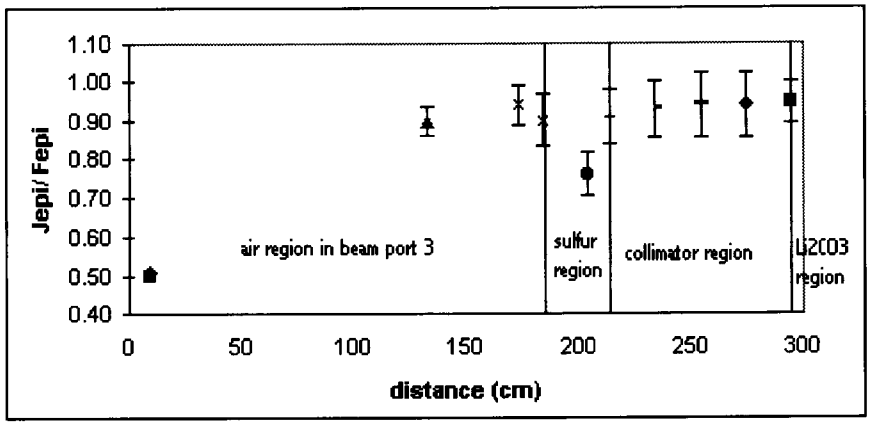

Figure 5.14 Calculated epithermal neutron current to flux ratio with relative error (DXTRAN sphere method)

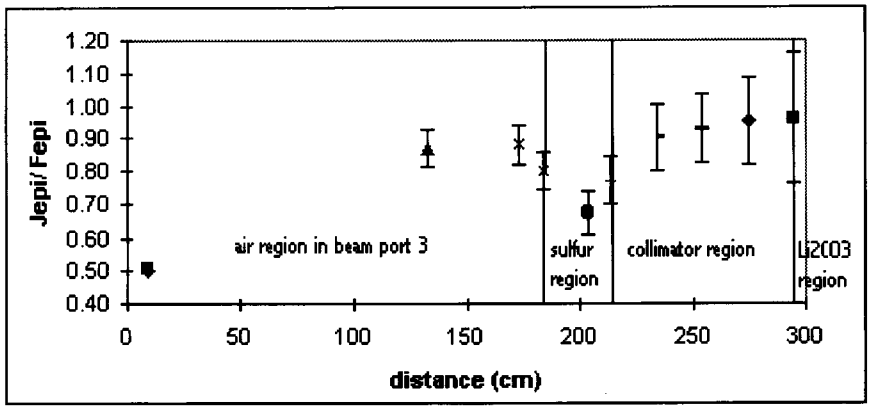

Figure 5.15 Calculated epithermal neutron current to flux ratio with relative error (importance ratio method)

A high epithermal neutron forward direction was obtained up to the sulfur filter plane. Subsequently, the epithermal neutron current to flux ratio fell off very rapidly in the sulfur region. Since the sulfur inside the aluminum can is a scattering material, the forward direction of the epithermal neutron beam was reduced. The high forward direction of the epithermal neutron beam was achieved again further down the beam port after the beam was collimated.

The final design (Figure 5.16) produced a high forward peaking of the epithermal neutron beam. Since the epithermal neutron current to flux ratio was 0.95 with a 5% relative error, it should generate more thermal neutron flux at the tumor location with little diverging effect of the epithermal neutron beam.

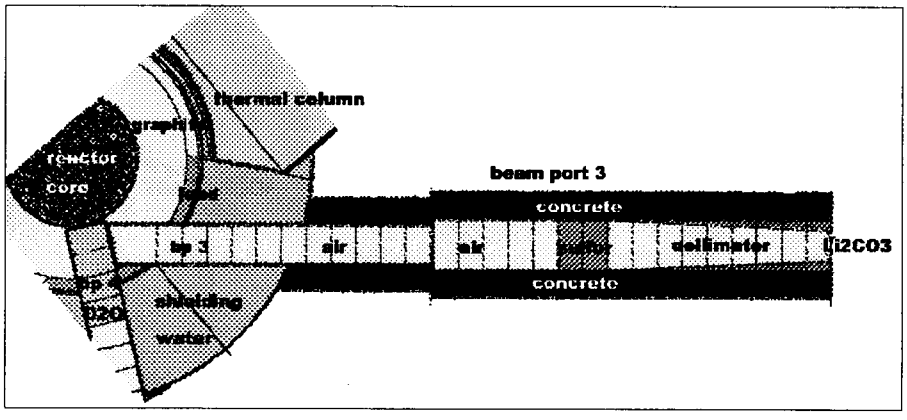

Figure 5.16 Final design of beam port 3

6. DISCUSSION

Since experimental measurement is the only way to confirm the MCNP calculations, neutron activation analysis was used as a tool to measure thermal and epithermal neutron fluxes. Calculated thermal and epithermal neutron fluxes were compared with the measured values at the same position.

6.1 Thermal Neutron and Epithermal Neutron Measurement Position

Thermal neutron and epithermal neutron fluxes were determined by gold foil irradiations with and without a cover of cadmium metal foil. The gold and gold with cadmium (Au/Cd) foil activations were performed by several other investigators (Oregon State University, 1997) at 1 cm above the bottom of the rabbit, 1 cm above the bottom of the rotating rack (Lazy Susan) and at the exit of beam port 3 and beam port 4 before modification. Comparisons of the experimental measurements and MCNP calculations for thermal and epithermal neutron fluxes are presented in Tables 14 and 15, respectively.

Table 14. Calculated (this study) and measured (Oregon State University, 1997) thermal neutron flux for an unmodified OSTR at 1 MW.

Position in the reactor	Calculated thermal neutron flux ($n\ cm^{-2}\ s^{-1}$)	Measured thermal neutron flux ($n\ cm^{-2}\ s^{-1}$)
1 cm above the bottom of rabbit	$9.35\times10^{12} \pm 2.5\%$ relative error	9.0×10^{12}
1 cm above the bottom of Lazy Susan	$3.25\times10^{12} \pm 1.6\%$ relative error	3.16×10^{12}
exit of beam port 4	$4.46\times10^{9} \pm 9.5\%$ relative error	4.10×10^{9}

6.2 Calculated and Measured Thermal and Epithermal Neutron Fluxes

The data in Tables 14 and 15 show good agreement between the calculated and measured values of the thermal neutron flux in the rabbit, the Lazy Susan, and the exit of beam port 4. Although MCNP calculations for the epithermal neutron flux in the rabbit and the exit of beam port 3 agree fairly well with experimental measurement, the experimental measurement and MCNP calculations for the epithermal neutron flux in the Lazy Susan and the exit of beam port 4 are not in good agreement

Table 15. Calculated (this study) and measured (Oregon State University, 1997) epithermal neutron flux for an unmodified OSTR at 1 MW.

Position in the reactor	Calculated epithermal neutron flux (n cm^{-2} s^{-1})	Measured epithermal neutron flux (n cm^{-2} s^{-1})
1 cm above the bottom of rabbit	4.54×10^{11} ± 1.7% relative error	4.0×10^{11}
1 cm above the bottom of Lazy Susan	2.43×10^{11} ± 1.9% relative error	1.06×10^{11}
exit of beam port 3	1.78×10^{8} ± 4.3% relative error	1.40×10^{8}
exit of beam port 4	2.15×10^{8} ± 8.3% relative error	1.30×10^{8}

Several aspects contribute to the discrepancies of the calculated and the measured results. The model in MCNP is an approximation of the real reactor system. In particular, the fuel element assumption in the MCNP model was a homogeneous distribution and did not account for fission product buildup. The beam port design described in this study was modified from the original design. Furthermore, the investigators performed these measurements in the past and the conditions during the measurements cannot be reproduced in the model. Consequently, the calculated neutron fluxes from the beam port were not totally in agreement with the neutron flux measurements.

7. CONCLUSION

7.1 Summary

The OSU TRIGA Mark-II reactor operating at 1 MW power was studied for generating a suitable epithermal neutron beam (energy range between 0.5 eV to 100 keV) for boron neutron capture therapy. The criticality of the reactor core was verified first. Secondly, the moderator and filter arrangement was designed to obtain a therapeutic beam with a high epithermal neutron intensity but low fast and thermal neutron contamination.

It was concluded that heavy water is the best moderator in the front part of beam port 4, whereas sulfur and lithium carbonate were effective materials as a fast neutron filter and thermal neutron filter in beam port 3, respectively. Furthermore, a silicon conical collimator improved the quality of the neutron beam by delivering a forward directional anisotropic epithermal neutron beam ($J/\Phi_{epi} = 0.95$ with a 5% relative error).

The Monte Carlo calculation indicated that an epithermal neutron flux of 1.28×10^{8} n $cm^{-2}s^{-1}$, a thermal neutron flux of 1.34×10^{7} n $cm^{-2}s^{-1}$ and a fast neutron flux of 1.14×10^{7} n $cm^{-2}s^{-1}$ could be obtained. Relative MCNP errors were in the 3 to 5% range. Nevertheless, the epithermal neutron flux was insufficient in magnitude for a short irradiation treatment time for BNCT. Fast neutron contamination is still somewhat higher than that desirable, 2.38×10^{-10} cGy $cm^{2}n^{-1}$, with a 5.2% relative error.

Due to the facts that the exit of the beam port is located far way from the source (reactor core) and the source area was small, a low epithermal neutron intensity was obtained. An epithermal neutron fluence of about 1.0×10^{13} n cm^{-2} is thought to be necessary for effective BNCT (Harling et al., 1990). For the calculated epithermal flux, a

treatment time of about 25 hours would be required, which is clearly unacceptable. However, for a similar reactor at 10 MW, the treatment time would be more acceptable.

7.2 Recommendations for Further Study

This design indicated that a therapeutic epithermal neutron beam can be generated from a research reactor such as the OSTR. However further study including gamma ray calculations and phantom dose calculations and measurements should be performed to improve the potential of this epithermal neutron beam.

Although MCNP simulation provided guidance for the epithermal beam design, experiments should be performed to verify the beam design. Moreover, the gamma flux and gamma dose rate should be investigated for further study of BNCT in order to specify the filter configuration for gamma rays.

Measurement of all dose components in a tissue equivalent phantom at the exit of beam port 3 is required to determine the advantage depth, advantage ratio and advantage depth dose rate.

Advantage depth is used to measure the penetration of the therapeutic beam, and advantage depth dose rate is the therapeutic dose at the advantage depth. Advantage ratio, which is defined as the ratio of the integral of the total therapeutic dose (tumor dose) to the integral of the total background dose (normal tissue), is important for dose distribution in phantoms. In this definition the integration is over the distance from entrance into the head to the tumor site.

The advantage of an optimum epithermal neutron beam and an effective tumor cell-specific boron compound will provide a high potential of boron neutron capture

therapy treatment, which will improve the survival rate for brain tumor patients in the future.

BIBLIOGRAPHY

Aizawa, O., K. Kanda, T. Nozaki and T. Matsumoto. 1980. Remodeling and dosimetry on the neutron irradiation facility of the Musashi Institute of Technology reactor for boron neutron capture therapy. Nuclear Technology 48:150-162.

Aizawa, O. 1990. Research on neutron beam design for BNCT at the Musashi reactor. Neutron Beam Design, Development, and Performance for Neutron Capture Therapy, ed. O. K. Harling et al., 219-227. Plenum Press, New York and London.

Auterinen, I. And P. Hiismaki. 1993. Epithermal BNCT neutron beam design for a TRIGA-II reactor. Advances in Neutron Capture Therapy, ed. A. H. Soloway et al., 81-84. Plenum Press, New York.

Barth, R. F., A. H. Soloway and R. G. Fairchild. 1990. Boron neutron capture therapy for cancer. Scientific American 263(4):100-109.

Briesmeister, J. F. ed., 1993. MCNP-a general Monte Carlo N-particle transport code, version 4a, Los Alamos National Laboratory.

Brugger, R. M. and W. H. Herleth. 1990. Intermediate energy neutron beams from the MURR. Neutron Beam Design, Development, and Performance for Neutron Capture Therapy, ed. O. K. Harling et al., 153-165. Plenum Press, New York and London.

Brugger, R. M., J. A. Shih and H. B. Liu. 1992. An epithermal neutron beam for neutron capture therapy at the Missouri University Research Reactor. Nuclear Technology 98:322-332.

Brugger, R. M., T. J. Less, G. G. Passmore. 1986. Beam of intermediate energy neutrons for neutron capture therapy. Transactions of the American Nuclear Society 53:24-25.

Burian, J., M. Marek and J. Rataj. 1992. Neutron beam parameters on LVR-15 reactor for neutron capture therapy. Progress in Neutron Capture Therapy for Cancer, ed. B. J. Allen et al., 83-86. Plenum Press, New York.

Cheng, K., K. Unlu, A. J. Teachout, N. M. Abdurrahman and B. W. Wehring. 1995. Gadolinium neutron capture therapy dosimetry measurements. Transactions of the American Nuclear Society, ed. J. A. Bernard, 73:30-31.

Choi, J. R., S. D. Clement, O. K. Harling and R. G. Zamenhof. 1990. Neutron capture therapy beams at the MIT research reactor. Neutron Beam Design, Development, and Performance for Neutron Capture Therapy, ed. O. K. Harling et al., 201-217. Plenum Press, New York and London.

Clement, S. D., J. R. Choi, R. G. Zamenhof, J. C. Yanch, and O. K. Harling. 1990. Monte Carlo methods of neutron beam design for neutron capture therapy at the MIT research reactor (MITR-II). Neutron Beam Design, Development, and Performance for Neutron Capture Therapy, ed. O. K. Harling et al., 51-67. Plenum Press, New York and London.

Constantine, G. 1990. Neutron capture therapy beam design at Harwell. Neutron Beam Design, Development, and Performance for Neutron Capture Therapy, ed. O. K. Harling et al., 71-81. Plenum Press, New York and London.

DeMora, J. M., H. L. He, A. Sainz, C. Butzow, D. Worthington, E. Schaefer, T. Moschetti, G. H. Miley. 1995. Conceptual design for a BNCT facility using an IEC fusion source. Transactions of the American Nuclear Society 72:104.

Deutsch, O. L. and B. W. Murray. 1975. Monte Carlo dosimetry calculation for boron neutron capture therapy in the treatment of brain tumors. Nuclear Technology 26:320-338.

Duderstadt, J.J and Hamilton L.J. 1976. Nuclear Reactor Analysis. John Wiley and Sons, New York.

Fairchild, R. G. 1986. Optimization of epithermal neutron beams for neutron capture therapy. 1986. Transactions of the American Nuclear Society 53:25-26.

Fairchild, R. G., V. Benary, J. K. Ezra, S. K. Saraf, R. M. Brugger, A. Shih, R. A. Gahbauer, J. H. Goodman, B. H. Laster, J. Gajewski, E. B. Ramsey, L. E. Reinstein, S. Fiarman, and Y. Kamen. 1992. An optimized epithermal neutron beam for neutron capture therapy (NCT) at the Brookhaven Medical Research Reactor (BMRR). Progress

in Neutron Capture Therapy for Cancer, ed. B. J. Allen et al., 1-5. Plenum Press, New York.

Godwin, J. T., L. E. Farr, W. H. Sweet and J. S. Robertson. 1955. Pathologic study of eight patients with glioblastoma multiforme treated by neutron capture therapy using boron-10. Cancer 8:601-615.

Harling, O.K., J. A. Bernard, and R. G. Zamenhof. 1990. Neutron beam design, development, and performance for neutron capture therapy. Plenum Press, New York.

Harling, O. K., J. C. Yanch, J. R. Choi, G. R. Solares, R. D. Rogus, D. J. Moulin, L. S. Johnson, I. O. Wirdzek, and J. A. Bernard. 1992. Boron neutron capture therapy and radiation synovectomy research at the Massachusetts Institute of Technology Research Reactor. Nuclear Science and Engineering 110:330-348.

Harling, O. K., J. A. Bernard, and R. G. Zamenhof. 1992. Critique MIT workshop on neutron beam design, development and performance for neutron capture therapy. Progress in Neutron Capture Therapy for Cancer, ed. B. J. Allen et al., 37-40. Plenum Press, New York.

Harrington, B. V. 1990. A calculational study of tangential and radial beams in HIFAR for neutron capture therapy. Neutron Beam Design, Development, and Performance for Neutron Capture Therapy, ed. O. K. Harling et al., 97-106. Plenum Press, New York and London.

Harrington B. V. and G. Constantine. 1995. Analysis of epithermal neutron beam experiments at the HIFAR reactor. Nuclear Technology 109:11-20.

Hatanaka, H. 1990. Clinical results of boron neutron capture therapy. Neutron Beam Design, Development, and Performance for Neutron Capture Therapy, ed. O. K. Harling et al., 15-19. Plenum Press, New York.

Kanda, K. 1975. Elimination of gamma rays from a thermal neutron field for medical and biological irradiation purposes. IAEA-SM-193/68, International Atomic Energy Agency.

Kaye, A. H. 1992. Photodynamic therapy of brain tumors. Progress in Neutron Capture Therapy for Cancer, ed. B. J. Allen et al.,613-616. Plenum Press, New York.

Kennedy, B. J. 1972. Chemotherapy of brain tumors. In Cancer Chemotherapy II, ed. I. Brodsky, S. B. Kahn and J. M. Moyer. Grune and Stratton Inc., New York.

Liu, H. B., R. M. Brugger, D. C. Rorer. 1993. Enhancement of the epithermal neutron beam at the Brookhaven Medical Research Reactor. Advance in Neutron Capture Therapy, ed. A. H. Soloway, 75-78. Plenum Press, New York and London.

Liu, H. B., R. M. Brugger, D. D. Greenberg, D. C. Rorer, J. P. Hu, and H. M. Hauptman. 1994. Enhancement of the epithermal neutron beam used for boron neutron capture therapy. International Journal of Radiation Oncology and Biological Physics 28(5):1149-1156.

Liu, H. B., and R. M. Brugger. 1994. Conceptual designs of epithermal neutron beams for boron neutron capture therapy from low power reactor. Nuclear Technology 108:151-156.

Liu, H. B., R. M. Brugger, D. C. Rorer, P. R. Tichler and H. Jih-Perng. 1994. Design of a high-flux epithermal neutron beam using ^{235}U fission plates at the Brookhaven Medical Research Reactor. Medical Physics 21(10):1627-1631.

Locher, G. L. 1936. Biological effects and therapeutic possibilities of neutrons. American Journal Roentgenological and Radium Therapy 36:1.

Maker, H. S. and G. M. Lehrer. 1972. Experimental factors in the structure, metabolism and growth of glial tumors. In Experimental Biology of Brain Tumors, ed. M. K. Wolff, E. G. Paoletti and D. Paoletti, 521. Illinois: Springfield.

Matsumoto, T. 1995. Design studies of an epithermal neutron beam for neutron capture therapy at the Musashi reactor. Journal of Nuclear Science and Technology 32(2):87-84.

Matsumoto, T. 1996. Design of neutron beams for boron neutron capture therapy for TRIGA reactor. Journal of Nuclear Science and Technology 33:171-178.

Moss, R. L., F. Stecher-Rasmussen, R. Huiskamp, L. Dewit and B. Mijnheer. 1992. The Petten BNCT project. Progress in Neutron Capture Therapy for Cancer, ed. B. J. Allen et al., 7-11. Plenum Press, New York.

Moss, R. L., F. Stecher-Rasmussen, K. Ravensberg, G. Constantine and P. Watkins. 1992. Design, construction of an epithermal neutron beam for BNCT at the high flux reactor Petten. Progress in Neutron Capture Therapy for Cancer, ed. B. J. Allen et al., 63-66. Plenum Press, New York

Moss, R. L. 1993. Review of reactor-based neutron beam development for BNCT applications. Advances in Neutron Capture Therapy, ed. A. H. Soloway et al., 1-7. Plenum Press, New York and London.

Neuman, W. A. 1990. Neutron beam studies for a medical therapy reactor. Neutron Beam Design, Development, and Performance for Neutron Capture Therapy, ed. O. K. Harling et al., 125-138. Plenum Press, New York and London.

Nigg, D. W., G. J. Storr, and F. J. Wheeler. 1993. Physics parameters for an epithermal neutron beam at the Georgia Institute of Technology. Advances in Neutron Capture Therapy, ed. A. H. Soloway et al., 71-73. Plenum Press, New York.

Oregon State University. 1997. Personal communication, Radiation Center Staff, unpublished data.

Perks, C. A., A. J. Mill, G. Constantine, K. G. Harrison, and J. A. B. Gibson. 1988. A review of boron neutron capture therapy (BNCT) and the design and dosimetry of a high-intensity, 24 keV, neutron beam for BNCT research. The British Journal of Radiology 61:1115-1126.

Rief, H., R. V. Heusden, and G. Perlini. 1993. Generating epithermal neutron beams for BNCT at TRIGA reactors. Advances in Neutron Capture Therapy, ed. A. H. Soloway et al., 85. Plenum Press, New York.

Ross, D., G. Constantine and D. R. Weaver. 1992. Modeling an epithermal neutron beam for a DIDO type reactor using MCNP-a Monte Carlo code. Progress in Neutron Capture Therapy for Cancer, ed. B. J. Allen et al., 67-69. Plenum Press, New York.

Ross, D., G. Constantine, D. R. Weaver and T. D. Beynon. 1993. Designing an epithermal neutron beam for boron neutron capture therapy for a DIDO type reactor using MCNP. Nuclear Instruments and Methods in Physics Research 334:596-606.

Russell, J. L., W. H. Miller, R. M. Brugger and W. H. Herleth. 1990. Georgia Tech research reactor epithermal beam. Neutron Beam Design, Development, and Performance for Neutron Capture Therapy, ed. O. K. Harling et al., 219-227. Plenum Press, New York and London.

Sakurai, Y., S. Fujihara, T. Kobayashi and K. Kanda. 1992. Re-evaluation of thermal neutron field of the KUR heavy water facility for biomedical uses (optimization of bismuth, heavy water and graphite layers). Progress in Neutron Capture Therapy for Cancer, ed. B. J. Allen et al., 101-105. Plenum Press, New York.

Schinazi, R. F., N. Goudgaon, J. Soria and D. C. Liotta. 1993. Synthesis, antiviral activity, cytotoxicity, and cellular pharmacology of 5-carboranyl-pyrimidine nucleosides. Advances in Neutron Capture Therapy, ed. A. H. Soloway et al., 285-288. Plenum Press, New York.

Shefer, R. E., R. E. Klinkowstein, J. C. Yanch and G. L. Brownell. 1992. An epithermal neutron source for BNCT using a tandem cascade accelerator. Progress in Neutron Capture Therapy for Cancer, ed. B. J. Allen et al.,119-121. Plenum Press, New York.

Shigehiro, A., A. Furuhashi, Y. Oka, A. A. Masatsugu, H. Kuga, and H. Tanaka. 1980. Development studies regarding the construction of epithermal enriched neutron field for medical purposes at the University of Tokyo YAYOI fast reactor. Nuclear Technology 48:204-214.

Shih, J. A. and R. M. Brugger. 1992. Gadolinium as a neutron capture therapy agent. Progress in Neutron Capture Therapy for Cancer, ed. B. J. Allen et al.,183-186. Plenum Press, New York.

Soloway, A. H. 1964. Boron compounds in cancer therapy. Progress in Boron Chemistry, 203. Pergamon Press, New York.

Soloway, A. H., F. Alam, R. F. Barth, A. K. M. Anisuzzaman and B. V. Bapat. 1990. Tumor targeting agents for neutron capture therapy. Neutron Beam Design,

Development, and Performance for Neutron Capture Therapy, ed. O. K. Harling et al., 37-45. Plenum Press, New York.

Storr, G. J., B. J. Allen, B. V. Harrington, L. R. Davis, M. M. Elcombe and H. Meriaty. 1992. Progress in Neutron Capture Therapy for Cancer, ed. B. J. Allen et al., 79-81. Plenum Press, New York.

Sweet, W. H. and M. Javid. 1952. The possible use of neutron capturing isotopes such as boron-10 in the treatment of neoplasmas I, intracranial tumor. Journal of Neurosurgery 9:200.

Taguchi, M. 1979. Reactor neutron application for brain tumor therapy in Japan. Technology Transfer Forum on Nuclear Development Technology. INTI, Argentina.

Wallace S. A., B. J. Allen and J. N. Mathur. 1995. Monte Carlo calculations of epithermal boron neutron capture therapy with heavy water. Physics in Medicine and Biology 40:1599-1606.

Wang, C. K., T. E. Blue and J. W. Blue. 1989. An experimental study of the moderator assembly for a low-energy proton accelerator neutron irradiation facility for BNCT. Neutron Beam Design, Development, and Performance for Neutron Capture Therapy, ed. O. K. Harling et al., 271-280. Plenum Press, New York and London.

Watkins, P., G. Constantine, F. Stecher-Rasmussen, W. Freudenreich, R. L. Moss and R. Ricchena. 1992. MCNP calculations for the design and characterisation of the PETTEN BNCT epithermal neutron beam. Progress in Neutron Capture Therapy for Cancer, ed. B. J. Allen et al, 71-73. Plenum Press, New York and London.

Wheeler, F. J., D. K. Parsons, B. L. Rushton and D. W. Nigg. 1989. Epithermal neutron beam design for neutron capture therapy at the Power Burst Facility and the Brookhaven Medical Research Reactor. Nuclear Technology 92:106-117.

Wheeler, F. J., D. K. Parsons, D. W. Nigg, D. E. Wessol, L. G. Miller, and R. G. Fairchild. 1990. Physics design for the Brookhaven Medical Research Reactor epithermal neutron source. Neutron Beam Design, Development, and Performance for Neutron Capture Therapy, ed. O. K. Harling et al., 83-94. Plenum Press, New York and London.

Whittmore, W. L. 1992. A compact TRIGA reactor for boron neutron capture therapy. Progress in Neutron Capture Therapy for Cancer. Progress in Neutron Capture Therapy for Cancer, ed. B. J. Allen et al., 57-62. Plenum Press, New York.

Yanch, J. C., X-L. Zhou, R. E. Shefer, R. E. Klinkowstein and G. L. Brownell. 1992. Design of an accelerator-based epithermal neutron beam for boron neutron capture therapy. Progress in Neutron Capture Therapy for Cancer, ed. B. J. Allen et al.,107-112. Plenum Press, New York.

Yanch, J. C., J. K. Kim, and M. J. Wilson. 1993. Design of a californium-based epithermal neutron beam for neutron capture therapy. Physics in Medicine and Biology 38:1145-1155.

Yanch, J. C. and O. K. Harling. 1993. Dosimetric effects of beam size and collimation of epithermal neutrons for boron neutron capture therapy. Radiation Research 135:131-145.

Yanch, J. C. and O. K. Harling, 1993. A comparison of epithermal neutron beams for NCT: effect of beam collimation on therapy parameters. Advances in Neutron Capture Therapy, ed. A. H. Soloway et al., 67-70. Plenum Press, New York and London.

Yoshiaki, O., I. Yanagisawa, and A. Shigehiro. 1981. A design study of the neutron irradiation facility for boron neutron capture therapy. Nuclear Technology 55:642-654.

Zamenhof, R., H. Madoc-Jones, O. Harling, D. Wazer, S. Saris, J. Yanch, G. Solares, G. Rogers. 1992. The neutron capture therapy research program at New England Medical Center and the Massachusetts Institute of Technology. Progress in Neutron Capture Therapy for Cancer, ed. B. J. Allen et al., 21-26. Plenum Press, New York.

APPENDIX

APPENDIX

A two-step MCNP calculation was performed. In the first step, the surface source write (SSW) file or KCODE fission volume source file was written to be used in the second step, the surface source read (SSR) file. The input file below presents the SSR file for the final design. The commented lines (beginning with a "c") are the first step calculation or SSW file which was used for the criticality calculation and the normalization factor.

MCNP Input for Oregon State University TRIGA Mark-II Reactor

```
OSU TRIGA bp4 (D2O) bp3 20.12 cm S, 91 cm Si cone R=6 cm, 0.1 cm Li2CO3
c void
13000   0 1 $ void outside reactor
13001   0 -1 601 $ void above reactor
13002   0 -1 -606 $ void below reactor
13003   0 -1 -1000 $ void outside bp4
13004   0 -1 3000 3001 $ void outside DXTRAN sphere
13005   0 877 -617 890 -601 606 886 -1 $ right side outside reactor
13006   0 -877 882 -601 871 890 886 $ above thermalizing column
13007   0 -877 882 -876 606 890 886 $ below thermalizing column
13008   0 -882 -617 890 -601 606 886 1041 902 $ left side outside reactor
13010   0 -1 -886 902 -601 606 $ left of thermalizing column
13011   0 -1 618 1044 858 -601 606 #30000 #13019 $ right of thermal column
13012   0 -612 617 890 1042 -601 606 -848 -618 $ left side outside reactor
13013   0 607 617 -618 890 -601 606 -1 $ right side outside reactor
13014   0 -612 848 1044 -858 617 -618 -601 606 1000 $ outside reactor bp3
13015   0 -902 1043 1000 -617 -601 606 -1 $ outside reactor bp4
13016   0 618 612 -607 -858 -601 606 -1 #13011 $ outside TC
13017   0 618 607 -858 -601 606 -1 $ outside TC
13018   0 618 -612 1044 -858 617 -601 606 -1 $ around bp3
13019   0 -1 -3000 858 617 -612 618 3001 -601 606 $ void outside DXTRAN sphere
13020   0 -1 -3000 858 617 1000 -618 3001 -601 606 $ void outside DXTRAN sphere
13021   0 -1 3000 -1044 $ void outside DXTRAN sphere
13022   0 -1 -618 3000 1044 -3001 $ void outside DXTRAN sphere
c Al cladding
15000   1 -2.7 -5 4 2 -3 #15003 vol=7302.0827 $ core vessel
15001   1 -2.7 -7 9 13 -701 -615 877 $ right side of reactor
15004   1 -2.7 -7 9 13 -701 -877 882 -617 $ in front of thermalizing column
15005   1 -2.7 -7 9 13 -701 -882 -613 #(-835 13 -701) #(-838 13 -701) $ between TC and Th column
15006   1 -2.7 -7 9 13 -701 613 615 617 $ in front of TC
15002   1 -2.7 -601 606 -890 889 #(-607 612 -601 606 889 -890 617)
      #(-877 882 -871 876 889 -890 -617) #(889 -890 -835 -617)
      #(889 -890 -838 617) $ around reactor tank
```

```
15003   1 -2.7 -617 2 -3 -835 vol=142.20728 $ disk at core vessel in front of bp4
c thermal column
16000   6 -1.0 701 -702 615 613 -601 606 617 $ water gap
16001   1 -2.7 702 -703 615 613 -601 606 617 vol=31514.3997 $ front Al cladding
16002   1 -2.7 615 -616 703 -607 -601 606 617 vol=3843.197 $ right angle
16003   1 -2.7 613 -614 703 612 -601 606 617 vol=3843.197 $ left angle
16004   1 -2.7 616 -618 -607 608 -601 606 $ right
16005   1 -2.7 614 -618 -611 612 -601 606 $ left
16006   1 -2.7 703 616 614 -608 611 -618 -601 602 $ top
16007   1 -2.7 703 616 614 -608 611 -618 -605 606 $ bottom
16008   10 -2.48 703 616 614 -609 610 -618 -602 603 $b4c top
16009   10 -2.48 703 616 614 -609 610 -618 -604 605 $ b4c bottom
16010   10 -2.48 616 -618 -608 609 -602 605 $ b4c right
16011   10 -2.48 614 -618 -610 611 -602 605 $ b4c left
16012   4 0.085205 703 616 614 -609 610 -619 -603 604 $ graphite
16013   4 0.085205 619 -618 -609 610 -603 604 $ graphite
c thermalizing column
17000   6 -1.0 701 -702 -877 882 -601 606 -617 vol=20828.981 $ water gap
17001   1 -2.7 702 -703 -877 882 -871 876 -617 vol=9943.8022 $ front Al
17002   1 -2.7 703 -877 878 -871 876 886 -617 vol=4229.17498 $ right Al
17003   1 -2.7 703 -881 882 -871 876 886 -617 vol=4229.17498 $ left Al
17004   1 -2.7 703 886 -617 -871 872 -878 881 vol=4367.551 $ top Al
17005   1 -2.7 703 886 -617 -875 876 -878 881 vol=4367.551 $ bottom Al
17006   10 -2.48 703 886 -617 -878 879 -872 875 vol=1059.7933 $ b4c right
17007   10 -2.48 703 886 -617 -880 881 -872 875 vol=1059.7933 $ b4c left
17008   10 -2.48 703 886 -617 -879 880 -872 873 vol=1062.5544 $ b4c top
17009   10 -2.48 703 886 -617 -879 880 -874 875 vol=1062.5544 $ b4c bottom
17010   4 0.085205 703 883 -873 874 -879 880 -617 vol=61012.553 $ graphite
17011   5 -11.4 -883 884 -873 874 -879 880 $ lead
17012   19 -1.029e-3 -884 885 -873 874 -879 880 $ air
17013   4 0.085205 -885 886 -873 874 -879 880 $ graphite
c core internals
18000   1 -2.7 -5 6 -2 vol=3597.67 $ top grid
18001   1 -2.7 -8 4 -2 vol=4268.05 $ bottom grid
18002   2 0.0958666 -6 7 -2 vol=6681.39 $ top end fittings
18003   2 0.0958666 -9 8 -2 vol=14368.3 $ bottom end fittings
c reflector region
19000   1 -2.7 -7 11 3 -10 1001 1002 1003 1004 1005 1006
      1007 1008 1009 1010 1011 1012 1013 1014 1015 1016 1017
      1018 1019 1020 1021 1022 1023 1024 1025 1026 1027 1028
      1029 1030 1031 1032 1033 1034 1035 1036 1037 1038 1039 1040
      1040 vol=41415.67284 $ around lazy susan
19001   4 0.085205 -7 11 10 -12 vol=118198.5445 $ graphite around lazy susan
19002   4 0.085205 -11 9 3 -12 #(-833 -835 -13) #(834 -838 -13) $ graphite
19003   4 0.085205 12 -13 -7 9 613 615 617 $ graphite in TC lead
19004   4 0.085205 12 -13 -7 9 -877 882 -617 $ graphite in Th. colum
19005   5 -11.4 12 -13 -615 617 -7 9 $ lead 1st quadrant
19006   5 -11.4 12 -13 877 -617 -7 9 $ lead 2nd quadrant
19007   5 -11.4 12 -13 -882 -617 -7 9 #(-835 12 -13 -868)
      #(-838 12 -13 -868) $ lead 3rd quadrant
19008   5 -11.4 12 -13 -613 617 -7 9 #(-838 12 -13 -868) $ lead 4th quadrant
c water region
20000   6 -1.0 -3 -601 5 $ above core
20001   6 -1.0 -3 606 -4 $ below core
20002   6 -1.0 -701 3 -601 7 $ above reflector
```

```
20003   6 -1.0 -701 3 606 -9 $ below reflector
20004   6 -1.0 701 -889 617 -615 -601 606 $ 1st quadrant
20005   6 -1.0 -889 615 607 -601 606 $ corner 1st quadrant
20006   6 -1.0 701 -889 -617 877 -601 606 $ 2nd quadrant
20007   6 -1.0 701 -889 -617 -882 -601 606 835 838 $ 3rd quadrant
20008   6 -1.0 701 -889 617 -613 -601 606 838 $ 4th quadrant
20009   6 -1.0 -889 613 -612 -601 606 $ corner 4th quadrant
20010   6 -1.0 702 -889 -877 882 -601 871 -617 $ above thermalizing column
20011   6 -1.0 702 -889 -877 882 606 -876 -617 $ below thermalizing column
c inside core rods and moderator
17      6 -1.0 26 29 32 35 38 41 44 47 50 53 55 58 61 64 67 70 73 76  $ inner core
        79 82 85 88 91 97 100 103 106 109 112 115 118 124 127 130 133
        -18 17 -19 -617
18      6 -1.0 26 29 32 35 38 41 44 47 50 53 55 58 61 64 67 70 73 76  $ inner top reflector region
        79 82 85 88 91 97 100 103 106 109 112 115 118 124 127 130 133 -7
        18 -19 -617
19      6 -1.0 26 29 32 35 38 41 44 47 50 53 55 58 61 64 67 70 73 76  $ inner bottom reflector region
        79 82 85 88 91 97 100 103 106 109 112 115 118 124 127 130 133
        -17 9 -19 -617
20      6 -1.0 82 85 88 91 94 97 100 103 106 109 112 115 118 121 124 $ outer core 1
        127 130 133 136 139 142 145 148 151 154 157 160 163 166 169 172
        175 178 181 184 187 190 193 196 199 202 205 -18 17 19 -20 -617
21      6 -1.0 82 85 88 91 94 97 100 103 106 109 112 115 118 121 124 $ outer top reflector 1
        127 130 133 136 139 142 145 148 151 154 157 160 163 166 169 172
        175 178 181 184 187 190 193 196 199 202 205 -7 18 19 -20 -617
22      6 -1.0 82 85 88 91 94 97 100 103 106 109 112 115 118 121 124  $ bottom reflector region 1
        127 130 133 136 139 142 145 148 151 154 157 160 163 166 169 172
        175 178 181 184 187 190 193 196 199 202 205 -17 9 19 -20 -617
23      6 -1.0 136 139 142 145 148 151 154 157 160 163 166 169 172 175 $ outer core 2
        178 181 184 187 190 193 196 199 202 205 -18 17 20 -21 -617
24      6 -1.0 136 139 142 145 148 151 154 157 160 163 166 169 172 175 $ outer top reflector 2
        178 181 184 187 190 193 196 199 202 205 -7 18 20 -21 -617
25      6 -1.0 136 139 142 145 148 151 154 157 160 163 166 169 172 175 $ bottom reflector region 2
        178 181 184 187 190 193 196 199 202 205 -17 9 20 -21 -617
26      6 -1.0 136 139 142 145 148 151 157 160 163 166 169 172 175 178 $ outer core 3
        181 184 187 193 196 199 202 205 208 211 214 217 218 221 224 227
        230 233 236 237 240 243 246 249 252 255 258 259 262 265 268 271
        274 277 278 281 293 296 -18 17 21 -22 -617
27      6 -1.0 136 139 142 145 148 151 157 160 163 166 169 172 175 178 $ outer top reflector 3
        181 184 187 193 196 199 202 205 208 211 214 217 218 221 224 227
        230 233 236 237 240 243 246 249 252 255 258 259 262 265 268 271
        274 277 278 281 293 296 -7 18 21 -22 -617
28      6 -1.0 136 139 142 145 148 151 157 160 163 166 169 172 175 178 $ bottom reflector region 3
        181 184 187 193 196 199 202 205 208 211 214 217 218 221 224 227
        230 233 236 237 240 243 246 249 252 255 258 259 262 265 268 271
        274 277 278 281 293 296 -17 9 21 -22 -617
29      6 -1.0 208 211 214 217 218 221 224 227 230 233 236 237 240 243 $ outer core 4
        246 249 252 255 258 259 262 265 268 271 274 277 278 281 293 296
        298 300 302 304 306 308 310 312 314 315 316 317 318 319 320 322
        324 326 328 330 332 333 334 335 336 337 338 339 341 343 345 347
        349 351 353 355 -18 17 22 -23 -617
30      6 -1.0 208 211 214 217 218 221 224 227 230 233 236 237 240 243 $ outer top reflector 4
        246 249 252 255 258 259 262 265 268 271 274 277 278 281 293 296
        298 300 302 304 306 308 310 312 314 315 316 317 318 319 320 322
        324 326 328 330 332 333 334 335 336 337 338 339 341 343 345 347
```

```
     349 351 353 355 -7 18 22 -23 -617
31     6 -1.0 208 211 214 217 218 221 224 227 230 233 236 237 240 243 $ bottom reflector region 4
     246 249 252 255 258 259 262 265 268 271 274 277 278 281 293 296
     298 300 302 304 306 308 310 312 314 315 316 317 318 319 320 322
     324 326 328 330 332 333 334 335 336 337 338 339 341 343 345 347
     349 351 353 355 -17 9 22 -23 -617
32     6 -1.0 298 300 302 304 306 308 310 312 314 315 316 317 318 319 $ outer core 5
     320 322 324 326 328 330 332 333 334 335 336 337 338 339 341 343
     345 347 349 351 353 355 -18 17 23 -24 -617
33     6 -1.0 298 300 302 304 306 308 310 312 314 315 316 317 318 319  $ outer top reflector 5
     320 322 324 326 328 330 332 333 334 335 336 337 338 339 341 343
     345 347 349 351 353 355 -7 18 23 -24 -617
34     6 -1.0 298 300 302 304 306 308 310 312 314 315 316 317 318 319  $ bottom reflector region 5
     320 322 324 326 328 330 332 333 334 335 336 337 338 339 341 343
     345 347 349 351 353 355 -17 9 23 -24 -617
35     6 -1.0 298 300 302 304 306 308 310 312 314 315 316 317 318 319  $ outer core 6
     320 322 324 326 328 330 332 333 334 335 336 337 338 339 341 343
     345 347 349 351 353 355 -18 17 24 -2 -617
36     6 -1.0 298 300 302 304 306 308 310 312 314 315 316 317 318 319  $ outer top reflector 6
     320 322 324 326 328 330 332 333 334 335 336 337 338 339 341 343
     345 347 349 351 353 355 -7 18 24 -2 -617
37     6 -1.0 298 300 302 304 306 308 310 312 314 315 316 317 318 319  $ bottom reflector region 6
     320 322 324 326 328 330 332 333 334 335 336 337 338 339 341 343
     345 347 349 351 353 355 -17 9 24 -2 -617
11017  6 -1.0 26 29 32 35 38 41 44 47 50 53 55 58 61 64 67 70 73 76  $ inner core
     79 82 85 88 91 97 100 103 106 109 112 115 118 124 127 130 133
     -18 17 -19 617
11018  6 -1.0 26 29 32 35 38 41 44 47 50 53 55 58 61 64 67 70 73 76  $ inner top reflector region
     79 82 85 88 91 97 100 103 106 109 112 115 118 124 127 130 133 -7
     18 -19 617
11019  6 -1.0 26 29 32 35 38 41 44 47 50 53 55 58 61 64 67 70 73 76  $ inner bottom reflector region
     79 82 85 88 91 97 100 103 106 109 112 115 118 124 127 130 133
     -17 9 -19 617
11020  6 -1.0 82 85 88 91 94 97 100 103 106 109 112 115 118 121 124 $ outer core 1
     127 130 133 136 139 142 145 148 151 154 157 160 163 166 169 172
     175 178 181 184 187 190 193 196 199 202 205 -18 17 19 -20 617
11021  6 -1.0 82 85 88 91 94 97 100 103 106 109 112 115 118 121 124 $ outer top reflector 1
     127 130 133 136 139 142 145 148 151 154 157 160 163 166 169 172
     175 178 181 184 187 190 193 196 199 202 205 -7 18 19 -20 617
11022  6 -1.0 82 85 88 91 94 97 100 103 106 109 112 115 118 121 124  $ bottom reflector region 1
     127 130 133 136 139 142 145 148 151 154 157 160 163 166 169 172
     175 178 181 184 187 190 193 196 199 202 205 -17 9 19 -20 617
11023  6 -1.0 136 139 142 145 148 151 154 157 160 163 166 169 172 175 $ outer core 2
     178 181 184 187 190 193 196 199 202 205 -18 17 20 -21 617
11024  6 -1.0 136 139 142 145 148 151 154 157 160 163 166 169 172 175 $ outer top reflector 2
     178 181 184 187 190 193 196 199 202 205 -7 18 20 -21 617
11025  6 -1.0 136 139 142 145 148 151 154 157 160 163 166 169 172 175 $ bottom reflector region 2
     178 181 184 187 190 193 196 199 202 205 -17 9 20 -21 617
11026  6 -1.0 136 139 142 145 148 151 157 160 163 166 169 172 175 178 $ outer core 3
     181 184 187 193 196 199 202 205 208 211 214 217 218 221 224 227
     230 233 236 237 240 243 246 249 252 255 258 259 262 265 268 271
     274 277 278 281 293 296 -18 17 21 -22 617
11027  6 -1.0 136 139 142 145 148 151 157 160 163 166 169 172 175 178 $ outer top reflector 3
     181 184 187 193 196 199 202 205 208 211 214 217 218 221 224 227
     230 233 236 237 240 243 246 249 252 255 258 259 262 265 268 271
```

```
     274 277 278 281 293 296 -7 18 21 -22 617
11028  6 -1.0 136 139 142 145 148 151 157 160 163 166 169 172 175 178 $ bottom reflector region 3
     181 184 187 193 196 199 202 205 208 211 214 217 218 221 224 227
     230 233 236 237 240 243 246 249 252 255 258 259 262 265 268 271
     274 277 278 281 293 296 -17 9 21 -22 617
11029  6 -1.0 208 211 214 217 218 221 224 227 230 233 236 237 240 243 $ outer core 4
     246 249 252 255 258 259 262 265 268 271 274 277 278 281 293 296
     298 300 302 304 306 308 310 312 314 315 316 317 318 319 320 322
     324 326 328 330 332 333 334 335 336 337 338 339 341 343 345 347
     349 351 353 355 -18 17 22 -23 617
11030  6 -1.0 208 211 214 217 218 221 224 227 230 233 236 237 240 243 $ outer top reflector 4
     246 249 252 255 258 259 262 265 268 271 274 277 278 281 293 296
     298 300 302 304 306 308 310 312 314 315 316 317 318 319 320 322
     324 326 328 330 332 333 334 335 336 337 338 339 341 343 345 347
     349 351 353 355 -7 18 22 -23 617
11031  6 -1.0 208 211 214 217 218 221 224 227 230 233 236 237 240 243 $ bottom reflector region 4
     246 249 252 255 258 259 262 265 268 271 274 277 278 281 293 296
     298 300 302 304 306 308 310 312 314 315 316 317 318 319 320 322
     324 326 328 330 332 333 334 335 336 337 338 339 341 343 345 347
     349 351 353 355 -17 9 22 -23 617
11032  6 -1.0 298 300 302 304 306 308 310 312 314 315 316 317 318 319 $ outer core 5
     320 322 324 326 328 330 332 333 334 335 336 337 338 339 341 343
     345 347 349 351 353 355 -18 17 23 -24 617
11033  6 -1.0 298 300 302 304 306 308 310 312 314 315 316 317 318 319  $ outer top reflector 5
     320 322 324 326 328 330 332 333 334 335 336 337 338 339 341 343
     345 347 349 351 353 355 -7 18 23 -24 617
11034  6 -1.0 298 300 302 304 306 308 310 312 314 315 316 317 318 319  $ bottom reflector region 5
     320 322 324 326 328 330 332 333 334 335 336 337 338 339 341 343
     345 347 349 351 353 355 -17 9 23 -24 617
11035  6 -1.0 298 300 302 304 306 308 310 312 314 315 316 317 318 319  $ outer core 6
     320 322 324 326 328 330 332 333 334 335 336 337 338 339 341 343
     345 347 349 351 353 355 -18 17 24 -2 617
11036  6 -1.0 298 300 302 304 306 308 310 312 314 315 316 317 318 319  $ outer top reflector 6
     320 322 324 326 328 330 332 333 334 335 336 337 338 339 341 343
     345 347 349 351 353 355 -7 18 24 -2 617
11037  6 -1.0 298 300 302 304 306 308 310 312 314 315 316 317 318 319  $ bottom reflector region 6
     320 322 324 326 328 330 332 333 334 335 336 337 338 339 341 343
     345 347 349 351 353 355 -17 9 24 -2 617
38     6 -1.0 -7 9 -25  vol=580.666  $ water region central thimble -#a1
39     7 0.085755 -7 9 25 -26  vol=32.8228  $ cladding central thimble -#a1
40     8 0.042234 -18 17 -27  vol=12.066  $ central zr rod ss-#b1
41     9 0.0928308 -18 17 27 -28  vol=385.479  $ fueled region ss-#b1
42     4 0.080193 -7 18 -28  vol=91.1953  $ gr reflector ss-#b1
43     4 0.080193 -17 9 -28  vol=91.9257  $ gr reflector ss-#b1
44     7 0.085755 -7 9 28 -29  vol=32.8228  $ cladding ss-#b1
45     8 0.042234 -18 17 -30  vol=12.066  $ central zr rod ss-#b2
46     9 0.0928308 -18 17 30 -31  vol=385.479  $ fueled region ss-#b2
47     4 0.080193 -7 18 -31  vol=91.1953  $ gr reflector ss-#b2
48     4 0.080193 -17 9 -31  vol=91.9257  $ gr reflector ss-#b2
49     7 0.085755 -7 9 31 -32  vol=32.8228  $ cladding ss-#b2
50     8 0.042234 -18 17 -33  vol=12.066  $ central zr rod ss-#b3
51     9 0.0928308 -18 17 33 -34  vol=385.479  $ fueled region ss-#b3
52     4 0.080193 -7 18 -34  vol=91.1953  $ gr reflector ss-#b3
53     4 0.080193 -17 9 -34  vol=91.9257  $ gr reflector ss-#b3
54     7 0.085755 -7 9 34 -35  vol=32.8228  $ cladding ss-#b3
```

```
8 0.042234 -18 17 -36  vol=12.066  $ central zr rod ss-#b4
9 0.0928308 -18 17 36 -37  vol=385.479  $ fueled region ss-#b4
4 0.080193 -7 18 -37  vol=91.1953  $ gr reflector ss-#b4
4 0.080193 -17 9 -37  vol=91.9257  $ gr reflector ss-#b4
7 0.085755 -7 9 37 -38  vol=32.8228  $ cladding ss-#b4
8 0.042234 -18 17 -39  vol=12.066  $ central zr rod ss-#b5
9 0.0928308 -18 17 39 -40  vol=385.479  $ fueled region ss-#b5
4 0.080193 -7 18 -40  vol=91.1953  $ gr reflector ss-#b5
4 0.080193 -17 9 -40  vol=91.9257  $ gr reflector ss-#b5
7 0.085755 -7 9 40 -41  vol=32.8228  $ cladding ss-#b5
8 0.042234 -18 17 -42  vol=12.066  $ central zr rod ss-#b6
9 0.0928308 -18 17 42 -43  vol=385.479  $ fueled region ss-#b6
4 0.080193 -7 18 -43  vol=91.1953  $ gr reflector ss-#b6
4 0.080193 -17 9 -43  vol=91.9257  $ gr reflector ss-#b6
7 0.085755 -7 9 43 -44  vol=32.8228  $ cladding ss-#b6
8 0.042234 -18 17 -45  vol=12.066  $ central zr rod ss-#c1
9 0.0928308 -18 17 45 -46  vol=385.479  $ fueled region ss-#c1
4 0.080193 -7 18 -46  vol=91.1953  $ gr reflector ss-#c1
4 0.080193 -17 9 -46  vol=91.9257  $ gr reflector ss-#c1
7 0.085755 -7 9 46 -47  vol=32.8228  $ cladding ss-#c1
8 0.042234 -18 17 -48  vol=12.066  $ central zr rod ss-#c2
9 0.0928308 -18 17 48 -49  vol=385.479  $ fueled region ss-#c2
4 0.080193 -7 18 -49  vol=91.1953  $ gr reflector ss-#c2
4 0.080193 -17 9 -49  vol=91.9257  $ gr reflector ss-#c2
7 0.085755 -7 9 49 -50  vol=32.8228  $ cladding ss-#c2
8 0.042234 -18 17 -51  vol=12.066  $ central zr rod ss-#c3
9 0.0928308 -18 17 51 -52  vol=385.479  $ fueled region ss-#c3
4 0.080193 -7 18 -52  vol=91.1953  $ gr reflector ss-#c3
4 0.080193 -17 9 -52  vol=91.9257  $ gr reflector ss-#c3
7 0.085755 -7 9 52 -53  vol=32.8228  $ cladding ss-#c3
10 -2.48 -7 18 -54  vol=91.1953  $ control rod poison control w/o fuel-#c4
19 -1.029e-3 -18 9 -54  vol=489.471  $ air region control w/o fuel-#c4
7 0.085755 -7 9 54 -55  vol=42.0765  $ cladding control w/o fuel-#c4
8 0.042234 -18 17 -56  vol=12.066  $ central zr rod ss-#c5
9 0.0928308 -18 17 56 -57  vol=385.479  $ fueled region ss-#c5
4 0.080193 -7 18 -57  vol=91.1953  $ gr reflector ss-#c5
4 0.080193 -17 9 -57  vol=91.9257  $ gr reflector ss-#c5
7 0.085755 -7 9 57 -58  vol=32.8228  $ cladding ss-#c5
8 0.042234 -18 17 -59  vol=12.066  $ central zr rod ss-#c6
9 0.0928308 -18 17 59 -60  vol=385.479  $ fueled region ss-#c6
4 0.080193 -7 18 -60  vol=91.1953  $ gr reflector ss-#c6
4 0.080193 -17 9 -60  vol=91.9257  $ gr reflector ss-#c6
7 0.085755 -7 9 60 -61  vol=32.8228  $ cladding ss-#c6
8 0.042234 -18 17 -62  vol=12.066  $ central zr rod ss-#c7
9 0.0928308 -18 17 62 -63  vol=385.479  $ fueled region ss-#c7
4 0.080193 -7 18 -63  vol=91.1953  $ gr reflector ss-#c7
4 0.080193 -17 9 -63  vol=91.9257  $ gr reflector ss-#c7
7 0.085755 -7 9 63 -64  vol=32.8228  $ cladding ss-#c7
8 0.042234 -18 17 -65  vol=12.066  $ central zr rod ss-#c8
9 0.0928308 -18 17 65 -66  vol=385.479  $ fueled region ss-#c8
4 0.080193 -7 18 -66  vol=91.1953  $ gr reflector ss-#c8
4 0.080193 -17 9 -66  vol=91.9257  $ gr reflector ss-#c8
7 0.085755 -7 9 66 -67  vol=32.8228  $ cladding ss-#c8
8 0.042234 -18 17 -68  vol=12.066  $ central zr rod ss-#c9
9 0.0928308 -18 17 68 -69  vol=385.479  $ fueled region ss-#c9
```

```
110   4 0.080193 -7 18 -69  vol=91.1953  $ gr reflector ss-#c9
111   4 0.080193 -17 9 -69  vol=91.9257  $ gr reflector ss-#c9
112   7 0.085755 -7 9 69 -70  vol=32.8228  $ cladding ss-#c9
113   10 -2.48 -7 18 -71  vol=91.1953  $ control rod poison con w/fuel-#c10
114   8 0.042234 -18 9 -72  vol=14.856  $ central zr rod con w/fuel-#c10
115   12 -5.0 -18 9 72 -71  vol=474.615  $ fueled region con w/fuel-#c10
116   7 0.085755 -7 9 71 -73  vol=32.8228  $ cladding con w/fuel-#c10
117   8 0.042234 -18 17 -74  vol=12.066  $ central zr rod ss-#c11
118   9 0.0928308 -18 17 74 -75  vol=385.479  $ fueled region ss-#c11
119   4 0.080193 -7 18 -75  vol=91.1953  $ gr reflector ss-#c11
120   4 0.080193 -17 9 -75  vol=91.9257  $ gr reflector ss-#c11
121   7 0.085755 -7 9 75 -76  vol=32.8228  $ cladding ss-#c11
122   8 0.042234 -18 17 -77  vol=12.066  $ central zr rod ss-#c12
123   9 0.0928308 -18 17 77 -78  vol=385.479  $ fueled region ss-#c12
124   4 0.080193 -7 18 -78  vol=91.1953  $ gr reflector ss-#c12
125   4 0.080193 -17 9 -78  vol=91.9257  $ gr reflector ss-#c12
126   7 0.085755 -7 9 78 -79  vol=32.8228  $ cladding ss-#c12
127   10 -2.48 -7 18 -80  vol=91.1953  $ control rod poison con w/fuel-#d1
128   8 0.042234 -18 9 -81  vol=14.856  $ central zr rod con w/fuel-#d1
129   12 -5.0 -18 9 81 -80  vol=474.615  $ fueled region con w/fuel-#d1
130   7 0.085755 -7 9 80 -82  vol=32.8228  $ cladding con w/fuel-#d1
131   8 0.042234 -18 17 -83  vol=12.066  $ central zr rod ss-#d2
132   9 0.0928308 -18 17 83 -84  vol=385.479  $ fueled region ss-#d2
133   4 0.080193 -7 18 -84  vol=91.1953  $ gr reflector ss-#d2
134   4 0.080193 -17 9 -84  vol=91.9257  $ gr reflector ss-#d2
135   7 0.085755 -7 9 84 -85  vol=32.8228  $ cladding ss-#d2
136   8 0.042234 -18 17 -86  vol=12.066  $ central zr rod ss-#d3
137   9 0.0928308 -18 17 86 -87  vol=385.479  $ fueled region ss-#d3
138   4 0.080193 -7 18 -87  vol=91.1953  $ gr reflector ss-#d3
139   4 0.080193 -17 9 -87  vol=91.9257  $ gr reflector ss-#d3
140   7 0.085755 -7 9 87 -88  vol=32.8228  $ cladding ss-#d3
141   8 0.042234 -18 17 -89  vol=12.066  $ central zr rod ss-#d4
142   9 0.0928308 -18 17 89 -90  vol=385.479  $ fueled region ss-#d4
143   4 0.080193 -7 18 -90  vol=91.1953  $ gr reflector ss-#d4
144   4 0.080193 -17 9 -90  vol=91.9257  $ gr reflector ss-#d4
145   7 0.085755 -7 9 90 -91  vol=32.8228  $ cladding ss-#d4
146   8 0.042234 -18 17 -92  vol=12.066  $ central zr rod ss-#d5
147   9 0.0928308 -18 17 92 -93  vol=385.479  $ fueled region ss-#d5
148   4 0.080193 -7 18 -93  vol=91.1953  $ gr reflector ss-#d5
149   4 0.080193 -17 9 -93  vol=91.9257  $ gr reflector ss-#d5
150   7 0.085755 -7 9 93 -94  vol=32.8228  $ cladding ss-#d5
151   8 0.042234 -18 17 -95  vol=12.066  $ central zr rod ss-#d6
152   9 0.0928308 -18 17 95 -96  vol=385.479  $ fueled region ss-#d6
153   4 0.080193 -7 18 -96  vol=91.1953  $ gr reflector ss-#d6
154   4 0.080193 -17 9 -96  vol=91.9257  $ gr reflector ss-#d6
155   7 0.085755 -7 9 96 -97  vol=32.8228  $ cladding ss-#d6
156   8 0.042234 -18 17 -98  vol=12.066  $ central zr rod ss-#d7
157   9 0.0928308 -18 17 98 -99  vol=385.479  $ fueled region ss-#d7
158   4 0.080193 -7 18 -99  vol=91.1953  $ gr reflector ss-#d7
159   4 0.080193 -17 9 -99  vol=91.9257  $ gr reflector ss-#d7
160   7 0.085755 -7 9 99 -100  vol=32.8228  $ cladding ss-#d7
161   8 0.042234 -18 17 -101  vol=12.066  $ central zr rod ss-#d8
162   9 0.0928308 -18 17 101 -102  vol=385.479  $ fueled region ss-#d8
163   4 0.080193 -7 18 -102  vol=91.1953  $ gr reflector ss-#d8
164   4 0.080193 -17 9 -102  vol=91.9257  $ gr reflector ss-#d8
```

```
7 0.085755 -7 9 102 -103  vol=32.8228  $ cladding ss-#d8
8 0.042234 -18 17 -104  vol=12.066  $ central zr rod ss-#d9
9 0.0928308 -18 17 104 -105  vol=385.479  $ fueled region ss-#d9
4 0.080193 -7 18 -105  vol=91.1953  $ gr reflector ss-#d9
4 0.080193 -17 9 -105  vol=91.9257  $ gr reflector ss-#d9
7 0.085755 -7 9 105 -106  vol=32.8228  $ cladding ss-#d9
10 -2.48 -7 18 -107  vol=91.1953  $ control rod poison con w/fuel-#d10
8 0.042234 -18 9 -108  vol=14.856  $ central zr rod con w/fuel-#d10
12 -5.0 -18 9 108 -107  vol=474.615  $ fueled region con w/fuel-#d10
7 0.085755 -7 9 107 -109  vol=32.8228  $ cladding con w/fuel-#d10
8 0.042234 -18 17 -110  vol=12.066  $ central zr rod ss-#d11
9 0.0928308 -18 17 110 -111  vol=385.479  $ fueled region ss-#d11
4 0.080193 -7 18 -111  vol=91.1953  $ gr reflector ss-#d11
4 0.080193 -17 9 -111  vol=91.9257  $ gr reflector ss-#d11
7 0.085755 -7 9 111 -112  vol=32.8228  $ cladding ss-#d11
8 0.042234 -18 17 -113  vol=12.066  $ central zr rod ss-#d12
9 0.0928308 -18 17 113 -114  vol=385.479  $ fueled region ss-#d12
4 0.080193 -7 18 -114  vol=91.1953  $ gr reflector ss-#d12
4 0.080193 -17 9 -114  vol=91.9257  $ gr reflector ss-#d12
7 0.085755 -7 9 114 -115  vol=32.8228  $ cladding ss-#d12
8 0.042234 -18 17 -116  vol=12.066  $ central zr rod ss-#d13
9 0.0928308 -18 17 116 -117  vol=385.479  $ fueled region ss-#d13
4 0.080193 -7 18 -117  vol=91.1953  $ gr reflector ss-#d13
4 0.080193 -17 9 -117  vol=91.9257  $ gr reflector ss-#d13
7 0.085755 -7 9 117 -118  vol=32.8228  $ cladding ss-#d13
8 0.042234 -18 17 -119  vol=12.066  $ central zr rod ss-#d14
9 0.0928308 -18 17 119 -120  vol=385.479  $ fueled region ss-#d14
4 0.080193 -7 18 -120  vol=91.1953  $ gr reflector ss-#d14
4 0.080193 -17 9 -120  vol=91.9257  $ gr reflector ss-#d14
7 0.085755 -7 9 120 -121  vol=32.8228  $ cladding ss-#d14
8 0.042234 -18 17 -122  vol=12.066  $ central zr rod ss-#d15
9 0.0928308 -18 17 122 -123  vol=385.479  $ fueled region ss-#d15
4 0.080193 -7 18 -123  vol=91.1953  $ gr reflector ss-#d15
4 0.080193 -17 9 -123  vol=91.9257  $ gr reflector ss-#d15
7 0.085755 -7 9 123 -124  vol=32.8228  $ cladding ss-#d15
8 0.042234 -18 17 -125  vol=12.066  $ central zr rod ss-#d16
9 0.0928308 -18 17 125 -126  vol=385.479  $ fueled region ss-#d16
4 0.080193 -7 18 -126  vol=91.1953  $ gr reflector ss-#d16
4 0.080193 -17 9 -126  vol=91.9257  $ gr reflector ss-#d16
7 0.085755 -7 9 126 -127  vol=32.8228  $ cladding ss-#d16
8 0.042234 -18 17 -128  vol=12.066  $ central zr rod ss-#d17
9 0.0928308 -18 17 128 -129  vol=385.479  $ fueled region ss-#d17
4 0.080193 -7 18 -129  vol=91.1953  $ gr reflector ss-#d17
4 0.080193 -17 9 -129  vol=91.9257  $ gr reflector ss-#d17
7 0.085755 -7 9 129 -130  vol=32.8228  $ cladding ss-#d17
8 0.042234 -18 17 -131  vol=12.066  $ central zr rod ss-#d18
9 0.0928308 -18 17 131 -132  vol=385.479  $ fueled region ss-#d18
4 0.080193 -7 18 -132  vol=91.1953  $ gr reflector ss-#d18
4 0.080193 -17 9 -132  vol=91.9257  $ gr reflector ss-#d18
7 0.085755 -7 9 132 -133  vol=32.8228  $ cladding ss-#d18
8 0.042234 -18 17 -134  vol=12.066  $ central zr rod ss-#e1
9 0.0928308 -18 17 134 -135  vol=385.479  $ fueled region ss-#e1
4 0.080193 -7 18 -135  vol=91.1953  $ gr reflector ss-#e1
4 0.080193 -17 9 -135  vol=91.9257  $ gr reflector ss-#e1
7 0.085755 -7 9 135 -136  vol=32.8228  $ cladding ss-#e1
```

```
8 0.042234 -18 17 -137  vol=12.066  $ central zr rod ss-#e2
9 0.0928308 -18 17 137 -138  vol=385.479  $ fueled region ss-#e2
4 0.080193 -7 18 -138  vol=91.1953  $ gr reflector ss-#e2
4 0.080193 -17 9 -138  vol=91.9257  $ gr reflector ss-#e2
7 0.085755 -7 9 138 -139  vol=32.8228  $ cladding ss-#e2
8 0.042234 -18 17 -140  vol=12.066  $ central zr rod ss-#e3
9 0.0928308 -18 17 140 -141  vol=385.479  $ fueled region ss-#e3
4 0.080193 -7 18 -141  vol=91.1953  $ gr reflector ss-#e3
4 0.080193 -17 9 -141  vol=91.9257  $ gr reflector ss-#e3
7 0.085755 -7 9 141 -142  vol=32.8228  $ cladding ss-#e3
8 0.042234 -18 17 -143  vol=12.066  $ central zr rod ss-#e4
9 0.0928308 -18 17 143 -144  vol=385.479  $ fueled region ss-#e4
4 0.080193 -7 18 -144  vol=91.1953  $ gr reflector ss-#e4
4 0.080193 -17 9 -144  vol=91.9257  $ gr reflector ss-#e4
7 0.085755 -7 9 144 -145  vol=32.8228  $ cladding ss-#e4
8 0.042234 -18 17 -146  vol=12.066  $ central zr rod ss-#e5
9 0.0928308 -18 17 146 -147  vol=385.479  $ fueled region ss-#e5
4 0.080193 -7 18 -147  vol=91.1953  $ gr reflector ss-#e5
4 0.080193 -17 9 -147  vol=91.9257  $ gr reflector ss-#e5
7 0.085755 -7 9 147 -148  vol=32.8228  $ cladding ss-#e5
8 0.042234 -18 17 -149  vol=12.066  $ central zr rod ss-#e6
9 0.0928308 -18 17 149 -150  vol=385.479  $ fueled region ss-#e6
4 0.080193 -7 18 -150  vol=91.1953  $ gr reflector ss-#e6
4 0.080193 -17 9 -150  vol=91.9257  $ gr reflector ss-#e6
7 0.085755 -7 9 150 -151  vol=32.8228  $ cladding ss-#e6
8 0.042234 -18 17 -152  vol=12.066  $ central zr rod ss-#e7
9 0.0928308 -18 17 152 -153  vol=385.479  $ fueled region ss-#e7
4 0.080193 -7 18 -153  vol=91.1953  $ gr reflector ss-#e7
4 0.080193 -17 9 -153  vol=91.9257  $ gr reflector ss-#e7
7 0.085755 -7 9 153 -154  vol=32.8228  $ cladding ss-#e7
8 0.042234 -18 17 -155  vol=12.066  $ central zr rod ss-#e8
9 0.0928308 -18 17 155 -156  vol=385.479  $ fueled region ss-#e8
4 0.080193 -7 18 -156  vol=91.1953  $ gr reflector ss-#e8
4 0.080193 -17 9 -156  vol=91.9257  $ gr reflector ss-#e8
7 0.085755 -7 9 156 -157  vol=32.8228  $ cladding ss-#e8
8 0.042234 -18 17 -158  vol=12.066  $ central zr rod ss-#e9
9 0.0928308 -18 17 158 -159  vol=385.479  $ fueled region ss-#e9
4 0.080193 -7 18 -159  vol=91.1953  $ gr reflector ss-#e9
4 0.080193 -17 9 -159  vol=91.9257  $ gr reflector ss-#e9
7 0.085755 -7 9 159 -160  vol=32.8228  $ cladding ss-#e9
8 0.042234 -18 17 -161  vol=12.066  $ central zr rod ss-#e10
9 0.0928308 -18 17 161 -162  vol=385.479  $ fueled region ss-#e10
4 0.080193 -7 18 -162  vol=91.1953  $ gr reflector ss-#e10
4 0.080193 -17 9 -162  vol=91.9257  $ gr reflector ss-#e10
7 0.085755 -7 9 162 -163  vol=32.8228  $ cladding ss-#e10
8 0.042234 -18 17 -164  vol=12.066  $ central zr rod ss-#e11
9 0.0928308 -18 17 164 -165  vol=385.479  $ fueled region ss-#e11
4 0.080193 -7 18 -165  vol=91.1953  $ gr reflector ss-#e11
4 0.080193 -17 9 -165  vol=91.9257  $ gr reflector ss-#e11
7 0.085755 -7 9 165 -166  vol=32.8228  $ cladding ss-#e11
8 0.042234 -18 17 -167  vol=12.066  $ central zr rod ss-#e12
9 0.0928308 -18 17 167 -168  vol=385.479  $ fueled region ss-#e12
4 0.080193 -7 18 -168  vol=91.1953  $ gr reflector ss-#e12
4 0.080193 -17 9 -168  vol=91.9257  $ gr reflector ss-#e12
7 0.085755 -7 9 168 -169  vol=32.8228  $ cladding ss-#e12
```

```
8 0.042234 -18 17 -170  vol=12.066  $ central zr rod ss-#e13
9 0.0928308 -18 17 170 -171  vol=385.479  $ fueled region ss-#e13
4 0.080193 -7 18 -171  vol=91.1953  $ gr reflector ss-#e13
4 0.080193 -17 9 -171  vol=91.9257  $ gr reflector ss-#e13
7 0.085755 -7 9 171 -172  vol=32.8228  $ cladding ss-#e13
8 0.042234 -18 17 -173  vol=12.066  $ central zr rod ss-#e14
9 0.0928308 -18 17 173 -174  vol=385.479  $ fueled region ss-#e14
4 0.080193 -7 18 -174  vol=91.1953  $ gr reflector ss-#e14
4 0.080193 -17 9 -174  vol=91.9257  $ gr reflector ss-#e14
7 0.085755 -7 9 174 -175  vol=32.8228  $ cladding ss-#e14
8 0.042234 -18 17 -176  vol=12.066  $ central zr rod ss-#e15
9 0.0928308 -18 17 176 -177  vol=385.479  $ fueled region ss-#e15
4 0.080193 -7 18 -177  vol=91.1953  $ gr reflector ss-#e15
4 0.080193 -17 9 -177  vol=91.9257  $ gr reflector ss-#e15
7 0.085755 -7 9 177 -178  vol=32.8228  $ cladding ss-#e15
8 0.042234 -18 17 -179  vol=12.066  $ central zr rod ss-#e16
9 0.0928308 -18 17 179 -180  vol=385.479  $ fueled region ss-#e16
4 0.080193 -7 18 -180  vol=91.1953  $ gr reflector ss-#e16
4 0.080193 -17 9 -180  vol=91.9257  $ gr reflector ss-#e16
7 0.085755 -7 9 180 -181  vol=32.8228  $ cladding ss-#e16
8 0.042234 -18 17 -182  vol=12.066  $ central zr rod ss-#e17
9 0.0928308 -18 17 182 -183  vol=385.479  $ fueled region ss-#e17
4 0.080193 -7 18 -183  vol=91.1953  $ gr reflector ss-#e17
4 0.080193 -17 9 -183  vol=91.9257  $ gr reflector ss-#e17
7 0.085755 -7 9 183 -184  vol=32.8228  $ cladding ss-#e17
8 0.042234 -18 17 -185  vol=12.066  $ central zr rod ss-#e18
9 0.0928308 -18 17 185 -186  vol=385.479  $ fueled region ss-#e18
4 0.080193 -7 18 -186  vol=91.1953  $ gr reflector ss-#e18
4 0.080193 -17 9 -186  vol=91.9257  $ gr reflector ss-#e18
7 0.085755 -7 9 186 -187  vol=32.8228  $ cladding ss-#e18
8 0.042234 -18 17 -188  vol=12.066  $ central zr rod ss-#e19
9 0.0928308 -18 17 188 -189  vol=385.479  $ fueled region ss-#e19
4 0.080193 -7 18 -189  vol=91.1953  $ gr reflector ss-#e19
4 0.080193 -17 9 -189  vol=91.9257  $ gr reflector ss-#e19
7 0.085755 -7 9 189 -190  vol=32.8228  $ cladding ss-#e19
8 0.042234 -18 17 -191  vol=12.066  $ central zr rod ss-#e20
9 0.0928308 -18 17 191 -192  vol=385.479  $ fueled region ss-#e20
4 0.080193 -7 18 -192  vol=91.1953  $ gr reflector ss-#e20
4 0.080193 -17 9 -192  vol=91.9257  $ gr reflector ss-#e20
7 0.085755 -7 9 192 -193  vol=32.8228  $ cladding ss-#e20
8 0.042234 -18 17 -194  vol=12.066  $ central zr rod ss-#e21
9 0.0928308 -18 17 194 -195  vol=385.479  $ fueled region ss-#e21
4 0.080193 -7 18 -195  vol=91.1953  $ gr reflector ss-#e21
4 0.080193 -17 9 -195  vol=91.9257  $ gr reflector ss-#e21
7 0.085755 -7 9 195 -196  vol=32.8228  $ cladding ss-#e21
8 0.042234 -18 17 -197  vol=12.066  $ central zr rod ss-#e22
9 0.0928308 -18 17 197 -198  vol=385.479  $ fueled region ss-#e22
4 0.080193 -7 18 -198  vol=91.1953  $ gr reflector ss-#e22
4 0.080193 -17 9 -198  vol=91.9257  $ gr reflector ss-#e22
7 0.085755 -7 9 198 -199  vol=32.8228  $ cladding ss-#e22
8 0.042234 -18 17 -200  vol=12.066  $ central zr rod ss-#e23
9 0.0928308 -18 17 200 -201  vol=385.479  $ fueled region ss-#e23
4 0.080193 -7 18 -201  vol=91.1953  $ gr reflector ss-#e23
4 0.080193 -17 9 -201  vol=91.9257  $ gr reflector ss-#e23
7 0.085755 -7 9 201 -202  vol=32.8228  $ cladding ss-#e23
```

```
330   8 0.042234 -18 17 -203  vol=12.066  $ central zr rod ss-#e24
331   9 0.0928308 -18 17 203 -204  vol=385.479  $ fueled region ss-#e24
332   4 0.080193 -7 18 -204  vol=91.1953  $ gr reflector ss-#e24
333   4 0.080193 -17 9 -204  vol=91.9257  $ gr reflector ss-#e24
334   7 0.085755 -7 9 204 -205  vol=32.8228  $ cladding ss-#e24
335   8 0.042234 -18 17 -206  vol=12.066  $ central zr rod ss-#f1
336   9 0.0928308 -18 17 206 -207  vol=385.479  $ fueled region ss-#f1
337   4 0.080193 -7 18 -207  vol=91.1953  $ gr reflector ss-#f1
338   4 0.080193 -17 9 -207  vol=91.9257  $ gr reflector ss-#f1
339   7 0.085755 -7 9 207 -208  vol=32.8228  $ cladding ss-#f1
655   6 -1.0 -7 9 -211  vol=613.489  $ water water -#f2
345   8 0.042234 -18 17 -212  vol=12.066  $ central zr rod ss-#f3
346   9 0.0928308 -18 17 212 -213  vol=385.479  $ fueled region ss-#f3
347   4 0.080193 -7 18 -213  vol=91.1953  $ gr reflector ss-#f3
348   4 0.080193 -17 9 -213  vol=91.9257  $ gr reflector ss-#f3
349   7 0.085755 -7 9 213 -214  vol=32.8228  $ cladding ss-#f3
350   8 0.042234 -18 17 -215  vol=12.066  $ central zr rod ss-#f4
351   9 0.0928308 -18 17 215 -216  vol=385.479  $ fueled region ss-#f4
352   4 0.080193 -7 18 -216  vol=91.1953  $ gr reflector ss-#f4
353   4 0.080193 -17 9 -216  vol=91.9257  $ gr reflector ss-#f4
354   7 0.085755 -7 9 216 -217  vol=32.8228  $ cladding ss-#f4
600   8 0.042234 -18 17 -400  vol=12.066  $ central zr rod ss-#f5
601   9 0.0928308 -18 17 400 -401  vol=385.479  $ fueled region ss-#f5
602   4 0.080193 -7 18 -401  vol=91.1953  $ gr reflector ss-#f5
603   4 0.080193 -17 9 -401  vol=91.9257  $ gr reflector ss-#f5
604   7 0.085755 -7 9 401 -218  vol=32.8228  $ cladding ss-#f5
356   8 0.042234 -18 17 -219  vol=12.066  $ central zr rod ss-#f6
357   9 0.0928308 -18 17 219 -220  vol=385.479  $ fueled region ss-#f6
358   4 0.080193 -7 18 -220  vol=91.1953  $ gr reflector ss-#f6
359   4 0.080193 -17 9 -220  vol=91.9257  $ gr reflector ss-#f6
360   7 0.085755 -7 9 220 -221  vol=32.8228  $ cladding ss-#f6
361   8 0.042234 -18 17 -222  vol=12.066  $ central zr rod ss-#f7
362   9 0.0928308 -18 17 222 -223  vol=385.479  $ fueled region ss-#f7
363   4 0.080193 -7 18 -223  vol=91.1953  $ gr reflector ss-#f7
364   4 0.080193 -17 9 -223  vol=91.9257  $ gr reflector ss-#f7
365   7 0.085755 -7 9 223 -224  vol=32.8228  $ cladding ss-#f7
366   8 0.042234 -18 17 -225  vol=12.066  $ central zr rod ss-#f8
367   9 0.0928308 -18 17 225 -226  vol=385.479  $ fueled region ss-#f8
368   4 0.080193 -7 18 -226  vol=91.1953  $ gr reflector ss-#f8
369   4 0.080193 -17 9 -226  vol=91.9257  $ gr reflector ss-#f8
370   7 0.085755 -7 9 226 -227  vol=32.8228  $ cladding ss-#f8
371   8 0.042234 -18 17 -228  vol=12.066  $ central zr rod ss-#f9
372   9 0.0928308 -18 17 228 -229  vol=385.479  $ fueled region ss-#f9
373   4 0.080193 -7 18 -229  vol=91.1953  $ gr reflector ss-#f9
374   4 0.080193 -17 9 -229  vol=91.9257  $ gr reflector ss-#f9
375   7 0.085755 -7 9 229 -230  vol=32.8228  $ cladding ss-#f9
376   8 0.042234 -18 17 -231  vol=12.066  $ central zr rod ss-#f10
377   9 0.0928308 -18 17 231 -232  vol=385.479  $ fueled region ss-#f10
378   4 0.080193 -7 18 -232  vol=91.1953  $ gr reflector ss-#f10
379   4 0.080193 -17 9 -232  vol=91.9257  $ gr reflector ss-#f10
380   7 0.085755 -7 9 232 -233  vol=32.8228  $ cladding ss-#f10
381   8 0.042234 -18 17 -234  vol=12.066  $ central zr rod ss-#f11
382   9 0.0928308 -18 17 234 -235  vol=385.479  $ fueled region ss-#f11
383   4 0.080193 -7 18 -235  vol=91.1953  $ gr reflector ss-#f11
384   4 0.080193 -17 9 -235  vol=91.9257  $ gr reflector ss-#f11
```

```
385   7 0.085755 -7 9 235 -236  vol=32.8228  $ cladding ss-#f11
605   8 0.042234 -18 17 -402  vol=12.066  $ central zr rod ss-#f12
606   9 0.0928308 -18 17 402 -403  vol=385.479  $ fueled region ss-#f12
607   4 0.080193 -7 18 -403  vol=91.1953  $ gr reflector ss-#f12
608   4 0.080193 -17 9 -403  vol=91.9257  $ gr reflector ss-#f12
609   7 0.085755 -7 9 403 -237  vol=32.8228  $ cladding ss-#f12
387   8 0.042234 -18 17 -238  vol=12.066  $ central zr rod ss-#f13
388   9 0.0928308 -18 17 238 -239  vol=385.479  $ fueled region ss-#f13
389   4 0.080193 -7 18 -239  vol=91.1953  $ gr reflector ss-#f13
390   4 0.080193 -17 9 -239  vol=91.9257  $ gr reflector ss-#f13
391   7 0.085755 -7 9 239 -240  vol=32.8228  $ cladding ss-#f13
392   8 0.042234 -18 17 -241  vol=12.066  $ central zr rod ss-#f14
393   9 0.0928308 -18 17 241 -242  vol=385.479  $ fueled region ss-#f14
394   4 0.080193 -7 18 -242  vol=91.1953  $ gr reflector ss-#f14
395   4 0.080193 -17 9 -242  vol=91.9257  $ gr reflector ss-#f14
396   7 0.085755 -7 9 242 -243  vol=32.8228  $ cladding ss-#f14
397   8 0.042234 -18 17 -244  vol=12.066  $ central zr rod ss-#f15
398   9 0.0928308 -18 17 244 -245  vol=385.479  $ fueled region ss-#f15
399   4 0.080193 -7 18 -245  vol=91.1953  $ gr reflector ss-#f15
400   4 0.080193 -17 9 -245  vol=91.9257  $ gr reflector ss-#f15
401   7 0.085755 -7 9 245 -246  vol=32.8228  $ cladding ss-#f15
402   8 0.042234 -18 17 -247  vol=12.066  $ central zr rod ss-#f16
403   9 0.0928308 -18 17 247 -248  vol=385.479  $ fueled region ss-#f16
404   4 0.080193 -7 18 -248  vol=91.1953  $ gr reflector ss-#f16
405   4 0.080193 -17 9 -248  vol=91.9257  $ gr reflector ss-#f16
406   7 0.085755 -7 9 248 -249  vol=32.8228  $ cladding ss-#f16
407   8 0.042234 -18 17 -250  vol=12.066  $ central zr rod ss-#f17
408   9 0.0928308 -18 17 250 -251  vol=385.479  $ fueled region ss-#f17
409   4 0.080193 -7 18 -251  vol=91.1953  $ gr reflector ss-#f17
410   4 0.080193 -17 9 -251  vol=91.9257  $ gr reflector ss-#f17
411   7 0.085755 -7 9 251 -252  vol=32.8228  $ cladding ss-#f17
412   8 0.042234 -18 17 -253  vol=12.066  $ central zr rod ss-#f18
413   9 0.0928308 -18 17 253 -254  vol=385.479  $ fueled region ss-#f18
414   4 0.080193 -7 18 -254  vol=91.1953  $ gr reflector ss-#f18
415   4 0.080193 -17 9 -254  vol=91.9257  $ gr reflector ss-#f18
416   7 0.085755 -7 9 254 -255  vol=32.8228  $ cladding ss-#f18
417   8 0.042234 -18 17 -256  vol=12.066  $ central zr rod ss-#f19
418   9 0.0928308 -18 17 256 -257  vol=385.479  $ fueled region ss-#f19
419   4 0.080193 -7 18 -257  vol=91.1953  $ gr reflector ss-#f19
420   4 0.080193 -17 9 -257  vol=91.9257  $ gr reflector ss-#f19
421   7 0.085755 -7 9 257 -258  vol=32.8228  $ cladding ss-#f19
610   4 0.080193 -7 9 -405  vol=580.666  $ graphite region gr-#f20
611   7 0.085755 -7 9 405 -259  vol=32.8228  $ cladding gr-#f20
663   4 0.080193 -7 9 -261  vol=580.666  $ graphite region gr-#f21
427   7 0.085755 -7 9 261 -262  vol=32.8228  $ cladding ss-#f21
664   4 0.080193 -7 9 -264  vol=580.666  $ graphite region gr-#f22
432   7 0.085755 -7 9 264 -265  vol=32.8228  $ cladding ss-#f22
665   4 0.080193 -7 9 -267  vol=580.666  $ graphite region gr-#f23
437   7 0.085755 -7 9 267 -268  vol=32.8228  $ cladding ss-#f23
666   4 0.080193 -7 9 -270  vol=580.666  $ graphite region gr-#f24
442   7 0.085755 -7 9 270 -271  vol=32.8228  $ cladding ss-#f24
667   4 0.080193 -7 9 -273  vol=580.666  $ graphite region gr-#f25
447   7 0.085755 -7 9 273 -274  vol=32.8228  $ cladding ss-#f25
668   4 0.080193 -7 9 -276  vol=580.666  $ graphite region gr-#f26
452   7 0.085755 -7 9 276 -277  vol=32.8228  $ cladding ss-#f26
```

```
669   4 0.080193 -7 9 -407  vol=580.666  $ graphite region gr-#f27
619   7 0.085755 -7 9 407 -278  vol=32.8228  $ cladding ss-#f27
454   8 0.042234 -18 17 -279  vol=12.066  $ central zr rod ss-#f28
455   4 0.080193 -7 18 -280  vol=91.1953  $ gr reflector ss-#f28
456   4 0.080193 -17 9 -280  vol=91.9257  $ gr reflector ss-#f28
457   7 0.085755 -7 9 280 -281  vol=32.8228  $ cladding ss-#f28
458   9 0.0928308 -18 282 279 -280  vol=38.5479  $ segment top ss-#f28
459   9 0.0928308 -282 283 279 -280  vol=38.5479  $ segment2 ss-#f28
460   9 0.0928308 -283 284 279 -280  vol=38.5479  $ segment3 ss-#f28
461   9 0.0928308 -284 285 279 -280  vol=38.5479  $ segment4 ss-#f28
462   9 0.0928308 -285 286 279 -280  vol=38.5479  $ segment5 ss-#f28
463   9 0.0928308 -286 287 279 -280  vol=38.5479  $ segment6 ss-#f28
464   9 0.0928308 -287 288 279 -280  vol=38.5479  $ segment7 ss-#f28
465   9 0.0928308 -288 289 279 -280  vol=38.5479  $ segment8 ss-#f28
466   9 0.0928308 -289 290 279 -280  vol=38.5479  $ segment9 ss-#f28
467   9 0.0928308 -290 17 279 -280  vol=38.5479  $ segment bottom ss-#f28
468   8 0.042234 -18 17 -291  vol=12.066  $ central zr rod ss-#f29
469   9 0.0928308 -18 17 291 -292  vol=385.479  $ fueled region ss-#f29
470   4 0.080193 -7 18 -292  vol=91.1953  $ gr reflector ss-#f29
471   4 0.080193 -17 9 -292  vol=91.9257  $ gr reflector ss-#f29
472   7 0.085755 -7 9 292 -293  vol=32.8228  $ cladding ss-#f29
473   8 0.042234 -18 17 -294  vol=12.066  $ central zr rod ss-#f30
474   9 0.0928308 -18 17 294 -295  vol=385.479  $ fueled region ss-#f30
475   4 0.080193 -7 18 -295  vol=91.1953  $ gr reflector ss-#f30
476   4 0.080193 -17 9 -295  vol=91.9257  $ gr reflector ss-#f30
477   7 0.085755 -7 9 295 -296  vol=32.8228  $ cladding ss-#f30
478   4 0.080193 -7 9 -297  vol=580.666  $ graphite region gr-#g1
479   7 0.085755 -7 9 297 -298  vol=32.8228  $ cladding gr-#g1
480   19 -1.029e-3 -7 830 -299 $ void of rabbit-#g2
670   19 -1.029e-3 -830 831 -299 $ void of rabbit-#g2
671   19 -1.029e-3 -831 9 -299 $ void of rabbit-#g2
481   1 -2.7 -7 9 299 -300  vol=32.8228  $ cladding gr-#g2
482   4 0.080193 -7 9 -301  vol=580.666  $ graphite region gr-#g3
483   7 0.085755 -7 9 301 -302  vol=32.8228  $ cladding gr-#g3
484   4 0.080193 -7 9 -303  vol=580.666  $ graphite region gr-#g4
485   7 0.085755 -7 9 303 -304  vol=32.8228  $ cladding gr-#g4
486   4 0.080193 -7 9 -305  vol=580.666  $ graphite region gr-#g5
487   7 0.085755 -7 9 305 -306  vol=32.8228  $ cladding gr-#g5
488   4 0.080193 -7 9 -307  vol=580.666  $ graphite region gr-#g6
489   7 0.085755 -7 9 307 -308  vol=32.8228  $ cladding gr-#g6
490   4 0.080193 -7 9 -309  vol=580.666  $ graphite region gr-#g7
491   7 0.085755 -7 9 309 -310  vol=32.8228  $ cladding gr-#g7
492   4 0.080193 -7 9 -311  vol=580.666  $ graphite region gr-#g8
493   7 0.085755 -7 9 311 -312  vol=32.8228  $ cladding gr-#g8
494   4 0.080193 -7 9 -313  vol=580.666  $ graphite region gr-#g9
495   7 0.085755 -7 9 313 -314  vol=32.8228  $ cladding gr-#g9
620   8 0.042234 -18 17 -408  vol=12.066  $ central zr rod ss-#g10
621   9 0.0928308 -18 17 408 -409  vol=385.479  $ fueled region ss-#g10
622   4 0.080193 -7 18 -409  vol=91.1953  $ gr reflector ss-#g10
623   4 0.080193 -17 9 -409  vol=91.9257  $ gr reflector ss-#g10
624   7 0.085755 -7 9 409 -315  vol=32.8228  $ cladding ss-#g10
625   8 0.042234 -18 17 -410  vol=12.066  $ central zr rod ss-#g11
626   9 0.0928308 -18 17 410 -411  vol=385.479  $ fueled region ss-#g11
627   4 0.080193 -7 18 -411  vol=91.1953  $ gr reflector ss-#g11
628   4 0.080193 -17 9 -411  vol=91.9257  $ gr reflector ss-#g11
```

```
629     7 0.085755 -7 9 411 -316  vol=32.8228  $ cladding ss-#g11
630     8 0.042234 -18 17 -412  vol=12.066  $ central zr rod ss-#g12
631     9 0.0928308 -18 17 412 -413  vol=385.479  $ fueled region ss-#g12
632     4 0.080193 -7 18 -413  vol=91.1953  $ gr reflector ss-#g12
633     4 0.080193 -17 9 -413  vol=91.9257  $ gr reflector ss-#g12
634     7 0.085755 -7 9 413 -317  vol=32.8228  $ cladding ss-#g12
635     8 0.042234 -18 17 -414  vol=12.066  $ central zr rod ss-#g13
636     9 0.0928308 -18 17 414 -415  vol=385.479  $ fueled region ss-#g13
637     4 0.080193 -7 18 -415  vol=91.1953  $ gr reflector ss-#g13
638     4 0.080193 -17 9 -415  vol=91.9257  $ gr reflector ss-#g13
639     7 0.085755 -7 9 415 -318  vol=32.8228  $ cladding ss-#g13
640     8 0.042234 -18 17 -416  vol=12.066  $ central zr rod ss-#g14
641     9 0.0928308 -18 17 416 -417  vol=385.479  $ fueled region ss-#g14
642     4 0.080193 -7 18 -417  vol=91.1953  $ gr reflector ss-#g14
643     4 0.080193 -17 9 -417  vol=91.9257  $ gr reflector ss-#g14
644     7 0.085755 -7 9 417 -319  vol=32.8228  $ cladding ss-#g14
645     8 0.042234 -18 17 -418  vol=12.066  $ central zr rod ss-#g15
646     9 0.0928308 -18 17 418 -419  vol=385.479  $ fueled region ss-#g15
647     4 0.080193 -7 18 -419  vol=91.1953  $ gr reflector ss-#g15
648     4 0.080193 -17 9 -419  vol=91.9257  $ gr reflector ss-#g15
649     7 0.085755 -7 9 419 -320  vol=32.8228  $ cladding ss-#g15
650     8 0.042234 -18 17 -420  vol=12.066  $ central zr rod ss-#g16
651     9 0.0928308 -18 17 420 -321  vol=385.479  $ fueled region ss-#g16
652     4 0.080193 -7 18 -321  vol=91.1953  $ gr reflector ss-#g16
653     4 0.080193 -17 9 -321  vol=91.9257  $ gr reflector ss-#g16
654     7 0.085755 -7 9 321 -322  vol=32.8228  $ cladding ss-#g16
504     4 0.080193 -7 9 -323  vol=580.666  $ graphite region gr-#g17
505     7 0.085755 -7 9 323 -324  vol=32.8228  $ cladding gr-#g17
506     4 0.080193 -7 9 -325  vol=580.666  $ graphite region gr-#g18
507     7 0.085755 -7 9 325 -326  vol=32.8228  $ cladding gr-#g18
508     4 0.080193 -7 9 -327  vol=580.666  $ graphite region gr-#g19
509     7 0.085755 -7 9 327 -328  vol=32.8228  $ cladding gr-#g19
510     4 0.080193 -7 9 -329  vol=580.666  $ graphite region gr-#g20
511     7 0.085755 -7 9 329 -330  vol=32.8228  $ cladding gr-#g20
512     4 0.080193 -7 9 -331  vol=580.666  $ graphite region gr-#g21
513     7 0.085755 -7 9 331 -332  vol=32.8228  $ cladding gr-#g21
514     6 -1.0 -7 9 -333  vol=613.489  $ water water -#g22
515     6 -1.0 -7 9 -334  vol=613.489  $ water water -#g23
516     6 -1.0 -7 9 -335  vol=613.489  $ water water -#g24
517     6 -1.0 -7 9 -336  vol=613.489  $ water water -#g25
518     6 -1.0 -7 9 -337  vol=613.489  $ water water -#g26
519     6 -1.0 -7 9 -338  vol=613.489  $ water water -#g27
520     6 -1.0 -7 9 -339  vol=613.489  $ water water -#g28
656     6 -1.0 -7 9 -341  vol=613.489  $ water water -#g29
657     6 -1.0 -7 9 -343  vol=613.489  $ water water -#g30
658     6 -1.0 -7 9 -345  vol=613.489  $ water water -#g31
659     6 -1.0 -7 9 -347  vol=613.489  $ water water -#g32
660     6 -1.0 -7 9 -349  vol=613.489  $ water water -#g33
661     6 -1.0 -7 9 -351  vol=613.489  $ water water -#g34
2003    6 -1.0 -7 1045 -353 vol=474.36507 $ 1st segment of rabbit #g35
2004    6 -1.0 9 -1046 -353 vol=128.09951 $ 2nd segment of rabbit #g35
2005    6 -1.0 -1045 1046 -353 vol=11.024055 $ 1cm above the bottom of rabbit
535     4 0.080193 -7 9 -354  vol=580.666  $ graphite region gr-#g36
536     7 0.085755 -7 9 354 -355  vol=32.8228  $ cladding gr-#g36
c lazy susan rack segment
```

```
5000    19 -1.029e-3 -7 1047 -1001 vol=85.19564
5001    19 -1.029e-3 -7 1047 -1002 vol=85.19564
5003    19 -1.029e-3 -7 1047 -1003 vol=85.19564
5004    19 -1.029e-3 -7 1047 -1004 vol=85.19564
5005    19 -1.029e-3 -7 1047 -1005 vol=85.19564
5006    19 -1.029e-3 -7 1047 -1006 vol=85.19564
5007    19 -1.029e-3 -7 1047 -1007 vol=85.19564
5008    19 -1.029e-3 -7 1047 -1008 vol=85.19564
5009    19 -1.029e-3 -7 1047 -1009 vol=85.19564
5010    19 -1.029e-3 -7 1047 -1010 vol=85.19564
5011    19 -1.029e-3 -7 1047 -1011 vol=85.19564
5012    19 -1.029e-3 -7 1047 -1012 vol=85.19564
5013    19 -1.029e-3 -7 1047 -1013 vol=85.19564
5014    19 -1.029e-3 -7 1047 -1014 vol=85.19564
5015    19 -1.029e-3 -7 1047 -1015 vol=85.19564
5016    19 -1.029e-3 -7 1047 -1016 vol=85.19564
5017    19 -1.029e-3 -7 1047 -1017 vol=85.19564
5018    19 -1.029e-3 -7 1047 -1018 vol=85.19564
5019    19 -1.029e-3 -7 1047 -1019 vol=85.19564
5020    19 -1.029e-3 -7 1047 -1020 vol=85.19564
5021    19 -1.029e-3 -7 1047 -1021 vol=85.19564
5022    19 -1.029e-3 -7 1047 -1022 vol=85.19564
5023    19 -1.029e-3 -7 1047 -1023 vol=85.19564
5024    19 -1.029e-3 -7 1047 -1024 vol=85.19564
5025    19 -1.029e-3 -7 1047 -1025 vol=85.19564
5026    19 -1.029e-3 -7 1047 -1026 vol=85.19564
5027    19 -1.029e-3 -7 1047 -1027 vol=85.19564
5028    19 -1.029e-3 -7 1047 -1028 vol=85.19564
5029    19 -1.029e-3 -7 1047 -1029 vol=85.19564
5030    19 -1.029e-3 -7 1047 -1030 vol=85.19564
5031    19 -1.029e-3 -7 1047 -1031 vol=85.19564
5032    19 -1.029e-3 -7 1047 -1032 vol=85.19564
5033    19 -1.029e-3 -7 1047 -1033 vol=85.19564
5034    19 -1.029e-3 -7 1047 -1034 vol=85.19564
5035    19 -1.029e-3 -7 1047 -1035 vol=85.19564
5036    19 -1.029e-3 -7 1047 -1036 vol=85.19564
5037    19 -1.029e-3 -7 1047 -1037 vol=85.19564
5038    19 -1.029e-3 -7 1047 -1038 vol=85.19564
5039    19 -1.029e-3 -7 1047 -1039 vol=85.19564
5040    19 -1.029e-3 -7 1047 -1040 vol=85.19564
c the segment 1 cm above the bottom of lazy susan
5041    19 -1.029e-3 -1047 11 -1001 vol=4.10433
5042    19 -1.029e-3 -1047 11 -1002 vol=4.10433
5043    19 -1.029e-3 -1047 11 -1003 vol=4.10433
5044    19 -1.029e-3 -1047 11 -1004 vol=4.10433
5045    19 -1.029e-3 -1047 11 -1005 vol=4.10433
5046    19 -1.029e-3 -1047 11 -1006 vol=4.10433
5047    19 -1.029e-3 -1047 11 -1007 vol=4.10433
5048    19 -1.029e-3 -1047 11 -1008 vol=4.10433
5049    19 -1.029e-3 -1047 11 -1009 vol=4.10433
5050    19 -1.029e-3 -1047 11 -1010 vol=4.10433
5051    19 -1.029e-3 -1047 11 -1011 vol=4.10433
5052    19 -1.029e-3 -1047 11 -1012 vol=4.10433
5053    19 -1.029e-3 -1047 11 -1013 vol=4.10433
5054    19 -1.029e-3 -1047 11 -1014 vol=4.10433
```

```
5055    19 -1.029e-3 -1047 11 -1015 vol=4.10433
5056    19 -1.029e-3 -1047 11 -1016 vol=4.10433
5057    19 -1.029e-3 -1047 11 -1017 vol=4.10433
5058    19 -1.029e-3 -1047 11 -1018 vol=4.10433
5059    19 -1.029e-3 -1047 11 -1019 vol=4.10433
5060    19 -1.029e-3 -1047 11 -1020 vol=4.10433
5061    19 -1.029e-3 -1047 11 -1021 vol=4.10433
5062    19 -1.029e-3 -1047 11 -1022 vol=4.10433
5063    19 -1.029e-3 -1047 11 -1023 vol=4.10433
5064    19 -1.029e-3 -1047 11 -1024 vol=4.10433
5065    19 -1.029e-3 -1047 11 -1025 vol=4.10433
5066    19 -1.029e-3 -1047 11 -1026 vol=4.10433
5067    19 -1.029e-3 -1047 11 -1027 vol=4.10433
5068    19 -1.029e-3 -1047 11 -1028 vol=4.10433
5069    19 -1.029e-3 -1047 11 -1029 vol=4.10433
5070    19 -1.029e-3 -1047 11 -1030 vol=4.10433
5071    19 -1.029e-3 -1047 11 -1031 vol=4.10433
5072    19 -1.029e-3 -1047 11 -1032 vol=4.10433
5073    19 -1.029e-3 -1047 11 -1033 vol=4.10433
5074    19 -1.029e-3 -1047 11 -1034 vol=4.10433
5075    19 -1.029e-3 -1047 11 -1035 vol=4.10433
5076    19 -1.029e-3 -1047 11 -1036 vol=4.10433
5077    19 -1.029e-3 -1047 11 -1037 vol=4.10433
5078    19 -1.029e-3 -1047 11 -1038 vol=4.10433
5079    19 -1.029e-3 -1047 11 -1039 vol=4.10433
5080    19 -1.029e-3 -1047 11 -1040 vol=4.10433
c outer region of bp3 (air region for DXTRAN sphere)
30000   19 -1.029e-3 -3001 -612 617 858 -3000 3002 vol=59464.74838 $ air region
30001   19 -1.029e-3 -3002 #3045 vol=531.17268 $ sphere tally at bp3
c beam port 4
4011    1 -2.7 -836 -833 899 vol=43.9499 $ al plate bp4
4012    20 -1.1 -836 -899 1048 vol=1989.587 $ al pipe bp4
4013    20 -1.1 -836 -1048 1049 $ al pipe bp4
4014    20 -1.1 -836 -1049 1050 $ al pipe bp4
4015    20 -1.1 -836 -1050 1051 $ al pipe bp4
4016    19 -1.029e-3 -836 -1051 1052 $ al pipe bp4
4017    19 -1.029e-3 -836 -1052 1053 $ al pipe bp4
4018    19 -1.029e-3 -836 -1053 1054 $ al pipe bp4
4019    19 -1.029e-3 -836 -1054 902 $ end of al pipe bp4
4020    19 -1.029e-3 -800 -902 903 vol=128.3135 $ al plate bp4
4021    19 -1.029e-3 -800 -903 904 $ steel plate bp4
4022    19 -1.029e-3 -800 -904 905 vol=5196.697 $ steel pipe bp4
4023    19 -1.029e-3 -800 -905 906 $ steel pipe bp4
4024    19 -1.029e-3 -800 -906 907 $ steel pipe bp4
4025    19 -1.029e-3 -800 -907 908 $ steel pipe bp4
4026    19 -1.029e-3 -800 -908 909 $ steel pipe bp4
4027    19 -1.029e-3 -800 -909 1000 $ end of steel pipe bp4
c al and steel cladding bp4
6011    1 -2.7 -835 836 -833 899 vol=4.42204 $ al cladding bp4
6012    1 -2.7 -835 836 -899 1048 vol=200.1833 $ al cladding bp4
6013    1 -2.7 -835 836 -1048 1049 $ al cladding bp4
6014    1 -2.7 -835 836 -1049 1050 $ al cladding bp4
6015    1 -2.7 -835 836 -1050 1051 $ al cladding bp4
6016    1 -2.7 -835 836 -1051 1052 $ al cladding bp4
6017    1 -2.7 -835 836 -1052 1053 $ al cladding bp4
```

```
6018    1 -2.7 -835 836 -1053 1054 $ al cladding bp4
6019    1 -2.7 -835 836 -1054 902 $ end of al cladding bp4
6020    16 -7.86 800 -801 -902 903 vol=33.43498 $ steel cladding bp4
6021    16 -7.86 800 -801 -903 904 $ steel cladding bp4
6022    16 -7.86 800 -801 -904 905 vol=1354.117 $ steel cladding bp4
6023    16 -7.86 800 -801 -905 906 $ steel cladding bp4
6024    16 -7.86 800 -801 -906 907 $ steel cladding bp4
6025    16 -7.86 800 -801 -907 908 $ steel cladding bp4
6026    16 -7.86 800 -801 -908 909 $ steel cladding bp4
6027    16 -7.86 800 -801 -909 1000 $ end of steel cladding bp4
c concrete surrounded al cladding bp4
14000   18 -2.3 835 -1041 890 902 -882 -617 vol=5757.936 $ concrete surrounded bp4
c concrete surrounded steel cladding bp4
14001   18 -2.3 801 -1043 -902 903 -617 vol=636.5283 $ concrete around steel clad bp4
14002   18 -2.3 801 -1043 -903 904 -617 $ concrete around steel clad bp4
14003   18 -2.3 801 -1043 -904 905 -617 vol=25779.4 $ concrete around steel clad bp4
14004   18 -2.3 801 -1043 -905 906 -617 $ concrete around steel clad bp4
14005   18 -2.3 801 -1043 -906 907 -617 $ concrete around steel clad bp4
14006   18 -2.3 801 -1043 -907 908 -617 $ concrete around steel clad bp4
14007   18 -2.3 801 -1043 -908 909 -617 $ concrete around steel clad bp4
14008   18 -2.3 801 -1043 -909 1000 -617 $ end of concrete around clad bp4
c beam port 3
3011    1 -2.7 -837 834 -842 vol=57.91666 $ al plate bp3
3012    19 -1.029e-3 -837 842 -1056 vol=1853.3333 $ al pipe bp3
3013    19 -1.029e-3 -837 1056 -1057 $ al pipe bp3
3014    19 -1.029e-3 -837 1057 -1058 $ al pipe bp3
3015    19 -1.029e-3 -837 1058 -1059 $ al pipe bp3
3016    19 -1.029e-3 -837 1059 -1060 $ al pipe bp3
3017    19 -1.029e-3 -837 1060 -1061 $ al pipe bp3
3018    19 -1.029e-3 -837 1061 -1062 $ al pipe bp3
3019    19 -1.029e-3 -837 1062 -1063 $ al pipe bp3
3020    19 -1.029e-3 -837 1063 -1064 $ al pipe bp3
3021    19 -1.029e-3 -837 1064 -1065 $ al pipe bp3
3022    19 -1.029e-3 -837 1065 -1066 $ al pipe bp3
3023    19 -1.029e-3 -837 1066 -848 vol=1882.9757 $ end of al pipe bp3
3024    19 -1.029e-3 -839 848 -849 $ al plate bp3
3025    19 -1.029e-3 -839 849 -850 $ steel plate bp3
3026    19 -1.029e-3 -839 850 -1067 vol=3294.8147 $ steel pipe bp3
3027    19 -1.029e-3 -839 1067 -1068 $ steel pipe bp3
3028    19 -1.029e-3 -839 1068 -1069 $ steel pipe bp3
3029    19 -1.029e-3 -839 1069 -1070 $ steel pipe bp3
3030    19 -1.029e-3 -839 1070 -1071 $ steel pipe bp3
c sulfur surrounded by aluminum can
3031    1 -2.7 -3004 1071 -1083 vol=31.79405 $ al
3032    23 -2.07 -3004 1083 -1072 vol=3198.481 $ sulfur inside al can
3033    23 -2.07 -3004 1072 -1084 $ sulfur inside al can
3034    1 -2.7 -3004 1084 -1073 $ al
3035    1 -2.7 -839 3004 1071 -1073 vol=129.0787 $ al cladding
c beam port 3
3036    19 -1.029e-3 -3003 1073 -1074 vol=3146.6792 $ steel pipe bp3
3037    19 -1.029e-3 -3003 1074 -1075 vol=2859.5649 $ steel pipe bp3
3038    19 -1.029e-3 -3003 1075 -1076 vol=2586.1860 $ steel pipe bp3
3039    19 -1.029e-3 -3003 1076 -1077 vol=2326.5423 $ steel pipe bp3
3040    19 -1.029e-3 -3003 1077 -1078 vol=2080.6339 $ steel pipe bp3
3041    19 -1.029e-3 -3003 1078 -1079 vol=1848.4608 $ steel pipe bp3
```

```
3042    19 -1.029e-3 -3003 1079 -1080 vol=1630.0230 $ steel pipe bp3
3043    19 -1.029e-3 -3003 1080 -1081 vol=1425.3204 $ steel pipe bp3
3044    19 -1.029e-3 -3003 1081 -1082 3002 vol=1186.9414 $ end bp3
3045    22 -2.11 -3003 1082 -858 vol=11.30973 $ Li2CO3 plate in bp3
c collimator for bp3 (cone collimator)
7033    24 -2.42 3003 -839 1073 -1074 vol=148.1356 $ collimator bp3
7034    24 -2.42 3003 -839 1074 -1075 vol=435.2498 $ collimator bp3
7035    24 -2.42 3003 -839 1075 -1076 vol=708.6288 $ collimator bp3
7036    24 -2.42 3003 -839 1076 -1077 vol=968.2724 $ collimator bp3
7037    24 -2.42 3003 -839 1077 -1078 vol=1214.1808 $ collimator bp3
7038    24 -2.42 3003 -839 1078 -1079 vol=1446.3539 $ collimator bp3
7039    24 -2.42 3003 -839 1079 -1080 vol=1664.7917 $ collimator bp3
7040    24 -2.42 3003 -839 1080 -1081 vol=1869.4943 $ collimator bp3
7041    24 -2.42 3003 -839 1081 -1082 vol=2075.4441 $ end bp3
7042    22 -2.11 3003 -839 1082 -858 vol=21.119545 $ Li2CO3
c al and steel cladding bp3
2011    1 -2.7 837 -838 834 -842 vol=12.69525 $ al cladding bp3
2012    1 -2.7 837 -838 842 -1056 vol=406.2479 $ al cladding bp3
2013    1 -2.7 837 -838 1056 -1057 $ al cladding bp3
2014    1 -2.7 837 -838 1057 -1058 $ al cladding bp3
2015    1 -2.7 837 -838 1058 -1059 $ al cladding bp3
2016    1 -2.7 837 -838 1059 -1060 $ al cladding bp3
2017    1 -2.7 837 -838 1060 -1061 $ al cladding bp3
2018    1 -2.7 837 -838 1061 -1062 $ al cladding bp3
2019    1 -2.7 837 -838 1062 -1063 $ al cladding bp3
2020    1 -2.7 837 -838 1063 -1064 $ al cladding bp3
2021    1 -2.7 837 -838 1064 -1065 $ al cladding bp3
2022    1 -2.7 837 -838 1065 -1066 $ al cladding bp3
2023    1 -2.7 837 -838 1066 -848 vol=412.7455 $ end of al cladding
2024    16 -7.86 839 -840 848 -849 vol=33.43498 $ steel cladding bp3
2025    16 -7.86 839 -840 849 -850 $ steel cladding bp3
2026    16 -7.86 839 -840 850 -1067 vol=534.9597 $ steel cladding bp3
2027    16 -7.86 839 -840 1067 -1068 $ steel cladding bp3
2028    16 -7.86 839 -840 1068 -1069 $ steel cladding bp3
2029    16 -7.86 839 -840 1069 -1070 $ steel cladding bp3
2030    16 -7.86 839 -840 1070 -1071 $ steel cladding bp3
2031    16 -7.86 839 -840 1071 -1072 $ steel cladding bp3
2032    16 -7.86 839 -840 1072 -1073 $ steel cladding bp3
2033    16 -7.86 839 -840 1073 -1074 $ steel cladding bp3
2034    16 -7.86 839 -840 1074 -1075 $ steel cladding bp3
2035    16 -7.86 839 -840 1075 -1076 $ steel cladding bp3
2036    16 -7.86 839 -840 1076 -1077 $ steel cladding bp3
2037    16 -7.86 839 -840 1077 -1078 $ steel cladding bp3
2038    16 -7.86 839 -840 1078 -1079 $ steel cladding bp3
2039    16 -7.86 839 -840 1079 -1080 $ steel cladding bp3
2040    16 -7.86 839 -840 1080 -1081 $ steel cladding bp3
2041    16 -7.86 839 -840 1081 -858 vol=518.1106 $ end of steel pipe bp3
c concrete surrounded al cladding bp3
14009   18 -2.3 838 -1042 890 -1063 617 -612 vol=7358.777 $ concrete around al clad bp3
14010   18 -2.3 838 -1042 1063 -1064 617 -612 vol=8562.989 $ concrete around al clad bp3
14011   18 -2.3 838 -1042 1064 -1065 617 -612 $ concrete around al clad bp3
14012   18 -2.3 838 -1042 1065 -1066 617 -612 $ concrete around al clad bp3
14013   18 -2.3 838 -1042 1066 -848 617 -612 $ concrete around al clad bp3
c concrete surrounded steel cladding bp3
14014   18 -2.3 840 -1044 617 -612 848 -849 vol=636.5283 $ concrete around steel clad bp3
```

```
14015   18 -2.3 840 -1044 617 -612 849 -850 $ concrete around steel clad bp3
14016   18 -2.3 840 -1044 617 -612 850 -1067 vol=10184.45 $ concrete around steel clad bp3
14017   18 -2.3 840 -1044 617 -612 1067 -1068 $ concrete around steel clad bp3
14018   18 -2.3 840 -1044 617 -612 1068 -1069 $ concrete around steel clad bp3
14019   18 -2.3 840 -1044 617 -612 1069 -1070 $ concrete around steel clad bp3
14020   18 -2.3 840 -1044 617 -612 1070 -1071 $ concrete around steel clad bp3
14021   18 -2.3 840 -1044 617 -612 1071 -1072 $ concrete around steel clad bp3
14022   18 -2.3 840 -1044 617 -612 1072 -1073 $ concrete around steel clad bp3
14023   18 -2.3 840 -1044 617 -612 1073 -1074 $ concrete around steel clad bp3
14024   18 -2.3 840 -1044 617 -612 1074 -1075 $ concrete around steel clad bp3
14025   18 -2.3 840 -1044 617 -612 1075 -1076 $ concrete around steel clad bp3
14026   18 -2.3 840 -1044 617 -612 1076 -1077 $ concrete around steel clad bp3
14027   18 -2.3 840 -1044 617 -612 1077 -1078 $ concrete around steel clad bp3
14028   18 -2.3 840 -1044 617 -612 1078 -1079 $ concrete around steel clad bp3
14029   18 -2.3 840 -1044 617 -612 1079 -1080 $ concrete around steel clad bp3
14030   18 -2.3 840 -1044 617 -612 1080 -1081 $ concrete around steel clad bp3
14031   18 -2.3 840 -1044 617 -612 1081 -858 vol=9863.683 $end of concrete around steel clad

1     so 1000  $ infinity
2     cz 26.67 $ cylinder of water
3     cz 27.31 $ cylinder of vessel
4     pz -36.2 $ bottom of reflector
5     pz 32.39 $ top of water
6     pz 30.78 $ bottom of upper grid plate
7     pz 27.79 $ top of rod
8     pz -34.29 $ top of lower grid plate
9     pz -27.86 $ bottom of rod
10     cz 37.47 $ cylinder of lazy susan
11     pz 6.0325 $ bottom of lazy susan
12     cz 47.63 $ cylinder of graphite
13     cz 52.55 $ cylinder of lead
c 14     pz -46.2 $ bottom of water
c 15     pz 42.39 $ top of water
c 16     cz 62.71 $ cylinder of water
17     pz -19.05 $ bottom of fuel
18     pz 19.05 $ top of fuel
19     cz 10.0803 $ region 0 core
20     cz 14.2557 $ region 1 core
21     cz 17.4596 $ region 2 core
22     cz 20.1606 $ region 3 core
23     cz 22.5403 $ region 4 core
24     cz 24.6916 $ region 5 core
25     cz 1.82245 $ graph
26     cz 1.87325 $ cladding central thimble -#a1
27     c/z 1.04648 3.91414 0.3175 $ zr rod
28     c/z 1.04648 3.91414 1.82245 $ fuel
29     c/z 1.04648 3.91414 1.87325 $ cladding ss-#b1
30     c/z -2.86766 2.86766 0.3175 $ zr rod
31     c/z -2.86766 2.86766 1.82245 $ fuel
32     c/z -2.86766 2.86766 1.87325 $ cladding ss-#b2
33     c/z -3.91414 -1.04648 0.3175 $ zr rod
34     c/z -3.91414 -1.04648 1.82245 $ fuel
35     c/z -3.91414 -1.04648 1.87325 $ cladding ss-#b3
36     c/z -1.04648 -3.91414 0.3175 $ zr rod
37     c/z -1.04648 -3.91414 1.82245 $ fuel
```

```
38  c/z -1.04648 -3.91414 1.87325 $ cladding ss-#b4
39  c/z 2.86766 -2.86766 0.3175 $ zr rod
40  c/z 2.86766 -2.86766 1.82245 $ fuel
41  c/z 2.86766 -2.86766 1.87325 $ cladding ss-#b5
42  c/z 3.91414 1.04648 0.3175 $ zr rod
43  c/z 3.91414 1.04648 1.82245 $ fuel
44  c/z 3.91414 1.04648 1.87325 $ cladding ss-#b6
45  c/z 0.0 7.98068 0.3175 $ zr rod
46  c/z 0.0 7.98068 1.82245 $ fuel
47  c/z 0.0 7.98068 1.87325 $ cladding ss-#c1
48  c/z -3.99034 6.91134 0.3175 $ zr rod
49  c/z -3.99034 6.91134 1.82245 $ fuel
50  c/z -3.99034 6.91134 1.87325 $ cladding ss-#c2
51  c/z -6.91134 3.99034 0.3175 $ zr rod
52  c/z -6.91134 3.99034 1.82245 $ fuel
53  c/z -6.91134 3.99034 1.87325 $ cladding ss-#c3
54  c/z -7.98068 0.0 1.82245 $ fuel
55  c/z -7.98068 0.0 1.88733 $ cladding control w/o fuel-#c4
56  c/z -6.91134 -3.99034 0.3175 $ zr rod
57  c/z -6.91134 -3.99034 1.82245 $ fuel
58  c/z -6.91134 -3.99034 1.87325 $ cladding ss-#c5
59  c/z -3.99034 -6.91134 0.3175 $ zr rod
60  c/z -3.99034 -6.91134 1.82245 $ fuel
61  c/z -3.99034 -6.91134 1.87325 $ cladding ss-#c6
62  c/z 0.0 -7.98068 0.3175 $ zr rod
63  c/z 0.0 -7.98068 1.82245 $ fuel
64  c/z 0.0 -7.98068 1.87325 $ cladding ss-#c7
65  c/z 3.99034 -6.91134 0.3175 $ zr rod
66  c/z 3.99034 -6.91134 1.82245 $ fuel
67  c/z 3.99034 -6.91134 1.87325 $ cladding ss-#c8
68  c/z 6.91134 -3.99034 0.3175 $ zr rod
69  c/z 6.91134 -3.99034 1.82245 $ fuel
70  c/z 6.91134 -3.99034 1.87325 $ cladding ss-#c9
71  c/z 7.98068 0.0 1.82245 $ fuel
72  c/z 7.98068 0.0 0.3175 $ zr rod
73  c/z 7.98068 0.0 1.87325 $ cladding con w/fuel-#c10
74  c/z 6.91134 3.99034 0.3175 $ zr rod
75  c/z 6.91134 3.99034 1.82245 $ fuel
76  c/z 6.91134 3.99034 1.87325 $ cladding ss-#c11
77  c/z 3.99034 6.91134 0.3175 $ zr rod
78  c/z 3.99034 6.91134 1.82245 $ fuel
79  c/z 3.99034 6.91134 1.87325 $ cladding ss-#c12
80  c/z 0.0 11.9456 1.82245 $ fuel
81  c/z 0.0 11.9456 0.3175 $ zr rod
82  c/z 0.0 11.9456 1.87325 $ cladding con w/fuel-#d1
83  c/z -4.08432 11.2243 0.3175 $ zr rod
84  c/z -4.08432 11.2243 1.82245 $ fuel
85  c/z -4.08432 11.2243 1.87325 $ cladding ss-#d2
86  c/z -7.67842 9.15162 0.3175 $ zr rod
87  c/z -7.67842 9.15162 1.82245 $ fuel
88  c/z -7.67842 9.15162 1.87325 $ cladding ss-#d3
89  c/z -10.3454 5.97408 0.3175 $ zr rod
90  c/z -10.3454 5.97408 1.82245 $ fuel
91  c/z -10.3454 5.97408 1.87325 $ cladding ss-#d4
92  c/z -11.7653 2.2225 0.3175 $ zr rod
```

```
93    c/z -11.7653 2.2225 1.82245 $ fuel
94    c/z -11.7653 2.2225 1.87325 $ cladding ss-#d5
95    c/z -11.303 -2.07264 0.3175 $ zr rod
96    c/z -11.303 -2.07264 1.82245 $ fuel
97    c/z -11.303 -2.07264 1.87325 $ cladding ss-#d6
98    c/z -10.3454 -5.97408 0.3175 $ zr rod
99    c/z -10.3454 -5.97408 1.82245 $ fuel
100   c/z -10.3454 -5.97408 1.87325 $ cladding ss-#d7
101   c/z -7.67842 -9.15162 0.3175 $ zr rod
102   c/z -7.67842 -9.15162 1.82245 $ fuel
103   c/z -7.67842 -9.15162 1.87325 $ cladding ss-#d8
104   c/z -4.08432 -11.2243 0.3175 $ zr rod
105   c/z -4.08432 -11.2243 1.82245 $ fuel
106   c/z -4.08432 -11.2243 1.87325 $ cladding ss-#d9
107   c/z 0.0 -11.9456 1.82245 $ fuel
108   c/z 0.0 -11.9456 0.3175 $ zr rod
109   c/z 0.0 -11.9456 1.87325 $ cladding con w/fuel-#d10
110   c/z 4.08432 -11.2243 0.3175 $ zr rod
111   c/z 4.08432 -11.2243 1.82245 $ fuel
112   c/z 4.08432 -11.2243 1.87325 $ cladding ss-#d11
113   c/z 7.67842 -9.15162 0.3175 $ zr rod
114   c/z 7.67842 -9.15162 1.82245 $ fuel
115   c/z 7.67842 -9.15162 1.87325 $ cladding ss-#d12
116   c/z 10.3454 -5.97408 0.3175 $ zr rod
117   c/z 10.3454 -5.97408 1.82245 $ fuel
118   c/z 10.3454 -5.97408 1.87325 $ cladding ss-#d13
119   c/z 11.7653 -2.2225 0.3175 $ zr rod
120   c/z 11.7653 -2.2225 1.82245 $ fuel
121   c/z 11.7653 -2.2225 1.87325 $ cladding ss-#d14
122   c/z 11.303 2.07264 0.3175 $ zr rod
123   c/z 11.303 2.07264 1.82245 $ fuel
124   c/z 11.303 2.07264 1.87325 $ cladding ss-#d15
125   c/z 10.3454 5.97408 0.3175 $ zr rod
126   c/z 10.3454 5.97408 1.82245 $ fuel
127   c/z 10.3454 5.97408 1.87325 $ cladding ss-#d16
128   c/z 7.67842 9.15162 0.3175 $ zr rod
129   c/z 7.67842 9.15162 1.82245 $ fuel
130   c/z 7.67842 9.15162 1.87325 $ cladding ss-#d17
131   c/z 4.08432 11.2243 0.3175 $ zr rod
132   c/z 4.08432 11.2243 1.82245 $ fuel
133   c/z 4.08432 11.2243 1.87325 $ cladding ss-#d18
134   c/z 0.0 15.9156 0.3175 $ zr rod
135   c/z 0.0 15.9156 1.82245 $ fuel
136   c/z 0.0 15.9156 1.87325 $ cladding ss-#e1
137   c/z -4.11988 15.3721 0.3175 $ zr rod
138   c/z -4.11988 15.3721 1.82245 $ fuel
139   c/z -4.11988 15.3721 1.87325 $ cladding ss-#e2
140   c/z -7.95782 13.782 0.3175 $ zr rod
141   c/z -7.95782 13.782 1.82245 $ fuel
142   c/z -7.95782 13.782 1.87325 $ cladding ss-#e3
143   c/z -11.2547 11.2547 0.3175 $ zr rod
144   c/z -11.2547 11.2547 1.82245 $ fuel
145   c/z -11.2547 11.2547 1.87325 $ cladding ss-#e4
146   c/z -13.782 7.95782 0.3175 $ zr rod
147   c/z -13.782 7.95782 1.82245 $ fuel
```

```
c/z -13.782 7.95782 1.87325 $ cladding ss-#e5
c/z -15.2019 4.20624 0.3175 $ zr rod
c/z -15.2019 4.20624 1.82245 $ fuel
c/z -15.2019 4.20624 1.87325 $ cladding ss-#e6
c/z -15.2019 0.2413 0.3175 $ zr rod
c/z -15.2019 0.2413 1.82245 $ fuel
c/z -15.2019 0.2413 1.87325 $ cladding ss-#e7
c/z -15.3721 -4.11988 0.3175 $ zr rod
c/z -15.3721 -4.11988 1.82245 $ fuel
c/z -15.3721 -4.11988 1.87325 $ cladding ss-#e8
c/z -13.782 -7.95782 0.3175 $ zr rod
c/z -13.782 -7.95782 1.82245 $ fuel
c/z -13.782 -7.95782 1.87325 $ cladding ss-#e9
c/z -11.2547 -11.2547 0.3175 $ zr rod
c/z -11.2547 -11.2547 1.82245 $ fuel
c/z -11.2547 -11.2547 1.87325 $ cladding ss-#e10
c/z -7.95782 -13.782 0.3175 $ zr rod
c/z -7.95782 -13.782 1.82245 $ fuel
c/z -7.95782 -13.782 1.87325 $ cladding ss-#e11
c/z -4.11988 -15.3721 0.3175 $ zr rod
c/z -4.11988 -15.3721 1.82245 $ fuel
c/z -4.11988 -15.3721 1.87325 $ cladding ss-#e12
c/z 0.0 -15.9156 0.3175 $ zr rod
c/z 0.0 -15.9156 1.82245 $ fuel
c/z 0.0 -15.9156 1.87325 $ cladding ss-#e13
c/z 4.11988 -15.3721 0.3175 $ zr rod
c/z 4.11988 -15.3721 1.82245 $ fuel
c/z 4.11988 -15.3721 1.87325 $ cladding ss-#e14
c/z 7.95782 -13.782 0.3175 $ zr rod
c/z 7.95782 -13.782 1.82245 $ fuel
c/z 7.95782 -13.782 1.87325 $ cladding ss-#e15
c/z 11.2547 -11.2547 0.3175 $ zr rod
c/z 11.2547 -11.2547 1.82245 $ fuel
c/z 11.2547 -11.2547 1.87325 $ cladding ss-#e16
c/z 13.782 -7.95782 0.3175 $ zr rod
c/z 13.782 -7.95782 1.82245 $ fuel
c/z 13.782 -7.95782 1.87325 $ cladding ss-#e17
c/z 15.2019 -4.20624 0.3175 $ zr rod
c/z 15.2019 -4.20624 1.82245 $ fuel
c/z 15.2019 -4.20624 1.87325 $ cladding ss-#e18
c/z 15.2019 -0.2413 0.3175 $ zr rod
c/z 15.2019 -0.2413 1.82245 $ fuel
c/z 15.2019 -0.2413 1.87325 $ cladding ss-#e19
c/z 15.3721 4.11988 0.3175 $ zr rod
c/z 15.3721 4.11988 1.82245 $ fuel
c/z 15.3721 4.11988 1.87325 $ cladding ss-#e20
c/z 13.782 7.95782 0.3175 $ zr rod
c/z 13.782 7.95782 1.82245 $ fuel
c/z 13.782 7.95782 1.87325 $ cladding ss-#e21
c/z 11.2547 11.2547 0.3175 $ zr rod
c/z 11.2547 11.2547 1.82245 $ fuel
c/z 11.2547 11.2547 1.87325 $ cladding ss-#e22
c/z 7.95782 13.782 0.3175 $ zr rod
c/z 7.95782 13.782 1.82245 $ fuel
c/z 7.95782 13.782 1.87325 $ cladding ss-#e23
```

```
203   c/z 4.11988 15.3721 0.3175 $ zr rod
204   c/z 4.11988 15.3721 1.82245 $ fuel
205   c/z 4.11988 15.3721 1.87325 $ cladding ss-#e24
206   c/z 0.0 19.8196 0.3175 $ zr rod
207   c/z 0.0 19.8196 1.82245 $ fuel
208   c/z 0.0 19.8196 1.87325 $ cladding ss-#f1
211   c/z -4.13512 19.4539 1.87325 $ cladding ss-#f2
212   c/z -8.0899 18.1686 0.3175 $ zr rod
213   c/z -8.0899 18.1686 1.82245 $ fuel
214   c/z -8.0899 18.1686 1.87325 $ cladding ss-#f3
215   c/z -11.6916 16.0909 0.3175 $ zr rod
216   c/z -11.6916 16.0909 1.82245 $ fuel
217   c/z -11.6916 16.0909 1.87325 $ cladding ss-#f4
400   c/z -14.7803 13.3071 0.3175 $ zr rod
401   c/z -14.7803 13.3071 1.82245 $ fuel
218   c/z -14.7803 13.3071 1.87325 $ cladding water -#f5
219   c/z -17.1323 10.1194 0.3175 $ zr rod
220   c/z -17.1323 10.1194 1.82245 $ fuel
221   c/z -17.1323 10.1194 1.87325 $ cladding ss-#f6
222   c/z -18.9154 6.1468 0.3175 $ zr rod
223   c/z -18.9154 6.1468 1.82245 $ fuel
224   c/z -18.9154 6.1468 1.87325 $ cladding ss-#f7
225   c/z -19.9898 2.07772 0.3175 $ zr rod
226   c/z -19.9898 2.07772 1.82245 $ fuel
227   c/z -19.9898 2.07772 1.87325 $ cladding ss-#f8
228   c/z -19.9898 -2.07772 0.3175 $ zr rod
229   c/z -19.9898 -2.07772 1.82245 $ fuel
230   c/z -19.9898 -2.07772 1.87325 $ cladding ss-#f9
231   c/z -18.9154 -6.1468 0.3175 $ zr rod
232   c/z -18.9154 -6.1468 1.82245 $ fuel
233   c/z -18.9154 -6.1468 1.87325 $ cladding ss-#f10
234   c/z -17.4523 -9.9441 0.3175 $ zr rod
235   c/z -17.4523 -9.9441 1.82245 $ fuel
236   c/z -17.4523 -9.9441 1.87325 $ cladding ss-#f11
402   c/z -14.7803 -13.3071 0.3175 $ zr rod
403   c/z -14.7803 -13.3071 1.82245 $ fuel
237   c/z -14.7803 -13.3071 1.87325 $ cladding water -#f12
238   c/z -11.6916 -16.0909 0.3175 $ zr rod
239   c/z -11.6916 -16.0909 1.82245 $ fuel
240   c/z -11.6916 -16.0909 1.87325 $ cladding ss-#f13
241   c/z -8.0899 -18.1686 0.3175 $ zr rod
242   c/z -8.0899 -18.1686 1.82245 $ fuel
243   c/z -8.0899 -18.1686 1.87325 $ cladding ss-#f14
244   c/z -4.13512 -19.4539 0.3175 $ zr rod
245   c/z -4.13512 -19.4539 1.82245 $ fuel
246   c/z -4.13512 -19.4539 1.87325 $ cladding ss-#f15
247   c/z 0.0 -19.8882 0.3175 $ zr rod
248   c/z 0.0 -19.8882 1.82245 $ fuel
249   c/z 0.0 -19.8882 1.87325 $ cladding ss-#f16
250   c/z 4.13512 -19.4539 0.3175 $ zr rod
251   c/z 4.13512 -19.4539 1.82245 $ fuel
252   c/z 4.13512 -19.4539 1.87325 $ cladding ss-#f17
253   c/z 8.0899 -18.1686 0.3175 $ zr rod
254   c/z 8.0899 -18.1686 1.82245 $ fuel
255   c/z 8.0899 -18.1686 1.87325 $ cladding ss-#f18
```

```
256     c/z 11.6916 -16.0909 0.3175 $ zr rod
257     c/z 11.6916 -16.0909 1.82245 $ fuel
258     c/z 11.6916 -16.0909 1.87325 $ cladding ss-#f19
405     c/z 14.7803 -13.3071 1.82245 $ fuel
259     c/z 14.7803 -13.3071 1.87325 $ cladding water -#f20
261     c/z 17.1323 -10.1194 1.82245 $ fuel
262     c/z 17.1323 -10.1194 1.87325 $ cladding ss-#f21
264     c/z 18.9154 -6.1468 1.82245 $ fuel
265     c/z 18.9154 -6.1468 1.87325 $ cladding ss-#f22
267     c/z 19.9898 -2.07772 1.82245 $ fuel
268     c/z 19.9898 -2.07772 1.87325 $ cladding ss-#f23
c 269     c/z 19.9898 2.07772 0.3175 $ zr rod
270     c/z 19.9898 2.07772 1.82245 $ fuel
271     c/z 19.9898 2.07772 1.87325 $ cladding ss-#f24
273     c/z 18.9154 6.1468 1.82245 $ fuel
274     c/z 18.9154 6.1468 1.87325 $ cladding ss-#f25
276     c/z 17.4523 9.9441 1.82245 $ fuel
277     c/z 17.4523 9.9441 1.87325 $ cladding ss-#f26
407     c/z 14.7803 13.3071 1.82245 $ fuel
278     c/z 14.7803 13.3071 1.87325 $ cladding water -#f27
279     c/z 11.6916 16.0909 0.3175 $ zr rod
280     c/z 11.6916 16.0909 1.82245 $ fuel
281     c/z 11.6916 16.0909 1.87325 $ cladding ss-#f28
282     pz 15.24 $ segment bottom1
283     pz 11.43 $ segment bottom2
284     pz 7.62 $ segment bottom3
285     pz 3.81 $ segment bottom4
286     pz 0.0 $ segment bottom5
287     pz -3.81 $ segment bottom6
288     pz -7.62 $ segment bottom7
289     pz -11.43 $ segment bottom8
290     pz -15.24 $ segment bottom9
291     c/z 8.0899 18.1686 0.3175 $ zr rod
292     c/z 8.0899 18.1686 1.82245 $ fuel
293     c/z 8.0899 18.1686 1.87325 $ cladding ss-#f29
294     c/z 4.13512 19.4539 0.3175 $ zr rod
295     c/z 4.13512 19.4539 1.82245 $ fuel
296     c/z 4.13512 19.4539 1.87325 $ cladding ss-#f30
297     c/z 0.0 23.8608 1.82245 $ graph
298     c/z 0.0 23.8608 1.87325 $ cladding gr-#g1
299     c/z -4.14274 23.4975 1.82245 $ graph
300     c/z -4.14274 23.4975 1.87325 $ cladding gr-#g2
301     c/z -8.16102 22.4206 1.82245 $ graph
302     c/z -8.16102 22.4206 1.87325 $ cladding gr-#g3
303     c/z -11.9304 20.6654 1.82245 $ graph
304     c/z -11.9304 20.6654 1.87325 $ cladding gr-#g4
305     c/z -15.3365 18.2778 1.82245 $ graph
306     c/z -15.3365 18.2778 1.87325 $ cladding gr-#g5
307     c/z -18.2778 15.3365 1.82245 $ graph
308     c/z -18.2778 15.3365 1.87325 $ cladding gr-#g6
309     c/z -20.6654 11.9304 1.82245 $ graph
310     c/z -20.6654 11.9304 1.87325 $ cladding gr-#g7
311     c/z -22.606 8.0772 1.82245 $ graph
312     c/z -22.606 8.0772 1.87325 $ cladding gr-#g8
313     c/z -23.4975 4.14274 1.82245 $ graph
```

```
314   c/z -23.4975 4.14274 1.87325 $ cladding gr-#g9
408   c/z -23.8608 0.0 0.3175 $ zr rod
409   c/z -23.8608 0.0 1.82245 $ fuel
315   c/z -23.8608 0.0 1.87325 $ cladding water -#g10
410   c/z -23.4975 -4.14274 0.3175 $ zr rod
411   c/z -23.4975 -4.14274 1.82245 $ fuel
316   c/z -23.4975 -4.14274 1.87325 $ cladding water -#g11
412   c/z -22.4206 -8.16102 0.3175 $ zr rod
413   c/z -22.4206 -8.16102 1.82245 $ fuel
317   c/z -22.4206 -8.16102 1.87325 $ cladding water -#g12
414   c/z -20.6654 -11.9304 0.3175 $ zr rod
415   c/z -20.6654 -11.9304 1.82245 $ fuel
318   c/z -20.6654 -11.9304 1.87325 $ cladding water -#g13
416   c/z -18.2778 -15.3365 0.3175 $ zr rod
417   c/z -18.2778 -15.3365 1.82245 $ fuel
319   c/z -18.2778 -15.3365 1.87325 $ cladding water -#g14
418   c/z -15.3365 -18.2778 0.3175 $ zr rod
419   c/z -15.3365 -18.2778 1.82245 $ fuel
320   c/z -15.3365 -18.2778 1.87325 $ cladding water -#g15
420   c/z -11.9304 -20.6654 0.3175 $ zr rod
321   c/z -11.9304 -20.6654 1.82245 $ graph
322   c/z -11.9304 -20.6654 1.87325 $ cladding gr-#g16
323   c/z -7.93242 -22.4206 1.82245 $ graph
324   c/z -7.93242 -22.4206 1.87325 $ cladding gr-#g17
325   c/z -4.14274 -23.4975 1.82245 $ graph
326   c/z -4.14274 -23.4975 1.87325 $ cladding gr-#g18
327   c/z 0.0 -23.8608 1.82245 $ graph
328   c/z 0.0 -23.8608 1.87325 $ cladding gr-#g19
329   c/z 4.14274 -23.4975 1.82245 $ graph
330   c/z 4.14274 -23.4975 1.87325 $ cladding gr-#g20
331   c/z 8.16102 -22.4206 1.82245 $ graph
332   c/z 8.16102 -22.4206 1.87325 $ cladding gr-#g21
333   c/z 11.9304 -20.6654 1.87325 $ cladding water -#g22
334   c/z 15.3365 -18.2778 1.87325 $ cladding water -#g23
335   c/z 18.2778 -15.3365 1.87325 $ cladding water -#g24
336   c/z 20.6654 -11.9304 1.87325 $ cladding water -#g25
337   c/z 22.606 -8.0772 1.87325 $ cladding water -#g26
338   c/z 23.4975 -4.14274 1.87325 $ cladding water -#g27
339   c/z 23.8608 0.0 1.87325 $ cladding water -#g28
341   c/z 23.4975 4.14274 1.87325 $ cladding gr-#g29
343   c/z 22.4206 8.16102 1.87325 $ cladding gr-#g30
345   c/z 20.6654 11.9304 1.87325 $ cladding gr-#g31
347   c/z 18.2778 15.3365 1.87325 $ cladding gr-#g32
349   c/z 15.3365 18.2778 1.87325 $ cladding gr-#g33
351   c/z 11.9304 20.6654 1.87325 $ cladding gr-#g34
353   c/z 7.93242 22.4206 1.87325 $ cladding gr-#g35
354   c/z 4.14274 23.4975 1.82245 $ graph
355   c/z 4.14274 23.4975 1.87325 $ cladding gr-#g36
701   cz 53.815 $ water gap
702   cz 56.46 $ cylinder of Al
703   cz 59.0 $ outer cylinder of Al
601   pz 60.96 $ top of TC
602   pz 59.691 $ b4c top of TC
603   pz 59.373 $ Al top of TC
604   pz -59.373 $ Al bottom of TC
```

```
605   pz -59.691 $ b4c bottom of TC
606   pz -60.96 $ bottom of TC
607   px 60.96 $ right side of TC
608   px 59.691 $ b4c right of TC
609   px 59.373 $ Al right of TC
610   px -59.373 $ Al left of TC
611   px -59.691 $ b4c left of TC
612   px -60.96 $ left side of TC
613   p 0 13.38 0 0 13.38 1 -60.96 63.623 0 $ left outer angle of TC
614   p 0 13.8 0 0 13.8 1 -59.373 63.623 0 $ left inner angle of TC
615   p 0 13.38 0 0 13.38 1 60.96 63.623 0 $ right outer angle of TC
616   p 0 13.8 0 0 13.8 1 59.373 63.623 0 $ right inner angle of TC
617   py 0.0 $ center line
618   py 219.405 $ front of region N
619   py 63.623 $ back of region A
830   pz 5.08 $ top of inner region
831   pz -5.08 $ bottom of inner region
833   1 px -27.4105 $ al pipe bp4
834   1 py 8.7313 $ al pipe bp3
835   1 cx 8.4138 $ outer radius al pipe bp4
838   2 cy 8.4138 $ outer radius al pipe bp3
868   px 0 $ center line
871   pz 30.48 $ top of thermalizing column
872   pz 29.211 $ b4c top of thermalizing column
873   pz 28.893 $ Al top of thermalizing column
874   pz -28.893 $ Al bottom of thermalizing column
875   pz -29.211 $ b4c bottom of thermalizing column
876   pz -30.48 $ bottom of thermalizing column
877   px 30.48 $ right side of thermalizing column
878   px 29.211 $ b4c right of thermalizing column
879   px 28.893 $ Al right of thermalizing column
880   px -28.893 $ Al left of thermalizing column
881   px -29.211 $ b4c left of thermalizing column
882   px -30.48 $ left side of thermalizing column
883   py -67.95 $ front lead block in thermalizing column
884   py -73.03 $ back lead block in thermalizing column
885   py -93.35 $ air block in thermalzing column
886   py -113.67 $ end of graphite in thermalizing column
889   cz 98.425 $ inner radius of reactor tank
890   cz 99.06 $ outer radius of reactor tank
837   2 cy 7.62 $ inner radius al pipe bp3
839   2 cy 10.16 $ inner radius steel pipe bp3
840   2 cy 10.9538 $ outer radius steel pipe bp3
842   1 py 9.0488 $ al pipe bp3
1056  2 py 19.2088 $ al pipe bp3
1057  2 py 29.3688 $ al pipe bp3
1058  2 py 39.5288 $ al pipe bp3
1059  2 py 49.6888 $ al pipe bp3
1060  2 py 59.8488 $ al pipe bp3
1061  2 py 70.0088 $ al pipe bp3
1062  2 py 80.1688 $ al pipe bp3
1063  2 py 90.3288 $ al pipe bp3
1064  2 py 100.4888 $ al pipe bp3
1065  2 py 110.6488 $ al pipe bp3
1066  2 py 120.8088 $ al pipe bp3
```

```
848    2 py 131.1313 $ end of al pipe bp3
849    2 py 131.7663 $ al plate bp3
850    2 py 132.4013 $ steel plate bp3
1067   2 py 142.5613 $ steel pipe bp3
1068   2 py 152.7213 $ steel pipe bp3
1069   2 py 162.8813 $ steel pipe bp3
1070   2 py 173.0413 $ steel pipe bp3
1071   2 py 183.2013 $ steel pipe bp3
1072   2 py 193.3613 $ steel pipe bp3
1073   2 py 203.5213 $ steel pipe bp3
1074   2 py 213.6813 $ steel pipe bp3
1075   2 py 223.8413 $ steel pipe bp3
1076   2 py 234.0013 $ steel pipe bp3
1077   2 py 244.1613 $ steel pipe bp3
1078   2 py 254.3213 $ steel pipe bp3
1079   2 py 264.4813 $ steel pipe bp3
1080   2 py 274.6413 $ steel pipe bp3
1081   2 py 284.8013 $ steel pipe bp3
858    2 py 294.6413 $ end of steel pipe bp3
836    1 cx 8.02 $ inner radius Al pipe bp4
800    1 cx 10.16 $ inner radius steel pipe bp4
801    1 cx 10.9538 $ outer radius steel pipe bp4
899    1 px -27.628 $ Al pipe bp4
1048   1 px -37.4741 $ Al pipe bp4
1049   1 px -47.3202 $ Al pipe bp4
1050   1 px -57.1663 $ A pipe bp4
1051   1 px -67.0124 $ Al pipe bp4
1052   1 px -76.8585 $ Al pipe bp4
1053   1 px -86.7046 $ Al pipe bp4
1054   1 px -96.5507 $ Al pipe bp4
902    1 px -105.8918 $ end of Al pipe bp4
903    1 px -106.5268 $ al plate of bp4
904    1 px -107.1618 $ steel plate bp4
905    1 px -132.8793 $ steel pipe bp4
906    1 px -158.5968 $ steel pipe bp4
907    1 px -184.3143 $ steel pipe bp4
908    1 px -210.0318 $ steel pipe bp4
909    1 px -235.7493 $ steel pipe bp4
1000   1 px -261.4668 $ end of steel pipe bp4
1001   c/z 5.06691 31.99123 1.143 $ lazy susan rack
1002   c/z 10.00906 30.80472 1.143 $ lazy susan rack
1003   c/z 14.70475 28.8597 1.143 $ lazy susan rack
1004   c/z 19.03836 26.20406 1.143 $ lazy susan rack
1005   c/z 22.90319 22.90319 1.143 $ lazy susan rack
1006   c/z 26.20406 19.03836 1.143 $ lazy susan rack
1007   c/z 28.8597 14.70475 1.143 $ lazy susan rack
1008   c/z 30.80472 10.00906 1.143 $ lazy susan rack
1009   c/z 31.99123 5.066912 1.143 $ lazy susan rack
1010   c/z 32.39 0 1.143 $ lazy susan rack
1011   c/z 31.99123 -5.06691 1.143 $ lazy susan rack
1012   c/z 30.80472 -10.0091 1.143 $ lazy susan rack
1013   c/z 28.8597 -14.7048 1.143 $ lazy susan rack
1014   c/z 26.20406 -19.0384 1.143 $ lazy susan rack
1015   c/z 22.90319 -22.9032 1.143 $ lazy susan rack
1016   c/z 19.03836 -26.2041 1.143 $ lazy susan rack
```

```
1017    c/z 14.70475 -28.8597 1.143 $ lazy susan rack
1018    c/z 10.00906 -30.8047 1.143 $ lazy susan rack
1019    c/z 5.066912 -31.9912 1.143 $ lazy susan rack
1020    c/z 0 -32.39 1.143 $ lazy susan rack
1021    c/z -5.06691 -31.9912 1.143 $ lazy susan rack
1022    c/z -10.0091 -30.8047 1.143 $ lazy susan rack
1023    c/z -14.7048 -28.8597 1.143 $ lazy susan rack
1024    c/z -19.0384 -26.2041 1.143 $ lazy susan rack
1025    c/z -22.9032 -22.9032 1.143 $ lazy susan rack
1026    c/z -26.2041 -19.0384 1.143 $ lazy susan rack
1027    c/z -28.8597 -14.7048 1.143 $ lazy susan rack
1028    c/z -30.8047 -10.0091 1.143 $ lazy susan rack
1029    c/z -31.9912 -5.06691 1.143 $ lazy susan rack
1030    c/z -32.39 0 1.143 $ lazy susan rack
1031    c/z -31.9912 5.066912 1.143 $ lazy susan rack
1032    c/z -30.8047 10.00906 1.143 $ lazy susan rack
1033    c/z -28.8597 14.70475 1.143 $ lazy susan rack
1034    c/z -26.2041 19.03836 1.143 $ lazy susan rack
1035    c/z -22.9032 22.90319 1.143 $ lazy susan rack
1036    c/z -19.0384 26.20406 1.143 $ lazy susan rack
1037    c/z -14.7048 28.8597 1.143 $ lazy susan rack
1038    c/z -10.0091 30.80472 1.143 $ lazy susan rack
1039    c/z -5.06691 31.99123 1.143 $ lazy susan rack
1040    c/z 0 32.39 1.143 $ lazy susan rack
1041    1 cx 18.4138 $ concrete surrounded al clad bp4
1042    2 cy 18.4138 $ concrete surrounded al clad bp3
1043    1 cx 20.9538 $ concrete surrounded steel clad bp4
1044    2 cy 20.9538 $ concrete surrouned steel clad bp3
1045    pz -15.24 $ 1 cm above the bottom of rabbit sample position
1046    pz -16.24 $ bottom of rabbit sample position
1047    pz 7.0325 $ 1 cm above the bottom of the lalzy susan sample position
3000    2 py 314.6413 $ outer region of bp3
3001    2 cy 30.9538 $ outer region of bp3
3002    s -225.91 216.62 -6.985 5.0594 $ sphere outside bp3
3003    2 ky 426.0644 0.002084 $ two sheets cone collimator R = 6 cm
1082    2 py 294.5413 $ Li2CO3 plate
3004    2 cy 10.06 $ al can surrounded sulfur
1083    2 py 183.3013 $ sulfur in bp3
1084    2 py 203.4213 $ sulfur in bp3

*tr1    0 0 -6.985 27 63 90 117 27 90 90 90 0
*tr2    -36.49 -9.37 -6.985 40 50 90 130 40 90 90 90 0
m1      13027 1.0 $ al
m2      6012 0.00009456 24000 0.005187 28000 0.00241866 26000  $ steel/h2o
        0.0180264 1001 0.04676 8016 0.02338
m4      6012 1.0 $ graphite
mt4     grph.01t $ graphite  salphabeta card
m5      82000 1.0 $ lead
m6      1001 0.6667 8016 0.3333 $ h2o
mt6     lwtr.01t $ h2o  salphabeta card
m7      6012 0.00031519 24000 0.01729 28000 0.0080622 26000 0.060088 $ steel
m8      40000.50c 1.0 $ zr
m9      1001 0.0561382 40000.50c 0.0350864 92235 0.000892797 92238  $ uzrh-full
        0.000378151 68166.00c 0.000258324 68167.00c 0.0000769439
mt9     h/zr.01t zr/h.01t $ uzrh-full  salphabeta card
```

```
m10     5010.50c 0.15824 5011.50c 0.64176 6012 0.2 $ b4c
m12     1001 0.04666 40000.50c 0.02916 92235 0.000753 92238 0.000323  $ uzrh-partial
      68166.00c 0.000267 68167.00c 0.000080
mt12    h/zr.01t zr/h.01t $ uzrh-partial  salphabeta card
m16     26000 1.0 $ steel
m18     1001 -0.010 8016 -0.529 11023 -0.016 12000 -0.002
      13027 -0.034 14000 -0.337 19000 -0.013 20000 -0.044
      26000 -0.014 6012 -0.001 $ concrete
m19     7014.50c 0.79 8016 0.21 $ air
m20     1002 0.6667 8016 0.3333 $ heavy water(D2O)
m22     3006 0.4 6012 0.2 8016 0.6 $ Li2CO3
m23     16032 1.0 $ sulfur
m24     14000 1.0 $ silicon
mode    n  $  card
c kcode   50000 1.05 5 100 $ card
c ksrc    4.24164 1.37398 0.0 3.19516 -2.54016 0.0 -0.71898 -3.58664 0.0
 c    -3.58664 -0.71898 0.0 -2.54016 3.19516 0.0 1.37398 4.24164 0.0
 c     8.30818 0.3275 0.0 7.23884 -3.66284 0.0 4.31784 -6.58384 0.0
 c    -3.66284 -6.58384 0.0 -6.58384 -3.66284 0.0 -7.65318 0.3275 0.0
 c    -6.58384 4.31784 0.0 -3.66284 7.23884 0.0 0.3275 8.30818 -4.405
 c     4.31784 7.23884 0.0 7.23884 4.31784 0.0 12.2731 0.3275 -4.405
 c     11.5518 -3.75682 0.0 9.47912 -7.35092 0.0 6.30158 -10.0179 0.0
 c     2.55 -11.4378 0.0 -1.74514 -10.9755 0.0 -5.64658 -10.0179 0.0
 c     -8.82412 -7.35092 0.0 -10.8968 -3.75682 0.0 -11.6181 0.3275
 c     -4.405 -10.8968 4.41182 0.0 -8.82412 8.00592 0.0 -5.64658
 c     10.6729 0.0 -1.895 12.0928 0.0 2.40014 11.6305 0.0 6.30158
 c     10.6729 0.0 9.47912 8.00592 0.0 11.5518 4.41182 0.0 16.2431
 c     0.3275 0.0 15.6996 -3.79238 0.0 14.1095 -7.63032 0.0 11.5822
 c     -10.9272 0.0 8.28532 -13.4545 0.0 4.53374 -14.8744 0.0 0.5688
 c     -14.8744 0.0 -3.79238 -15.0446 0.0 -7.63032 -13.4545 0.0
 c     -10.9272 -10.9272 0.0 -13.4545 -7.63032 0.0 -15.0446 -3.79238
 c     0.0 -15.5881 0.3275 0.0 -15.0446 4.44738 0.0 -13.4545 8.28532
 c     0.0 -10.9272 11.5822 0.0 -7.63032 14.1095 0.0 -3.87874 15.5294
 c     0.0 0.0862 15.5294 0.0 4.44738 15.6996 0.0 8.28532 14.1095 0.0
 c     11.5822 11.5822 0.0 14.1095 8.28532 0.0 15.6996 4.44738 0.0
 c     20.1471 0.3275 0.0 19.7814 -3.80762 0.0 18.4961 -7.7624 0.0
 c     16.4184 -11.3641 0.0 10.4469 -16.8048 0.0 6.4743 -18.5879 0.0
 c     2.40522 -19.6623 0.0 -1.75022 -19.6623 0.0 -5.8193 -18.5879 0.0
 c     -9.6166 -17.1248 0.0 -15.7634 -11.3641 0.0 -17.8411 -7.7624 0.0
 c     -19.1264 -3.80762 0.0 -19.5607 0.3275 0.0 -19.1264 4.46262 0.0
 c     -17.8411 8.4174 0.0 -15.7634 12.0191 0.0 -9.79186 17.4598 0.0
 c     -5.8193 19.2429 0.0 -1.75022 20.3173 0.0 2.40522 20.3173 0.0
 c     6.4743 19.2429 0.0 10.2716 17.7798 0.0 18.4961 8.4174 0.0
 c     19.7814 4.46262 0.0 -15.1803 13.3071 0.0 -15.1803 -13.3071 0.0
 c     -24.2608 0.0 0.0 -23.8975 -4.14274 0.0 -21.0654 -11.9304 0.0
 c     -18.6778 -15.3365 0.0 -15.8365 -18.2778 0.0 -12.3304 -20.6654 0.0
c *f7:n   41 46 51 56 61 66 71 76 81 89 94 99 104 109 118 123 132
c       137 142 147 152 157 162 167 176 181 186 191 196 201 206
c       211 216 221 226 231 236 241 246 251 256 261 266 271 276
c       281 286 291 296 301 306 311 316 321 326 331 336 346 351
c       601 357 362 367 372 377 382 606 388 393 398 403 408 413
c       418 458 459 460 461 462 463 464 465 466 467 469 474 621
c       626 631 636 641 646 651 115 129 173 T $ fission energy deposition
c ssw     2(15003) pty n sym 0
ssr     old 2 new 2 col 0 wgt 1 psc 0
```

```
nonu    2 858r
dxt:n   -225.91 216.62 -6.985 5.9594 5.9594
dxc:n   0.001 716r 5j 0.01 11r 5j 0.01 20r 84j 0.4 7r 7j
dd1     0.5 3000
dbcn    12j 764585 4j $ random number stride is 5 time of 152917 (default)
esplt:n 2 0.1 2 0.001 2 0.0001 2 0.000001 0.75 5e-7 $ split energy
f4:n    15003 4011 15i 4027 3011 33i 3045 30001 $ flux over the end of bp3
f24:n   15003 4011 15i 4027 3011 33i 3045 30001 $ flux over the end of bp3 cells
area    380j 222.39972 222.39972 4148.95 6470.733 19j
        5860.252 10438.01448 11253.53573 222.39972
        182.41469 182.41469 182.41469 182.41469
        182.41469 182.41469 182.41469 182.41469
        182.41469 182.41469 182.41469 182.41469
        324.29279 324.29279 324.29279 324.29279
        324.29279 324.29279
        317.9405 317.9405 317.9405
        324.29279 324.29279 324.29279
        324.29279 324.29279 324.29279
        324.29279 324.29279 324.29279
        3954.763 9931.46659 10707.41129 222.39972
        202.06849 202.06849 202.06849 202.06849
        202.06849 202.06849 202.06849 202.06849
        324.29279 324.29279 324.29279 324.29279
        324.29279 324.29279 324.29279 324.29279
        40j 790.42093 3710.56338 20482.47683 21527.17202
        5j 156.56167 2315.380 324.29279 1271.762 317.9405 317.9405
f1:n    1074 $ current over a surface bp 3 after sulfur
f2:n    1074 $ flux over a surface bp 3 after sulfur
fs1     -3003 -839 $ current tally segment
fs2     -3003 -839 $ flux tally segment
sd1     267.7753 56.5175 324.2928 $ segment divisor card for current tally
sd2     267.7753 56.5175 324.2928 $ segment divisor card for flux tally
f11:n   1070 $ current over a surface bp 3 before sulfur
f12:n   1070 $ flux over a surface bp 3 before sulfur
fs11    -839 -840 $ current tally segment
fs12    -839 -840 $ flux tally segment
sd11    324.2928 52.6535 376.9463 $ segment divisor card for current tally
sd12    324.2928 52.6535 376.9463 $ segment divisor card for flux tally
f21:n   858 $ current over a surface bp 3 at the end of bp3
f22:n   858 $ flux over a surface bp 3 at the end of bp3
fs21    -3003 -839 $ current tally segment
fs22    -3003 -839 $ flux tally segment
sd21    113.0973 211.1955 324.2928 $ segment divisor card for current tally
sd22    113.0973 211.1955 324.2928 $ segment divisor card for flux tally
f31:n   842 $ current over a surface bp 3 (second surface)
f32:n   842 $ flux over a surface bp 3 (second surface)
fs31    -837 -838 $ current tally segment
fs32    -837 -838 $ flux tally segment
sd31    182.4147 39.9850 222.3997 $ segment divisor card for current tally
sd32    182.4147 39.9850 222.3997 $ segment divisor card for flux tally
f41:n   834 $ current over a surface bp 3 first surface
f42:n   834 $ flux over a surface bp 3 first surface
fs41    -837 -838 $ current tally segment
fs42    -837 -838 $ flux tally segment
sd41    182.4147 39.9850 222.3997 $ segment divisor card for current tally
```

```
sd42    182.4147 39.9850 222.3997 $ segment divisor card for flux tally
f51:n   850 $ current over a surface bp 3 (steel pipe)
f52:n   850 $ flux over a surface bp 3 (steel pipe)
fs51    -839 -840 $ current tally segment
fs52    -839 -840 $ flux tally segment
sd51     324.2928 52.6535 376.9463 $ segment divisor card for current tally
sd52     324.2928 52.6535 376.9463 $ segment divisor card for flux tally
f61:n   1071 $ current over a surface bp 3 before sulfur
f62:n   1071 $ flux over a surface bp 3 before sulfur
fs61    -3004 -839 $ current tally segment (aluminum can of sulfur)
fs62    -3004 -839 $ flux tally segment (aluminum can of sulfur)
sd61    317.9405 6.3523 324.2928 $ segment divisor card for current tally
sd62    317.9405 6.3523 324.2928 $ segment divisor card for flux tally
f71:n   1073 $ current over a surface bp 3 (first surface)
f72:n   1073 $ flux over a surface bp 3 (first surface)
fs71    -3003 -839 $ current tally segment
fs72    -3003 -839 $ flux tally segment
sd71     295.3581 28.9347 324.2928 $ segment divisor card for current tally
sd72     295.3581 28.9347 324.2928 $ segment divisor card for flux tally
f81:n   1076 $ current over a surface bp 3
f82:n   1076 $ flux over a surface bp 3
fs81    -3003 -839 $ current tally segment
fs82    -3003 -839 $ flux tally segment
sd81     241.5444 82.7484 324.2928 $ segment divisor card for current tally
sd82     241.5444 82.7484 324.2928 $ segment divisor card for flux tally
f91:n   1078 $ current over a surface bp 3 (first surface)
f92:n   1078 $ flux over a surface bp 3 (first surface)
fs91    -3003 -839 $ current tally segment
fs92    -3003 -839 $ flux tally segment
sd91     193.138 131.1548 324.2928 $ segment divisor card for current tally
sd92     193.138 131.1548 324.2928 $ segment divisor card for flux tally
f101:n   1080 $ current over a surface bp 3 (first surface)
f102:n   1080 $ flux over a surface bp 3 (first surface)
fs101    -3003 -839 $ current tally segment
fs102    -3003 -839 $ flux tally segment
sd101    150.139 174.1538 324.2928 $ segment divisor card for current tally
sd102    150.139 174.1538 324.2928 $ segment divisor card for flux tally
e0      5.0e-7 1.0e-1 10 $ thermal epithermal and fast neutron energy
de24    2.5e-8 1.0e-7 1.0e-6 1.0e-5 1.0e-4 1.0e-3 1.0e-2 1.0e-1 5.0e-1 1
df24    3.85e-6 4.17e-6 4.55e-6 4.35e-6 4.17e-6 3.70e-6 3.57e-6 2.08e-5
        7.14e-5 1.18e-4
fm4     8.2056209e16 $ multiplier card (normalize factor for 1 MW reactor)
fm24    8.2056209e16 $ multiplier card (normalize factor for 1 MW reactor)
fm1     8.2056209e16 $ multiplier card (normalize factor for 1 MW reactor)
fm2     8.2056209e16 $ multiplier card (normalize factor for 1 MW reactor)
fm11    8.2056209e16 $ multiplier card (normalize factor for 1 MW reactor)
fm12    8.2056209e16 $ multiplier card (normalize factor for 1 MW reactor)
fm21    8.2056209e16 $ multiplier card (normalize factor for 1 MW reactor)
fm22    8.2056209e16 $ multiplier card (normalize factor for 1 MW reactor)
fm31    8.2056209e16 $ multiplier card (normalize factor for 1 MW reactor)
fm32    8.2056209e16 $ multiplier card (normalize factor for 1 MW reactor)
fm41    8.2056209e16 $ multiplier card (normalize factor for 1 MW reactor)
fm42    8.2056209e16 $ multiplier card (normalize factor for 1 MW reactor)
fm51    8.2056209e16 $ multiplier card (normalize factor for 1 MW reactor)
fm52    8.2056209e16 $ multiplier card (normalize factor for 1 MW reactor)
```

```
fm61    8.2056209e16 $ multiplier card (normalize factor for 1 MW reactor)
fm62    8.2056209e16 $ multiplier card (normalize factor for 1 MW reactor)
fm71    8.2056209e16 $ multiplier card (normalize factor for 1 MW reactor)
fm72    8.2056209e16 $ multiplier card (normalize factor for 1 MW reactor)
fm81    8.2056209e16 $ multiplier card (normalize factor for 1 MW reactor)
fm82    8.2056209e16 $ multiplier card (normalize factor for 1 MW reactor)
fm91    8.2056209e16 $ multiplier card (normalize factor for 1 MW reactor)
fm92    8.2056209e16 $ multiplier card (normalize factor for 1 MW reactor)
fm101    8.2056209e16 $ multiplier card (normalize factor for 1 MW reactor)
fm102    8.2056209e16 $ multiplier card (normalize factor for 1 MW reactor)
cut:n   j 0
print
c ctme    4000
prdmp   j j j 3
imp:n   0 21r 1 836r
c imp:n   0 21r 1 694r
c       1 0.87m 2.44m 2.15m 2.69m 2.26m 1.66m 1.62m 1.75m 1.66m 1.21m
c       1.02m 3.05m 2.31m 3.12m 1.37m 1.19m $ bp4
c       0.75 0.87m 2.44m 2.15m 2.69m 2.26m 1.66m 1.62m 1.75m 1.66m 1.21m
c       1.02m 3.05m 2.31m 3.12m 1.37m 1.19m $ cladding bp4
c       4.0 1.66m 1.21m 1.02m 3.05m 2.31m 3.12m 1.37m 1.19m $ concrete bp4
c       1 0.48m 2.81m 1.53m 1.51m 1.53m 1.57m 1.68m 1.68m 1.59m 1.42m
c       1.37m 1.29m 1.25m 1.25m 1.13m 1.38m 1.24m 1.21m 1.15m 1.14m
c       1.14m 1.01m 1.09m 1.13m 1.27m 1.02m 1.26m 1.04m 1.18m
c       1.5m 1.15m 1.15m 1.15m 1 $ bp3
c       4.0 1.09m 1.13m 1.27m 1.02m 1.26m 1.04m 1.18m 1.5m 1 $ collimator bp3
c       0.75 0.48m 2.81m 1.53m 1.51m 1.53m 1.57m 1.68m 1.68m 1.59m 1.42m
c       1.37m 1.29m 1.25m 1.25m 1.13m 1.38m 1.24m 1.21m 1.15m 1.14m
c       1.14m 1.01m 1.09m 1.13m 1.27m 1.02m 1.26m 1.04m
c       1.18m 1.03m $ cladding bp3
c       3.96 1.59m 1.42m 1.37m 1.29m 1.25m 1.25m 1.13m 1.38m 1.24m
c       1.21m 1.15m 1.14m 1.14m 1.01m 1.09m 1.13m 1.27m 1.02m
c       1.26m 1.04m 1.18m 1.03m $ concrete bp3
```